Pulse Radiolysis of Gases H Atom Yields, OH Reactions, and Kinetics of H2O Systems

Nielsen, Ole John

Publication date:
1984

Document Version
Publisher's PDF, also known as Version of record

Risø-R-480

RISØ

Risø-R-480

Pulse Radiolysis of Gases H atom yields, OH reactions, and kinetics of H_2O systems

Ole John Nielsen

Risø National Laboratory, DK-4000 Roskilde, Denmark
April 1984

?

RISØ-R-480

PULSE RADIOLYSIS OF GASES
H atom yields, OH reactions, and kinetics of H_2S systems

Ole John Nielsen
Chemistry Department

Abstract. The pulse radiolysis equipment and technique are described and its relevance to atmospheric chemistry is discussed.

Pulse radiolysis of a number of different chemical systems have been described and computer simulations have been used to check the validity of the proposed mechanisms:

1) The hydrogen atom yield in the pulse radiolysis of H_2 was measured by four independent calibration techniques, using reactions of H with O_2, ClNO, and HI. The H atom yield was compared with O_2 yields in pure O_2 and in O_2/SF_6 mixtures which lead to a value G(H) = 17.6. The rate constants at room temperature of the following reactions were determined:

$$H + O_2 + H_2 \rightarrow HO_2 \qquad k = 2.17 \times 10^{10}\ [H_2]\ M^{-2}s^{-1}$$
$$H + ClNO \rightarrow HCl + NO \qquad k = 9.24 \times 10^{9}\ M^{-1}s^{-1}$$
$$I + NO + H_2 \rightarrow INO + H_2 \qquad k = 3.7 \times 10^{9}\ [H_2]\ M^{-2}s^{-1}$$

2) OH radical reactions with tetraalkyllead at room temperature and with ethane, methane, and a series of Cl- and F-substituted methanes at 300-400 K were studied. Arrhenius par-

(Continued on next page)

April 1984
Risø National Laboratory, DK 4000 Roskilde, Denmark

ameters, A and E_a, were determined for several reactions. The lifetime of $Pb(CH_3)_4$ and $Pb(C_2H_5)_4$ in ambient air is estimated.

$k(OH + Pb(CH_3)_4) = 3.8 \times 10^9\ M^{-1}s^{-1}$
$k(OH + PB(C_2H_5)_4) = 7.0 \times 10^9\ M^{-1}s^{-1}$
$k(OH + C_2H_6) = 9.7 \times 10^9 \times \exp(-2330/RT)\ M^{-1}s^{-1}$
$k(OH + CH_3Cl) = 3.2 \times 10^9 \times \exp(-2510/RT)\ M^{-1}s^{-1}$
$k(OH + CH_2Cl_2) = 4.1 \times 10^9 \times \exp(-2220/RT)\ M^{-1}s^{-1}$
$k(OH + CHFCl_2) = 1.1 \times 10^9 \times \exp(-3550/RT)\ M^{-1}s^{-1}$

CF_2Cl_2 was found to be a very efficient third body, M, in the reaction $OH + OH + M \rightarrow H_2O_2 + M$.

3) In the H_2S systems the HS extinction coefficient at 3242 Å was determined to $9.5 \times 10^2\ cm^{-1}\ mol^{-1}$. The following rate constants at room temperature were determined:

$k(H + H_2S \rightarrow H_2 + HS) = 4\text{-}6 \times 10^8\ M^{-1}s^{-1}$
$k(HS + HS \rightarrow products) = (1.9 \pm 0.1) \times 10^{10}\ M^{-1}s^{-1}$
$k(HS + S + M \rightarrow HS_2 + M) = (2.5 \pm 1) \times 10^{10}\ [M]\ M^{-2}s^{-1}$
$k(HS_2 + HS_2 + M \rightarrow H_2S_4 + M) = (8.5 \pm 3) \times 10^{10}\ [M]\ M^{-2}s^{-1}$

INIS-descriptors: ATMOSPHERIC CHEMISTRY; CHEMICAL REACTION KINETICS; CHEMICAL REACTION YIELD; COMPUTERIZED SIMULATION; HYDROGEN SULFIDES; HYDROXYL RADICALS; LEAD COMPLEXES; PULSE TECHNIQUES; RADIOLYSIS

UDC 541.15 : 551.510.4

ISBN 87-550-1002-4
ISSN 0106-2840

Risø repro 1984

CONTENTS

FOREWORD

This report has been submitted to the University of Copenhagen in partial fullfilment of the requirements for obtaining the degree lic. scient. (Ph.D.). Most of the work was carried out at the Chemistry Department of Risø National Laboratory during the period 1978-1982, with Drs. Palle Pagsberg (Risø) and Børge Bak (University of Copenhagen) as advisers. As parts of the work have already been published elsewhere, the author has sought to make this report relatively short and hopefully easily comprehensible for readers without prior knowledge of gas phase pulse radiolysis. As the first Ph.D. student in gas phase pulse radiolysis at Risø, I hope this report can be valuable to future students in helping to solve their problems.

The author is greatly indebted to Palle Pagsberg for his continuing support and interest in the work. Furthermore, the author wishes to thank the staff of the Chemistry Department at Risø for creating such a stimulating environment. Finally, he thanks Risø for supplying the facilities and financial support.

1. INTRODUCTION

Pulse radiolysis, here defined as irradiation by a short pulse of fast electrons, combined with some kind of transient detection method can provide different kinds of information useful in many areas and often complementary to information obtainable by other techniques. In general, a pulse-radiolysis investigation is limited to studies of transient species and kinetics in reaction processes following irradiation of a particular chemical system. However, as the reader will hopefully have realized after reading this report, the technique within this area is one of the most powerful available.

Pulse radiolysis was developed as an analog to the very similar flash photolysis technique which had been applied more than a decade before sources of pulsed high-energy radiation became available. The developmental work on pulse radiolysis was carried out on liquid system. With the availability of accelerators in the sixties, liquid densities was necessary for sufficient interaction of the system under study with the ionizing radiation, to prove an observable concentration of transient species. The technique of pulse radiolysis was first applied on liquid systems by Matheson and Dorfman (1960) and extended to gases about four years later by Sauer and Dorfman (1964). In this report, vapours of compounds which are normally liquid at room temperature are considered gases. In order for gases to absorb enough energy from high-energy (2 MeV or greater) electron beams, high pressures (10-100 atm) were initially used. Gas phase work at an atmosphere or less was made possible by advances in detection techniques and the development of accelerators with improved pulse power. At Risø's Chemistry Department gas phase pulse radiolysis was started in 1972 after my tutor, Palle Pagsberg, had got the idea during a stay with Sheffield Gordon at the Argonne National Laboratory (USA). The gas phase pulse radiolysis system was developed around an already installed field-emission accelerator, Febetron 705B. Since this

accelerator was also used for investigations of liquid systems the development of the gas phase system was a slow and non-continuous process.

The direct study of transient species and reaction kinetics has two basic requirements. First, the process must be initiated at a time scale shorter than or comparable to the processes being observed. Second, the species and processes to be studied must be associated with a detectable change in one or more physical parameters.

The Febetron 705B with a pulse duration of 30 ns meets the first requirement. The primary effect of the ionizing radiation is production of positive ions, secondary electrons, excited atoms, and/or molecules. Neutral fragments, free radicals, atoms, and molecules are formed in a microsecond or less (Sauer, 1976). These products may in turn react to give final stable species.

The stopping power of gases at a pressure of 1 atm is very low for 2 MeV electrons. Only a small fraction of the total energy is absorbed while the electrons pass through 10 cm of gas at 1 atm. Regarding the yields of transient species the low stopping power may be considered a serious drawback in the pulse radiolysis of gases.

With the Febetron 705B in a normal experimental situation free radicals in concentrations at about 10^{-6} M are produced and this is sufficient for detection in most cases using our kinetic absorption spectroscopy system. In the excellent review on pulse radiolysis studies of gases by Sauer (1976) various detection methods are discussed.

The low stopping power for 2 MeV electrons ensures a fairly homogeneous energy deposition and radical production throughout the gas sample. Change in temperature due to the energy deposition and heat from chemical reactions amounts to a maximum of one to two degrees. Such a small change can generally be ignored with respect to its effect on reaction rates. Concen-

tration gradients and local heating, which are problems frequently encountered in flash photolysis experiments are largely avoided by the pulse radiolysis techniques.

Another advantage of our pulse radiolysis technique is that the observed half-lives of the transients are normally much shorter than the time required for diffusion to the walls of the reaction cell. Hence, in pulse radiolysis we avoid wall effects which can be a serious problem in low-pressure discharge flow reactors which are widely used for studies of free-radical gas phase kinetics.

For the two reasons summarized above pulse radiolysis has some advantages compared with other gas kinetic techniques. However, it should be pointed out that the interpretation of experimental kinetic data obtained by pulse radiolysis may often be difficult due to the inherent complexity of the reaction system.

These problems arise because of the simultaneous production of different transient species which may all react with each other. This is unavoidable except for pure diatomic systems like H_2, where the only product after irradiation is the H-atom. For water there are three species, H, O, and OH and it will be necessary to take into account all possible reactions. A complete analysis may seem like a hopeless task. However, with sufficient experience in experimental gas kinetics it is often possible to find strategies whereby information about individual elementary reactions can be extracted even in complex reaction mixtures. The application of small amounts of additives serving as specific radical scavengers is an example of a method to change the kinetics in a predictable way.

An analysis of experimental data obtained by pulse radiolysis requires more sophisticated methods to separate out the effect of any selected reaction on the observed all-over kinetics which contain contributions from a number of simultaneous reactions. The use of computer modelling to simulate the reaction kinetics has been shown to be a powerful tool in the analysis of experimental data. Also computer modelling may predict ef-

fects of changing experimental parameters as irradiation dose, chemical composition, pressure, and temperature. Finally, the computer simulations may be used to test the validity of a proposed kinetic model.

The pulse radiolysis system in our laboratory was designed to be used for low pressure (2 atm and below) using kinetic absorption spectroscopy in the UV and visible region.

When operational, the system was used to study a number a different chemical systems. After two introductory chapters this report describes some of the studies performed using our pulse radiolysis system.

2. PULSE RADIOLYSIS AND ATMOSPHERIC CHEMISTRY

Human activities cause emissions of a great number of gases from the Earth's surface to the atmosphere. These emissions interact with the environment. If the effect is undesirable the emissions are generally termed pollution. This issue can be of both local and international importance. The latter is easily illustrated by the current debate on the potential risk of depletion of what has become known as the ozone layer caused by the release of chlorofluorocarbons (CFCs).

Since the 1950's rapid advancement in chemical analytical techniques and high-speed computers has led to an explosion of knowledge concerning atmospheric composition. The atmosphere has been found to be a reservoir for a myrad of trace gaseous species. In spite of the relatively low concentration of these trace species they can have a major impact on our environment. Atmospheric scientists use computer modelling to give predictions about the effect of society's activities on atmospheric chemistry. To set up a realistic model of the atmosphere is a formidable task due to the overwhelming complexity of chemical

kinetics and transport dynamics. Current models incorporate more than 200 chemical reactions. The results from these very complex model calculations are only as good as the quality of input data, e.g. rate constants for the involved chemical reactions. Values of rate constants used in model calculations are revised as new and better experimental measurements are published (Derwent et al., 1981; Baulch et al. 1982).

The key species in atmospheric chemistry appears to be the hydroxyl radical, OH (Chameides and Davis 1982). Therefore, a large amount of experimental work has been devoted to OH reactions. Two techniques have been used in these studies primarily. One is based on discharge flow reactors where the downstream steady-state concentration of OH is monitored by resonance fluorescence. The other technique is flash photolysis combined with either resonance fluorescence or resonance absorption detection of OH. These two experimental techniques give results which in most cases are in good agreement. When two different techniques yield the same result it seems that rate constants so obtained may be taken with confidence for the given experimental conditions. However, for both methods the applied range of pressures is in general much below 1 atm. The reason for this is the fast quenching of the resonant state at higher pressures.

Due to the pressure dependence observed recently in some elementary reactions (Baum, 1982), it has been realized that measurements of rate constants at higher pressures are very important. Measurements around 1 atm require a technique like pulse radiolysis. Despite the several advantages of the pulse radiolysis technique it is used only at a few other laboratories around the world, probably mainly because of the expensive equipment needed.

3. EXPERIMENTAL

The experimental set-up is shown schematically in Figure 3.1, and has been described in detail by Hansen et al. (1979). The field-emission accelerator (Febetron 705B) provides single pulses of 2 MeV electrons with a pulse duration of 30 ns and a maximum current of about 3000 Amperes. Important properties of the electron pulse are its maximum energy, pulse current, time profile, cross-sectional homogenity, and divergence. Details of a Febetron accelerator shown schematically in Figure 3.2 may be found elsewhere (Charbonnier et al. 1975; Sauer 1982). Briefly, a series of capacitor modules in parallel, with their central spark gaps in open circuit are charged from a high-voltage power supply. Via the short pulse adapter the high-voltage output is discharged into the field-emission tube and passed out of the tube window. The pulse-to-pulse repeatability is specified as 5%. Sometimes a higher difference in pulses was observed. Once since 1978 the field emission tube was changed. This caused a slight change in observed dose.

The stainless steel cell for irradiation of gas samples is shown in Figure 3.3 and adapted from Gordon et al. (1971). The optical arrangement in the cell, originally described by White (1942), consists of a set of conjugate mirrors that allow multiple passages of the analyzing light through the sample. Usually this system can improve the signal-to-noise ratio in absorption measurements. The wavelength dependence of mirror reflectivity plays an important role when optimizing the signal-to-noise ratio using different numbers of traversals. Because signal-to-noise ratio is proportional to the square root of the light intensity, the gain in this ratio due to the increase in absorption must outweigh the effect of loss of intensity due to additional reflections. Below 300 nm the wavelength dependence of mirror reflectivity plays an increasing role with as the wavelength decreases. Most of the experiments were carried out using 12 traversals corresponding to an optical pathlength of 120 cm.

The damaging effect on the mirrors by chemicals in the cell required frequent changing of mirrors with some inconvenience.

The gas mixtures were either premixed in an all-glass vacuum line or prepared by admitting one component at a time to the cell. The partial pressure is read using a MKS Baratron 170 series absolute electronic membrane manometer with a resolution of 10^{-5} bar. Electric heating and temperature control provides a range of sample temperatures from 300 to 400 K. A platinum thermometer is used to measure the temperature of the reaction mixture near the central part of the cell.

Unless specifically stated the chemicals used were of the highest commercial purity and were used directly.

The principal features of the optical system are shown in Figure 3.4. The analyzing light source is a 150-watt high-pressure UV Varian xenon lamp with short axial arc and parabolic reflector. The sapphire exit window transmits the Xe-continuum down to about 1900 Å. An optical train of suprasil lenses and aluminized mirrors carries the analyzing light through the sample cell and shielding wall to the entrance slit of the Hilger and Watts 1 meter monochromator (spectrograph) with a 1200-groove/mm grating blazed at 3000 Å to obtain high efficiency down into the UV-region and a reciprocal dispersion of 8 Å/mm. The weakly divergent light beam from the xenon lamp is focused onto a discriminating slit plane to form an image of the xenon arc. This slit serves two purposes and is essential for the performance of the entire optical system. One is to select that fraction of the light which can be transmitted through the monochromator entrance slit. This avoids the major part of the light, which can contribute only to unwanted scattered light and photolysis. Secondly, the slit combined with the dispersion of the first lens acts as a band-pass filter, which enhances the light intensity around a particular wavelength determined by the distance between the lens and the slit plane. This feature is found to be important also for the optical feedback to the xenon lamp pulser which receives a spectral representative light signal via a quartz plate beam splitter and a fiber optic cable.

The xenon lamp pulser is most essential to the performance in the UV region where the light intensity can be increased by a factor of 20-50 and still be intensity stabilized to within a few per cent on a millisecond time-scale. For a given wavelength the distance between the telescope lens pair and neighbouring lenses is chosen so that the circular image of the limiting aperture fills out the collecting monochromator slit for maximum light efficiency. The application of a total of seven lenses results in a large loss of light intensity (about 4-6% per surface) which makes the use of the lamp pulser indispensable. However, a major advantage of the system is that the lenses act as a premonochromator resulting in a stray light level lower than a few per cent in the UV-region.

The light intensity out of the exit slit of the monochromator is monitored using a Hamamatzu R 955 photomultiplier coupled to a current input operational amplifier with ajustable offset. The transient signals are stored in a Biomation 8100 waveform digitizer interfaced to a PDP8 minicomputer that controls the transfer and storage of raw data.

Each transient curve is composed of 2000 time-equidistant samples of the transmitted light intensity in an 8-bit representation corresponding to a resolution of 1/256. The minimum sampling time is 10 nsec, the maximum sampling time is determined by the stability of the analyzing light intensity. Our experiments have never required longer sampling times than were available. Comment lines specifying the experimental conditions are attached to each kinetic curve during composition of the raw data file. Algorithms are available to produce absorption versus time or other relevant plot types that can be inspected on a display screen and may be plotted on an X-Y recorder.

Selected raw data can be transferred to magnetic tapes, which are brought to a large central computer where the experimental data become available as disk files. Different computer programs were written and modified for treatment of the raw kinetic data. These computer programs contain many options and will not be described in detail here. Constant absorbance, A_∞, may be sub-

tracted from the measured absorbance. The signal-to-noise ratio of the raw data may be improved, if necessary, by averaging repetitive runs or by applying of smoothing procedures. Analytical first- and second-order decay curves may be fitted to the experimental curves using least-squares procedures. In general, the analysis involves a study of a functional dependence of the shape of the kinetic curves following a change in the concentration of one of the reactants.

As mentioned earlier, we often deal with very complex reaction systems. A most powerful tool is computer simulation of the complete set of chemical reactions involved. A computer program, CHEMSIMUL, developed by O. Lang Rasmussen (1983) from Risø's Computer Department was used. As input, this program accepts reaction schemes in the usual chemical notation, e.g., $OH + OH \rightarrow H_2O + O$, $k = 3 \times 10^9\ M^{-1}s^{-1}$ etc. The program translates these chemical equations into the relevant set of differential equations which are solved by numerical integration after specification of initial conditions, e.g., concentrations, irradiation dose, etc. The effect of parametric variations can be studied using a graphical computer terminal. It will be seen later that computer simulation is indispensable in the analysis of complex cases like $OH + CF_2Cl_2$. Problems involved in deriving rate constants using computer simulation are described later.

4. PULSE RADIOLYSIS OF H_2 SYSTEMS, H ATOM YIELDS AND REACTIONS

4.1. Introduction

These studies will not be described in every detail since they have already been published elsewhere (Nielsen, Sillesen, Luther and Troe 1982). Pulse radiolysis of H_2 provides a well-defined source of H atoms in the gas phase. This has been used to study, e.g. series of H atom reactions with added molecules like O_2, C_6H_6, and related compounds (Bishop and Dorfman 1970; Sauer and

Ward 1967), spectra of radicals were recorded and radical-radical reactions investigated (e.g., Hamilton 1975; Hamilton and Lii 1977; Lii et al. 1979). Normally, absolute values of rate constants for reactions between H atoms and a species can be measured directly if pseudo-first-order conditions are established using a large excess of the reactant. However, derivation of absolute absorption coefficients for produced radicals as well as rate constants in cases where pseudo-first-order conditions cannot be established requires knowledge of the H-atom yield after irradiation of H_2. This fundamental property in radiation chemistry is also known as the G value of hydrogen, G(H). G(X) refers to the number of a product X formed on irradiation per 100 eV of energy absorbed. Surprisingly, there has only been one experimental (Hamilton and Lii 1975) and one theoretical (Armstrong and Willis 1976) estimate of G(H) in H_2. The problem is of course to convert all the H atoms produced into something that is stable and convenient to detect.

In this investigation four different titration reactions were used for determination of G(H) in H_2. The methods used are detection of HO_2 formation in irradiated H_2-O_2 mixtures via the reaction

$$H + O_2 + M \rightarrow HO_2 + M \qquad (1)$$

the detection of ONCl consumption in irradiated H_2-ONCl mixtures via the reaction

$$H + ONCl \rightarrow HCl + NO \qquad (2)$$

the detection of HI consumption in irradiated H_2-HI mixtures via the reaction

$$H + HI \rightarrow H_2 + I \qquad (3)$$

and the detection of I_2 formation in irradiated H_2-HI-NO mixtures via the reaction

$$I + I + NO + M \rightarrow I_2 + NO + M \qquad (4)$$

All these reaction systems are kinetically well characterized. They allow the determination of H atom yields with an accuracy which is given essentially by the accuracies of the absorption coefficients of HO_2, ONCl, HI, and I_2.

4.2. Results

4.2.1. H_2-O_2 mixtures

Mixtures with O_2 pressures between 0.8 and 50 mbar in H_2 at total pressures of 1 bar were irradiated. The formation of HO_2 was monitored at a wavelength of 230 nm. After its formation, HO_2 disappears at a very slow rate, with a half-life longer than 2 ms as seen in Figure 4.1.

The formation of HO_2

$$H + O_2 + H_2 \rightarrow HO_2 + H_2$$

followed a pseudo-first-order rate low:

$$d[HO_2]/dt = k_1'([HO_2]_{t=0} - [HO_2]_t) = k_1[H_2][O_2][H].$$

The data for k_1' are illustrated in Figure 4.2 for a total pressure of 1 bar and correspond to $k_1 = (2.17 \pm 0.2) \times 10^{10}$ $M^{-2}s^{-1}$. Figure 4.3 shows the HO_2 absorbances measured after initial formation, for various O_2 pressures. The measurements show a slight linear increase of the yield with added O_2 concentration. This must be due to the direct radiolysis of added O_2 to O atom. A certain fraction of these O atoms are formed in an excited state (probably $O(^1D)$ and $C(^1S)$), which can react fast with H_2, $k = 1.6 \times 10^{11}$ $M^{-1}s^{-1}$ at 300 K (Baulch et al. 1980) to form H atoms that give additional HO_2 via reaction 1. This is discussed in detail by Nielsen et al. (1982).

The HO_2 yield corresponding to the radiolysis of pure H_2 (where one could not get HO_2) is obtained from the intercept in Figure

4.3. This HO_2 absorbance is equal to 1.78×10^{-2}. When the HO_2 absorption coefficient of $\varepsilon = 587\ M^{-1}\ cm^{-1}$ at $\lambda = 230$ nm (Pankert and Johnston 1972) is used, this corresponds to an HO_2 yield and thereby H atom yield of 2.52×10^{-7} M. As seen from Figure 4.4, the HO_2 yield was found to be directly proportional to H_2 pressure between 180-1000 mbar.

4.2.2. H_2-ONCl mixtures

Mixtures of H_2 and ONCl (10^{-6} to 10^{-5} M) were irradiated at a total pressure of 1 bar. ONCl consumption by reaction 2 was monitored at $\lambda = 230$ nm. The measured rate of ONCl disappearance

$$d[ONCl]/dt = -k_2'([ONCl]_t - [ONCl]_{t=0}) = -k_2[H][ONCl]$$

is illustrated in Figure 4.5 and corresponds to $k_2 = (9.2 \pm 0.9) \times 10^9\ M^{-1}s^{-1}$. The change in ONCl absorbance due to reaction 2 is directly related to the H atom yield. Figure 4.6 shows the independence of this absorbance change from initial ONCl concentration. With the most recent value of the ONCl absorption coefficient at $\lambda = 230$ nm $\varepsilon = 830\ M^{-1}\ cm^{-1}$ (Illies and Takacs 1976) this absorbance change corresponds to an ONCl consumption and thereby H atom yield of 2.59×10^{-7} M.

4.2.3. H_2-HI mixtures

HI consumption by reaction 3 was monitored at 230 nm after irradiation of mixtures of HI, pressures 0.2 to 0.7, and H_2 at a total pressure of 1 bar. The observed rate of HI disappearance was consistent with the literature value of $k_3 = 1.6 \times 10^{10}\ M^{-1}s^{-1}$ (Lorenz et al. 1979). The absorbance change was found to be 6.23×10^{-3}, which with $\varepsilon = 200\ M^{-1}\ cm^{-1}$ (Huebert and Martin 1968) corresponds to a HI concentration change and thereby H atom yield of 2.60×10^{-7} M. Measured points are the open circles in Figure 4.8.

4.2.4. H_2-HI-NO mixtures

Recombination of I atoms from reaction 3 in the previous system

is slow under our conditions. However, small amounts of NO accelerate the I recombination without disturbing the reaction system (van den Bergh and Troe 1975; van den Bergh and Troe 1976). The initial reaction 3 is followed by

$$I + NO + H_2 \rightarrow INO + H_2 \qquad (5)$$

Since [NO] < [HI] HNO formation by

$$H + NO + H_2 \rightarrow HNO + H_2 \qquad (6)$$

$k_6 = 2 \times 10^{10}\ M^{-2}s^{-1}$, could not compete with reaction 3. Under our conditions reaction 5 is followed by

$$I + INO \rightarrow I_2 + NO \qquad (7)$$

$k_7 = 1.7 \times 10^{11}\ M^{-1}s^{-1}$. Van den Bergh and Troe (1975; 1976) found that I_2 was also formed through a much slower reaction channel

$$2\ INO \rightarrow I_2 + 2\ NO \qquad (8)$$

Under our conditions the amount of I_2 formed this way was less than 5% and therefore neglected.

Formation of I_2 was monitored at 490 nm and followed a pseudo-first-order rate law

$$d[I_2]/dt = k_4'([I_2]_{t=0} - [I_2]_t)$$

For quasi-stationary INO concentration k_4' is equal to $2k_5[NO][H_2]$ such that

$$d[I_2]/dt = 2k_5[NO][H_2]([I_2]_{t=0} - [I_2]_t) .$$

Figure 4.7 shows measured k_4' at a total pressure of 1 bar as a function of NO concentration. These data give $k_5 = (2.7 \pm 0.3) \times 10^9\ M^{-1}s^{-1}$. No effect of varying HI pressure from 1 to 50 mbar on the I_2 formation rate was detected. With a value of ε =

454 $M^{-1}cm^{-1}$ (Tellinghuisen, 1973) the I_2 yields in Figure 4.8 have been derived. A slight increase of the I_2 yield with increasing HI pressure is observed. Since I_2 formation was independent of HI pressure this increase cannot be attributed to

$$HI + INO \rightarrow I_2 + HNO \qquad (9)$$

However, in analogy with the H_2-O_2 system there is direct radiolysis of HI to H and I. The mechanism $H + HI \rightarrow H_2 + I$, $I + I \rightarrow I_2$ gives one I_2 per two dissociated HI molecules. An extrapolation of the I_2 yields to zero HI pressure gives $2[I_2]$ and thereby the H atom yield to 2.75×10^{-7} M.

4.3. Discussion

4.3.1. H atom yields

The accuracy of the values for the H atom yields depends mainly on the accuracy of the absorption coefficients of the titration species HO_2, ONCl, HI, and I_2. In Table 4.1 all H atom yields are given.

For HO_2 the ε value taken from experiments by Paukert and Johnston (1972) has been comfirmed several times (Hamilton 1975; Hochanadel et al. 1972) and its uncertainty is estimated to be about 10%.

Besides the most recent ε value for ONCl an older value of $\varepsilon = 1140\ M^{-1}cm^{-1}$ exists (Ballash and Armstrong 1974). However, this value would give a value of 1.89×10^{-7} M for the H atom yield, which is out of range compared to the three other determinations. These experiments therefore favour the lower value of ε.

In the care of HI the absorption coefficient is known very accurately (Huebert and Martin 1968). This is true also in the case of I_2 (Tellinghuisen 1973).

The determined H atom yields shown in Table 4.1, using the four different kinetic systems, are in very close agreement. The average value weighted by the number of measurements in each system is $[H] = (2.59 \pm 0.3) \times 10^{-7}$ M. It has also been shown (Nielsen et al., 1982) that the effect of electron and ion reactions in an initial short period after the pulse involving H_2 as well as the other components in the different mixtures will be within the uncertainty of the experimental data.

Table 4.1. Hydrogen Yields of Pulse Radiolysis in 1 bar of H_2 Measured by Different Titration Reactions

mixture	reaction	no. of experiments	H atom yield/(mol l^{-1})
H_2-O_2	$H+O_2+M \rightarrow HO_2+M$	54	2.52×10^{-7}
H_2-ClNO	$H+ClNO \rightarrow HCl+NO$	26	2.59×10^{-7}
H_2-HI	$H+HI \rightarrow H_2+I$	5	2.60×10^{-7}
H_2-HI-NO	$H+HI \rightarrow H_2+I$	19	2.75×10^{-7}
	$2I+NO+H_2 \rightarrow I_2+NO+H_2$		
			av 2.59×10^{-7}

4.3.2. Dosimetry and G value

In order to derive the G value for H atom formation in the pulse radiolysis of H_2, it is necessary to compare the H atom yield with dosimetry in our system under identical conditions.

The formation of O_3 in O_2 and O_2-SF_6 systems has been used for dosimetry in gas phase pulse radiolysis. Concentrations of O_3 can be measured using the absorption coefficient at O_3 maximum at 255 nm, $\varepsilon(O_3) = 3067\ M^{-1}cm^{-1}$ as determined by Inn and Tanaka (1953). In this way two separate determinations of $G(O_3)$ in pure O_2 using Febetron 705 dose rates have been made, $G(O_3) = 13.8 \pm 0.7$ (Ghormly et al. 1969) and $G(O_3) = 12.8 \pm 0.6$ (Boyd et al., 1969 Willis et al. 1970) were obtained from dosimetry based on the temperature rise in aluminium plates. Ghormly et al.

reported little or no dose-rate dependence while Boyd et al. reported independence of pressure (30-800 torr O_2) and of dose rate (10^{26} - $2 \cdot 10^{27}$ eV $g^{-1}s^{-1}$). However, this is in disagreement with Johnson and Wilkey (1969), who found $G(O_3)$ decreasing approximately linearly 20% going from 200 to 2000 torr O_2. The $G(O_3)$ was found to be constant over the same pressure range when SF_6 (1 mole %) was added to the O_2. Also dose-rate dependence disappeared upon addition of 0.5-3 mole % SF_6 (Willis et al. 1970). This is because SF_6 as an electron scavenger eliminates production of O_3 by ionic mechanisms. While Willis et al. (1970) observed a 52% decrease from 12.8 to 6.2 upon adding 0.5-3 mole % SF_6, Johnson and Wilkey (1969) measured a 38% drop upon the addition of 1 mole % SF_6. In the present work a similar low (33 ± 1) % decrease in O_3 yield upon adding SF_6 was measured repeatedly. This was reproduced several times before and after the exchange of a much used field emission tube with a new one. In this case the $G(O_3)$ in pure O_2 was preferred, because it has been measured by two different groups who obtained rather good agreement (Ghormley et al. 1969; Boyd et al. 1969). Of these two values $G(O_3)$ = 12.8 was chosen as it has been confirmed several times.

The ratio of H-atom yield in 1 bar H_2 to the O_3 yield in 1 bar of pure O_2 was found to be $[H]/[O_3] = 2.59 \times 10^{-1}/1.26 \times 10^{-6} = 0.206$. The calculation of energy absorption in H_2 depends only of the stopping power relative to that of O_2 (Sauer 1976). Then the G-value of H-atom formation in H_2 is given by the expression $G(H) = ([H]/[O_3])(S[O_2]/S[H_2])G(O_3)$ where S denotes the respective stopping powers. Using $S(O_2)/S(H_2) = 6.71$ (Huyton and Woodward 1970) and $G(O_3) = 12.8$, $G(H) = 17.6$ for H-atom production in H_2 is found.

The accuracy of this value is given by a 10% uncertainty in the $[H]/[O_3]$ ratio and the uncertainties of stopping power ratio and $G(O_3)$. Taking the 5% uncertainty of $G(O_3)$ from Willis et al. (1970) an accuracy of 20% is estimated for G(H).

This value can be compared with $G(H) \leq 13$ estimated by Hamilton and Lii (1977) in pulse radiolysis of H_2-O_2 systems. However,

their dose was 6.5 times higher than in this study. This means that the H + HO_2 reaction can no longer be neglected. Including H + HO_2 in a computer simulation it was found that the apparent H-atom yield indicated by HO_2 absorption will be 20% lower than the real H-atom yield. This brings the two measurements into closer agreement. The reason for the disagreement with the theoretical estimate of G(H) = 13.8 by Armstrong and Willis (1976) is not easily pointed out as it is dependent not only upon the chosen model but also upon the many different emperical data which enter into the model.

4.3.3. Rate constants

In addition to the H-atom yield, three rate constants were derived from these experiments. Table 4.2 summarizes these results and compares them with data found in the literature. The rate constants derived in this study are in very good agreement also with data obtained by different experimental techniques.

Table 4.2. Rate Constants for Elementary Reactions Studied in This Work (T = 295 K)

reaction	rate constant/ ($cm^3\ mol^{-1}s^{-1}$)	ref.
$H+O_2+M \rightarrow HO_2+M$	$2.17\times10^{16}[H_2]$	This work
	$1.7\times10^{16}[H_2]$	Bishop and Dorfman (1970)
	$2.14\times10^{16}[H_2]$	Wong and Davies (1974)
	$4.35\times10^{15}[H_2]$	Ahumada et al. (1972)
$H+ClNO \rightarrow HCl+NO$	9.24×10^{12}	This work
	9.88×10^{12}	Wagner et al. (1976)
	1.63×10^{13}	Dunn et al. (1971)
$I+NO+M \rightarrow INO+M$	$3.7\times10^{15}[H_2]$	This work
	$3.7\times10^{15}[H_2]$	Van den Bergh (1977)
	$2.2\times10^{15}[He]$	Van den Bergh (1977)

5. OH RADICAL REACTIONS

5.1. Introduction

As already mentioned it is well known that the OH radical plays an important role in the chemistry of the atmosphere. Development of computer kinetic models for simulating atmospheric chemistry has made accurate measurements of OH rate constants an important research goal. Together with this, advances in experimental techniques have caused the number of available OH rate constant data to increase dramatically during the last 10 years.

The OH-radical was first proposed as a separate species in 1924 by Watson (1924), and in 1928 the absorption spectrum of OH was obtained (Bonhoeffer and Reichardt 1928). In 1935 Oldenberg (1935) was able to follow the decay of the OH-radical in an electrical discharge in water vapour.

In 1961 Leighton (1961) suggested that OH was one of the intermediates playing an important role in photochemical air polution. Figure 5.1 shows the common division of the atmosphere into four regions based on temperature gradient. There are two major sources of OH in the atmosphere. First, excited $O(^1D)$ atoms, formed in the ozone photolysis at the shorter ($\lambda < 315$ nm) wavelengths of sunlight, react with water:

$$O(^1D) + H_2O \rightarrow 2\ OH \qquad (10)$$

The majority of $O(^1D)$ atoms will be quenched to $O(^3P)$ by collisions with N_2 and O_2

$$O(^1D) + M \rightarrow O(^3P) + M \ (M = O_2 \text{ or } N_2) \ . \qquad (11)$$

However, reaction 10 is so fast ($1.4 \times 10^{11}\ m^{-1}s^{-1}$) that about 5% of the $O(^1D)$ atoms will react through reaction 10. Secondly,

OH is formed from photolysis of HONO, which is a good absorber of sunlight for wavelengths less than 400 nm

$$HONO + h\nu \rightarrow HO + NO \quad . \qquad (12)$$

HONO is formed from

$$NO_2 + NO + H_2O \rightarrow 2\ HONO \quad . \qquad (13)$$

The instantaneous OH-concentration depends upon height, latitude, altitude, season, solar intensity, time of day, and present concentrations of a number of species. Estimates and measurements of OH-concentrations will be dealt with later. The OH-radical is highly reactive toward most of the impurities found in polluted air. Unlike many atoms, radicals of hydrocarbons, and alkoxy radicals, the OH-radical is unreactive toward atmospheric O_2, and thus lives long enough to react with compounds present as impurities even at very low levels. There have been three excellent reviews of OH gas phase reactions in the literature (Drysdale and Lloyd 1970; Atkinson et al. 1979; Baulch and Campbell 1981). Gordon and Mulac (1975) were the first to use pulse radiolysis to obtain OH rate constants directly. Based on a calculated initial OH yield they determined a rate constant for the total second-order disappearance of OH of 2×10^{10} $M^{-1}s^{-1}$. This value was indirectly confirmed by another simultaneous pulse radiolysis study of water vapour (Boyd et al. 1973). Our experiments differ mainly in one aspect: Around room temperature where the partial pressure of water is fairly low we back up with Ar to a total pressure of 1 bar to maintain the stopping power which is approximately proportional to the density of the gas mixture. This means that the Ar absorbs most of the energy and transfers it to the water producing H and OH

$$Ar^* + H_2O \rightarrow H + OH + Ar \qquad (14)$$

Absorption of UV light in one of the OH band systems has been used to monitor OH-concentrations in a variety of experimental systems. The UV absorption spectrum of OH is well known and an excellent summary of fundamental data is given by Dieke and

Crosswhite (1962). Figure 5.2 shows the most frequently used OH absorption band (0,0; $A^2\Sigma^+ \leftarrow X^2\Pi$) obtained by Welge and Stuhl (1967). We have monitored OH at 2 different wavelengths, around 3081.6 Å where Q_{13} and P_{11} absorb, and around 3090 Å where there are three Q_2 lines and some unresolved lines. In most cases the absorption around 3090 Å was used.

Normally the quantitative measure of light absorption is given by the Lambert-Beer law

$$A = \log (I_0/I) = \varepsilon l c \qquad (15)$$

where A is the absorbance defined in terms of the observed initial (I_0) and transmitted (I) light intensities after traversal of an optical path length of 1 cm through a substance with the absorbing species present in a concentration of c M. The extinction coefficient ε in $M^{-1}cm^{-1}$ is a constant characterizing the absorbing species. The Lambert-Beer law holds strictly for monochromatic light. In practice an analyzing light beam may be considered monochromatic after passing a spectrographic device with a spectral band pass which is about 1/10 of the line width of the spectral feature under investigation. To get a satisfying signal-to-noise ratio the bandwidth of the monochromator is often set so wide that this condition is far from fulfilled. In the OH case the bandwidth has to be set so wide that even several absorption lines become significant. When this is the case deviations from the Lambert-Beer have been observed (Callear and Tyerman 1966; Gordon et al. 1971) and a modified expression has been proposed

$$A = (\varepsilon l c)^n \qquad (16)$$

where n is a fractional power between 0 and 1 which has to be determined experimentally. The applicability of this relation has been investigated in detail by Bourene et al. (1974). The exponent n depends upon the lineshape and the monochromator slit setting. In this study n was determined in two different ways: One is by varying the optical path length in the cell. Two, by varying the initial OH concentration, c, consequently by varying

the irradiation dose by means of steel diaphragms. Thereafter n is derived by linear regression, $\log(A) = n(\log(\varepsilon lc))$. In most cases at both wavelengths n values derived by the two different methods were in good agreement. I found n in the range 0.83-0.63. When the observed absorption lines are very sharp, as for OH, a slight temperature change (1-2 ^{o}C) will disturb the monochromator setting enough to change the observed absorbance and thereby n. Further variations in dose from pulse-to-pulse will cause uncertainties in determinations of n. Since the absorption is small (around 0.1 at l = 120 cm) only small variations in optical path length and irradiation dose have been used, which again will cause uncertainties in the determination of n because of the small number of data points. Since the Ar-sensitized radiolysis of pure water vapour serves as the OH source and since it is our basic system it seems appropriate to deal with this system in somewhat more detail. Also this will show how to approach the kinetics in the pulse radiolysis of mixtures.

5.2. Pulse radiolysis of water vapour

There has always been a great interest in all aspects of the chemistry of water probably because of its vast natural abundance. Also radiolysis of water vapour has been studied extensively by different techniques. An excellent review is given by Dixon (1970).

Our Ar-sensitized radiolysis has the exact same result as radiolysis of pure H_2O namely production of H and OH within a short time scale (less than 1 μs). OH can recombine in two ways:

Table 5.1. Quadratic array giving the reactions considered in the pulse radiolysis of H_2O-Ar mixtures

		1 OH	2 H	3 O	4 O_2	5 HO_2	6 H_2O_2	7 H_2
1	OH	11	12	13		15	16	17
2	H		22	23	24	25	26	
3	O			33		35		
4	O_2							
5	HO_2					55		
6	H_2O_2							
7	H_2							

No.	Reaction	Rate Constant in $M^{-1}s^{-1}$ (300 K)
11a	$OH + OH \rightarrow H_2O + O$	$k_{11a} = 1.1 \times 10^9$
11b	$OH + OH + M \rightarrow H_2O_2 + M$	$k_{11b} = 3.8 \times 10^9$
12	$OH + H + M \rightarrow H_2O + M$	$k_{12} = 3.5 \times 10^9$
13	$OH + O \rightarrow H + O_2$	$k_{13} = 2.4 \times 10^{10}$
15	$OH + HO_2 \rightarrow H_2O + O_2$	$k_{15} = 2.4 \times 10^{10}$
16	$OH + H_2O_2 \rightarrow H_2O + HO_2$	$k_{16} = 4.9 \times 10^8$
17	$OH + H_2 \rightarrow H_2O + H$	$k_{17} = 4.5 \times 10^6$
22	$H + H + M \rightarrow H_2 + M$	$k_{22} = 5.0 \times 10^7$
23	$H + O + M \rightarrow OH + M$	$k_{23} = 3.0 \times 10^8$
24	$H + O_2 + M \rightarrow HO_2 + M$	$k_{24} = 3.0 \times 10^8$
25a	$H + HO_2 \rightarrow OH + OH$	$k_{25a} = 1.9 \times 10^{10}$
25b	$H + HO_2 \rightarrow H_2 + O_2$	$k_{25b} = 8.4 \times 10^9$
25c	$H + HO_2 \rightarrow H_2O + O$	$k_{25c} < 5.7 \times 10^8$
26a	$H + H_2O_2 \rightarrow H_2O + OH$	$k_{26a} = 2.4 \times 10^6$
26b	$H + H_2O_2 \rightarrow H_2 + HO_2$	$k_{26b} = 1.9 \times 10^6$
33	$O + O + M \rightarrow O_2 + M$	$k_{33} = 1.6 \times 10^7$
35	$O + HO_2 \rightarrow OH + O_2$	$k_{35} = 2.1 \times 10^{10}$
55	$HO_2 + HO_2 \rightarrow H_2O_2 + O_2$	$k_{55} = 1.5 \times 10^9$

Rate constants for third order reactions are converted to pseudo-second-order using [Ar] = 1/24 M. The numbering is used only in this table.

$$OH + OH \rightarrow H_2O + O \qquad (17)$$

$$OH + OH + M \rightarrow H_2O_2 + M \ (M = Ar \text{ and } H_2O) \qquad (18)$$

These reactions gave two new species in the system, O and H_2O_2, which can react with OH and H. It is easily seen that in this way the kinetic system for system as simple as H_2O will quickly become very complex. To be sure to consider all imaginable reactions the quadratic array shown in Table 5.1 is set up. In this table third-order rate constants are converted to pseudo-second-order using an Ar concentration of 1/24 M, neglecting the small H_2O concentration as third body. When nothing else is explicitly stated the rate constants have been taken from the extensive compilation of Hampson (1980), which was the most recent review when this work was carried out. None of the rate constants of the reactions in Table 5.1 which has been considered in the latest evaluation by the CODATA Task Group on chemical kinetics (Baulch et al. 1982) has changed significantly. To run the kinetic model set up in Table 5.1 knowledge of the initial OH concentration, $[OH]_o$, is needed. Based on ozone dosimetry and assuming that the yield of OH in H_2O-Ar mixtures is the same as that in pure H_2O vapour, G(OH) = 6.25 (Boyd et al., 1973), which is not a justified assumption, $[OH]_o = (1 \pm 0.5) \times 10^{-6}$ M was estimated.

In Table 5.2 OH half-lives from simulated models using three different $[OH]_o$ are compared with a typical experimental result.

It is seen from Table 5.2, assuming the complete model to be correct, that the $[OH]_o$ is probably closer to 0.5×10^{-6}.

It is also seen that a simpler model gives τ values in close agreement with those of the complete model. In the pure H_2O system the decay of OH is governed mainly by the reactions:

$$OH + OH \rightarrow H_2O + O \qquad (17)$$

$$OH + OH + M \rightarrow H_2O_2 + M \qquad (18)$$

Table 5.2. Comparison of simulated OH half lives, τ, with an experimental result.

$[OH]_o$	τ from complete model	τ from simple model[a]
0.5×10^{-6} M	132 µs	137 µs
1.0×10^{-6} M	68 µs	69 µs
1.5×10^{-6} M	44 µs	46 µs

$\tau_{exp} = 148 \pm 15$ µs

a) The simple model includes only the first three reactions (11a, 11b, 12).

$$OH + H + M \rightarrow H_2O + M \qquad (19)$$

The remaining 15 consecutive reactions in the model play a very minor role in our pulse-radiolysis experiments. Under these conditions the decay of OH is described to a good approximation by the differential equation:

$$-d[OH]/dt = 2\,k_{17}[OH]^2 + 2\,k_{18}[OH]^2[M] + k_{19}[OH][H][M] \qquad (20)$$

Figure 5.3 shows an example of the transient absorbance of OH monitored in the Ar-sensitized radiolysis of H_2O. The absorbance decreases to half of the maximum value in the course of 100 µs and this so-called "natural OH half-life" must be ascribed to the reactions 17, 18, and 19. Another characteristic feature is the long second-order tail following the steep initial part of the decay.

The high reactivity of OH in many H-abstraction reactions,

$$R\text{-}H + {}^{\bullet}OH \rightarrow R^{\bullet} + H\text{-}OH, \qquad (21)$$

is due to the high bond dissociation energy, D(H-OH) = 119 kcal/mole, which exceeds the bond dissociation energies D(R-H) in most compounds like alkanes and substituted alkanes.

By adding a compound, RH, reacting with OH a characteristic effect on the OH decay is observed, as shown in Figure 5.3. Comparison in Figure 5.3 reveals suppression of the second order tail, and the half-life is reduced as well. In this case an additional term must be added to Equation 20:

$$-d[OH]/dt = 2\,k_{17}[OH]^2 + 2\,k_{18}[OH]^2[M] + k_{19}[OH][H][M] + k_{21}[OH][RH]. \quad (22)$$

This differential equation serves as the basis for determining k_{21}. In general, the corrections for the contributions from reactions 17, 18, and 19 to the observed overall OH decay rate can be accomplished by studying the effect of reaction 21 over sufficiently large range RH concentrations. In the range of RH concentrations giving:

$$k_{21}[RH] \gg 2\,k_{17}[OH] + 2\,k_{18}[OH][M] + k_{19}[19][M] \quad (23)$$

the differential Equation 22 degenerates into

$$-d[OH]/dt = k_{21}[RH][OH] \quad (24)$$

corresponding to a simple exponential decay

$$[OH]_t = [OH]_o \exp(-k_{21}[RH]_o\, t) \quad (25)$$

with a half-life, τ, of

$$\tau = \ln^2/(k_{21}[RH]_o) \; . \quad (26)$$

This situation is referred to as pseudo-first-order. Equation 26 may be used to obtain a quick estimate of k_{21} from a single experiment in which the $[RH]_o$ was sufficient to change the observed OH half-life down to a small fraction of the half-life in the RH-free system.

Problems arise in studies of slower reactions where it may be difficult to fulfil inequality 23. From computer simulations it was found that it is still possible to calculate k_{21} based on a smaller variation in the observed half-life using

$$1/\tau = 1/\tau_o + k_{21}[RH]_o/\ln 2 \qquad (27)$$

where τ_o is the half-life in the pure system. According to Equation 27 a plot of $1/\tau$ versus corresponding $[RH]_o$ values is linear with a slope equal to $k_{21}/\ln 2$. This also allows a simple determination of k_{21} based on measured half-lives and corresponding $[RH]_o$. This method is still based on the pseudo-first-order approximation.

A very interesting example of behaviour different from the one outlined above was the adding of CF_2Cl_2 as an unreactive substrate, which, however, could still give decreasing OH half-lives with increasing CF_2Cl_2 concentrations. This effect must be assigned to a completely different mechanism which is evident from the complete decay curves which conserves the long second-order tail although half-lives do decrease with increasing CF_2Cl_2 concentrations.

A more complete procedure to distinguish between first and second-order kinetics is to analyse plots of ln(A) versus time, where A is the transient OH absorbance. Rearranging Equation 23:

$$-\frac{d[OH]/dt}{[OH]} = k_{21}[RH] \qquad (28)$$

$$-\frac{d\ \ln[OH]}{dt} = k_{21}[RH] \qquad (29)$$

$$\ln(A) \propto \ln[OH] = -k_{21}[RH]_t \qquad (30)$$

it is seen that such a plot is linear in the pseudo-first-order approximation. Any significant contributions from reactions of OH with itself or other transients will give the plot a more-or-less pronounced curvature. The slope may be $k_{21}[RH]$ plus a small correction term which may be hard to detect due to the experimental noise level. The correction term is eliminated by plotting $d(\ln(A))/dt$ versus $[RH]_o$ for a series of decay curves. The slope of this plot, $(d(d(\ln(A)))/dt)/d([RH])$, is equal to k_{21}.

Using either of the two last methods yields k_{21} values within the experimental uncertainties. The methods outlined above have been tested against noise-free computer-simulated decay curves. This is very instructive as a basis for evaluating the experimental data in the sense of defining what to expect.

5.3. Reactivity of OH with tetraalkyllead compounds

5.3.1. Introduction

This study was the author's first pulse-radiolysis investigation. Being completely inexperienced with the experimental set-up and the data handling the study was ended before achieving what would now be considered satisfactory thoroughness. Lead contamination of the cell and mirrors caused the experimental work to be very tedious and the study to be stopped at an earlier stage than originally intended.

Tetraalkyllead compounds, R_4Pb, predominantly tetramethyl- (Me_4Pb) and tetraethyllead (Et_4Pb), have been added to petrol as anti-knock agents for more than fifty years. The world-wide production of organolead compounds used for anti-knock addition was about 300,000 tons in 1975. Most of the R_4Pb in petrol is decomposed to lead halogenides and oxides during combustion in the automobile engine. However, spillage of leaded petrol, evaporation, and incomplete combustion are sources of atmospheric pollution by organolead compounds. The annual emission of R_4Pb in 1975 in the western world was estimated to be about 7,000 tons (Grandjean and Nielsen 1979). The 24 h mean value of volatile R_4Pb in street air under heavy traffic conditions may be as high

as 200 ng m^{-3} (Jonghe et al. 1981, Laveskog 1971, Nielsen et al. 1981) and it constitutes typically 5-10% of the total amount of particulate lead present (Nielsen 1982). Moreover, there is some circumstantial, but inconclusive evidence, that biomethylation of inorganic lead compounds to Me_4Pb takes place in the environment (Chau and Wong 1982, Jernelöv and Beijer 1982). The chemical properties and the toxic actions of organolead are different from those of inorganic lead compounds; the former is considered more toxic, but it is not yet possible to evaluate the health risks associated with long-term low-level exposure to organolead compounds (Grandjean and Nielsen 1979). A recent investigation of the content of organolead compounds in human brains (Nielsen et al. 1978) indicates that current environmental exposures to these compounds could have reached an unsafe level.

A few years ago the lifetime of TAL in the atmosphere was thought to be very short (National Academy of Sciences 1972, Public Health Service 1970, Robinson 1975, Snyder 1967), but Grandjean and Nielsen (1977) found this to be erroneous. During the present investigation Harrison and Laxen (1978) published an extensive investigation of the decomposition reactions of Me_4Pb and Et_4Pb vapour in the atmosphere and considered that the main sink process is the reaction with hydroxyl radicals. The rate constants for the Me_4Pb-OH and the Et_4Pb-OH reaction were determined relative to toluene and m-xylene using a system designed to simulate photochemical smog conditions in which the OH-radical is the principal reactive species. The use of a smog chamber could introduce errors in the experimentally determined values of the rate constants (see below). As the rate constants for the reactions between OH and Me_4Pb and OH and Et_4Pb are very important for evaluating their atmospheric lifetimes, more independent determinations of rate constants should be carried out preferably with the aid of different techniques. Therefore, in this study the rate constants for the Me_4Pb-OH and Et_4Pb-OH reactions have been determined following the decay of OH-absorption in the presence of Me_4Pb and Et_4Pb vapour. The OH-radicals were produced by pulse radiolysis of a mixture of water vapour and argon.

5.3.2. Experimental

Formation and decay of OH was studied by monitoring the OH-absorption around 3089 Å. A spectral bandpass of 1 Å was necessary in order to obtain a reasonable signal-to-noise ratio. The fractional power, n, in the modified version of the Lambert-Beer law was determined to be 0.73 studying only one of the two methods (dose variation) mentioned earlier. Destilled samples of Me_4Pb and Et_4Pb were used. They were introduced in the cell in µl quantities using a syringe through a rubber membrane.

5.3.3. Results

Upon addition of R_4Pb to the pure argon-water system, the OH-decay could be described in terms of pseudo-first-order kinetics (see Figure 5.4.). Measuring half-lives τ and using only the simple Equation 26, $k(OH + Me_4Pb) = (3.8 \pm 0.8) \cdot 10^9\ M^{-1}s^{-1}$ and $k(OH + Et_4Pb) = (7.0 + 1.0) \cdot 10^9\ M^{-1}s^{-1}$ were derived. The primary products in these reactions must be unstable intermediates and we have considered the following reactions for, e.g. Me_4Pb:

$$\cdot OH + Me_4Pb \rightarrow H_2O + Me_3PbCH_2\cdot \qquad (31)$$

$$\cdot OH + Me_4Pb \rightarrow Me\cdot + Me_3PbOH \qquad (32)$$

$$\cdot OH + Me_4Pb \rightarrow MeOH + Me_3Pb\cdot \qquad (33)$$

The hydrogen abstraction reaction 31 seems likely to occur because it is exothermic and there are a large number of hydrogen atoms on the "surface" of the molecule. Very likely D(Pb-OH) is greater than D(Pb-C) and hence (32) are expected to be exothermic, which for similar reasons will also be the case for reaction 33. A pentavalent intermediate $HOPbR_4$ could perhaps be involved in (32) and (33). Measurement of the activation energies may give a hint as to the nature of the reaction. Attempts should be made to determine the distribution of stable products.

5.3.4. Discussion

For reasons of comparison the rate constants are converted into

ppm^{-1} h^{-1} units. The Me_4Pb-OH rate constant found in this study, $5.6 \cdot 10^5$ ppm^{-1} h^{-1}, is slightly smaller but in very good agreement with the value, $7.8 \cdot 10^5$ ppm^{-1} h^{-1}, found by Harrison and Laxen (1978). However, Et_4Pb was found to be only twice as reactive towards OH, $10.3 \cdot 10^5$ ppm^{-1} h^{-1}, whereas Harrison and Laxen (1978) report a rate constant of $70.2 \cdot 10^5$ ppm^{-1} h^{-1}. As mentioned earlier, their rate constants, in contrast to ours, were determined relative to toluene and m-xylene and under smog-chamber-like conditions. Generally relatively good agreement between absolute OH rate constants obtained from smog chamber studies and those determined in elementary reaction studies using different techniques has been demonstrated (Darnall et al. 1975, Lloyd et al. 1976).

When determining absolute OH rate constants from smog chamber studies attention should be paid to small build-ups of concentrations of, for example, $O(^3P)$, HO_2 and particulary O_3. Reactions between the investigated compound and these reactive species will cause the determined OH rate constant to be too high. Extreme care should be taken when relative rate constants are determined from smog chamber studies. If the compound being investigated and the reference compound have very different reactivities towards one of these minor components: $O(^3P)$, HO_2, or O_3 errors could be introduced in the determined relative rate constants.

The destruction rate and half-life of R_4Pb in reactions with a species X are taken to be given by:

$$\frac{d[R_4Pb]}{dt} = k\,[X][R_4Pb] \qquad (34)$$

$$\tau = \ln 2/(k\,[X]) \qquad (35)$$

where k is the rate constant and [X] the instantaneous concentration of the reactive species X. Percentage breakdown per time unit can be expressed as

$$100(1-\exp(-k\ [X])) \qquad (36)$$

choosing appropriate units for k and [X].

The reaction mixture used by Harrison and Laxen (1978) was very similar to that optimized by Lloyd et al. (1976) in order to produce a high OH-concentration and decay O_3 formation. Lloyd et al. (1976) detected about 0.02 ppm O_3 during their experiments which ran for about 3 h, the same duration as those of Harrison and Laxen (1978). Assuming that their O_3 concentrations were the same as those of Harrison and Laxen (1978), the Et_4Pb-OH decay rates are overestimated by 1-10%. Interference from $O(^3P)$ can be considered to be negligible. Thus, unless HO_2 and/or other species present in the smog chamber are more important and unnoticed factors in the decomposition of Et_4Pb, the cause of the discrepancy between our results and those of Harrison and Laxen (1978) cannot be explained at the present time. Me_4Pb has an analogous tetrahedric structure to that of neo-pentane. The neo-pentane-OH rate constant, $0.9 \cdot 10^5$ ppm^{-1} h^{-1}, (Greiner 1970) is nearly one order of magnitude below that of the Me_4Pb-OH reaction. No conclusions about the mechanism of this reaction can be drawn on the basis of the present data. Harrison and Laxen (1978) explain the greater reactivity of OH towards Me_4Pb than towards neo-pentane by claiming that the lead atom should weaken the C-H bonds in the methyl groups relative to those in neo-pentane and implying that this should ease the assumed H atom abstraction by the OH-radical. This assertion contrasts with the prediction by McKean et al. (1978) that the lead atom strengthens the C-H bonds relative to those in neo-pentane.

The lead-to-carbon bond dissociation energies of 36 kcal mol^{-1} in Me_4Pb and 31 kcal mol^{-1} in Et_4Pb (Shapiro and Frey 1968) are considerably lower than those of C-C bonds and of C-H bonds in $M(CH_3)_4$ M = C, Si, Ge, Sn, and Pb; the latter are about 100 kcal mol^{-1} (McKean et al. 1973). This suggests that the dominant active sites for the OH attack could be the lead-to-carbon bonds.

Chaudhry and Gowenlock (1969) have studied the kinetics of the abstraction of the H-atom from Me_4Pb by methyl radicals at about

140 °C. They show that the H-atom abstraction by methyl radicals is one path way for the decomposition of Me_4Pb. However, they have apparently not considered the possibility of methyl group abstraction to give ethane and trimethylplumbyl radicals. Furthermore, the replacement of methyl groups in Me_4Pb with methyl radicals might have been the dominant reaction without interfering with the measurements of H atom abstraction.

It is not possible to make any relevant comparisons for the Et_4Pb-OH rate constant.

In both the Me_4Pb-OH and the Et_4Pb-OH cases a growing continuous absorption is observed on a millisecond time scale. This is due to an increase in the turbidity in the gas from nucleations of low-volatile lead compounds.

Since both tetraalkyllead and trialkyllead compounds are considered more toxic than dialkyllead and inorganic lead compounds (Grandjean and Nielsen 1979), the important factors are not limited only to the decomposition rates of R_4Pb itself, and further studies are needed to clarify the complete mechanism and the identity of intermediates and final products.

5.3.4.1. Estimate of the lifetime of R_4Pb in the atmosphere

The breakdown rates of R_4Pb in the atmosphere will depend upon the metereological conditions, such as solar intensity and temperature, and the concentrations of other trace components present. Harrison and Laxen (1978) have demonstrated the influence of solar light and presence of ozone and hydroxyl radicals. Considering only the two first factors, sunlight and ozone, the average decomposition rates of Me_4Pb and Et_4Pb in air have been estimated to be about 1.7% h^{-1} and 8% h^{-1}, respectively in summer and 0.4 and 2.6% h^{-1} in winter at 55° N latitude (Nielsen 1982). From Equations 4-6 it can be seen that the two parameters required to calculate the TAL-breakdown via OH attack, are the rate constant and the OH-concentration.

The instantaneous OH-concentration depends upon latitude, altitude, season, solar intensity, time of day, and present concentrations of NO, NO_2, HNO_2, CO and hydrocarbons. Numerous estimates of OH-concentrations have been made from model calculations (Chameides and Tan 1981, Ehhalt 1974, Graedel et al. 1976, Hov et al. 1978, Lin 1977, Lovelock 1977, Volz et al. 1981, Warneck 1974, Weinstock and Niki 1972) varying three orders of magnitude in the range 10^5-10^8 molecules cm^{-3}.

Only few direct OH-concentration measurements are reported in the literature. The peak values were in the range $1 \cdot 10^7$ - $5 \cdot 10^7$ molecules cm^{-3} (corresponding to $4 \cdot 10^{-7}$ - $2 \cdot 10^{-6}$ ppm) in the three investigations (Davis et al. 1979, Perner et al. 1976 and 1981, Wang et al. 1975 and 1981).

Volz et al. (1981) determined the content of ^{14}CO in the atmosphere at rural and remote sites at different latitudes and different times of the year. By means of these results the seasonal and latitudinal variation of the tropospheric concentration of OH-radicals was calculated. These results will be used here. The average concentration of hydroxyl radicals was calculated to be about 1×10^{-7} ppm in summer and much less than 2×10^{-9} ppm in winter at 55° N latitude. For winter a value of 5×10^{-11} ppm will be used. The geometric mean values of the rate constants determined for the Me_4Pb-OH and Et_4Pb-OH reactions are 6.6×10^5 and 27×10^5 ppm^{-1} h^{-1}, respectively. Thus, the depletion-rate for Me_4Pb and Et_4Pb in summer is calculated to be 6 and 20% h^{-1}, respectively, and 0.003 and 0.01% h^{-1}, respectively, in winter for their reaction with HO.

The major reactions recognized will imply that the total decomposition rate of Me_4Pb and Et_4Pb at conditions typical for 24 h period in summer at 55° N latitude will be about 8 and 30% h^{-1}, respectively. The dominant reactions are those with HO. Considering the disagreements in the estimates of the HO-concentrations in the atmosphere, the disagreement in the rate constant for the Et_4Pb-OH reaction, and the possibility that an unrecognized reaction in the atmosphere perhaps is the dominant sink process for Et_4Pb, it is estimated that the half-

life of Et_4Pb at typical conditions in summer will be in the 0.1 - 9 h range with 2 h as the most plausible value. The half-life of Me_4Pb will be in the 1 - 30 h with 9 h range as the most plausible value.

The decomposition rates of Me_4Pb and Et_4Pb at typical conditions in winter are calculated to be 0.4 and 3% h^{-1}, respectively. The principal aspect in the estimate of the lifetimes in winter is the mode of decomposition of R_4Pb in dark in pure air: surface-catalyzed reactions or vapour phase oxidation by oxygen (Nielsen 1982). Some observations suggest the former possibility (Radziuk et al. 1979). The half-life of Me_4Pb at typical conditions in winter will be in the 3 - 15 day range with 7 days as the most plausible value. The half-life of Et_4Pb will be in the 10 - 60 h range with 25 h as the most plausible value.

The stabilities in ambient air of R_4Pb and especially that of Me_4Pb are high enough to cause transportation over large distances, even to the most remote locations.

5.4. Kinetics of OH-reactions with CH_4, C_2H_6, and some Cl- and F-substituted hydrocarbons at 300-400 K

5.4.1. Introduction

Besides being of fundamental interest this work is also related to the current debate on the potential risk of depletion of stratospheric ozone caused by the release of chlorofluorocarbons (CFCs). In Denmark there is a great interest in this problem. Professor Buchardt from the University of Copenhagen has written an excellent review on this subject (Buchardt 1981). The pulse radiolysis group has done a three-year project for the Nordic Counsil of Ministers on tropospheric degradation mechanism for CFCs. This work has been described in two reports (Nielsen, Bjarnov, Pagsberg and Sillesen 1982; Bjarnov, Munk, Nielsen, Pagsberg and Sillesen 1983). All the results from this three-year project has been presented here in Chapter 5.4.3 even though this project was not done by me alone.

Because of the many natural variations in ozone concentration it has been stated "most probable" (Penner 1982) that a significant trend caused by man-made CFC emissions cannot be detected until around 1995. Therefore, all predictions on ozone depletion are at present based on model calculations. The results of these very complex model calculations change as new and better measurements of rate constants are published (Derwent and Eggleton 1981). However, there is remarkable agreement between different models using the most recently updated chemistry, as seen from Table 5.3 (Watson 1982).

Table 5.3. Percentage change in total ozone calculated for continued release of CFC-11 and CFC-12 at 1976 levels.

Model	Steady-state O_3 change
AER	-6.1
LLL	-5.0
AERE-HARWELL	-6.5
NOAA	-4.5
DU PONT 1-D	-7.0
DU PONT 2-D	-6.2
EERM	-7.0
HARVARD	-7.2
IAS 1-D	-4.8
IAS 2-D	-7.0
NASA	-8.7

A future ozone depletion might have serious consequences for life by allowing more UV-radiation to reach the Earth's surface. The most recent report on the subject from National Academy of Sciences (National Research Council, 1982) states: "Current scientific understanding, expressed in both one- and two-di-

mentional models indicates that if production of CF_2Cl_2 and $CFCl_3$ were to continue in the future at the rate prevalent in 1977, the steady-state reduction in total global ozone, in the absence of other perturbations, could be between 5 and 9%. Comparable results from 1979 ranged from 15% to 18%. The differences between current findings and those reported in 1979 are attributed to refinements in values of important reaction rates" (Underlining by the author).

Molina and Rowland (1974) were the first to point out that $CFCl_3$ (CFC-11) and CF_2Cl_2(CFC-12) appear to last long enough in the atmosphere so that their decomposition products could significantly add to the chlorine burden in the stratosphere. On the basis of present production and emission levels, these two compounds are still the CFC's of greatest concern. However, many other CFC's could eventually affect ozone. Large amounts of various CFC's i.e. $CHClF_2$ (CFC-22) and CH_3CCl_3 (methylchloroform) are being produced in increasing quantities for use as solvents, refrigerants, and propellants in aerosol cans. The amount of these substances that eventually reach the stratosphere depends not only on the quantities produced but also on the fraction actually released into the atmosphere and the fraction that survives to reach the stratosphere. Unless there is some rapid process for their removal, gases released into the troposphere will distribute themselves world-wide within 3-4 years. Transport to the stratosphere takes longer (~ 10 years).

There are 4 major mechanisms by which most molecular species are either destroyed in or removed from the atmosphere: reaction with OH, photolysis, rainout, and uptake by the oceans. For most compounds either containing H or unsaturated compounds reactions with OH is by far the most important destruction mechanisms. These compounds react so fast with trospospheric OH that only a small fraction reaches the stratosphere. However, completely halogenated CFC's, like CFC-11 and CFC-12, react very slowly if at all in the trosposphere. These two molecules, like many others, do not photolyse in the troposphere but in the stratosphere as the intensity of short wavelength radiation increases with altitude.

Destruction of stratospheric ozone takes place through various catalytic cycles including free radical species. The most important of these catalytic cycles is:

$$Cl + O_3 \rightarrow ClO + O_2 \quad (37)$$

$$ClO + O \rightarrow Cl + O_2 \quad (38)$$

$$\text{Net: } O + O_3 \rightarrow 2\ O_2 \quad (39)$$

It is seen that the net effect is to destroy one ozone molecule without using up either Cl or ClO. This means the ClO_x can react over and over again and each ClO_x species can remove thousands of ozone molecules before it is removed by some other process. Since it takes only a small ClO_x concentration to do a lot of damage it is very important to be able to assess the amount of CFC's reaching the stratosphere.

To a certain extent the choice of compounds for this investigation was dictated by what was available and easy to handle experimentally. Ethane and methane were chosen as reference compounds because their OH rate constant is well established through a large number of different investigations. The series of CH_3Cl, CH_2Cl_2, and $CHCl_3$ was chosen to study the effect of halogen substitution. CHF_2Cl (CFC-22) and CH_3CCl_3 were chosen because their concentration in the atmosphere is increasing exponentially (Khalil 1981). Of the incompletely halogenated CFC's these two compounds have relatively low OH rate constants and thereby long atmospheric lifetimes. Please note the difference in the definitions of atmospheric species lifetime and half-life, the first being defined as the time taken for the concentration of the specific species to decrease by a factor 1/e (1/2.72) of its initial value if all sources were turned off suddenly. The last compound CF_2Cl_2 (CFC-12) was chosen as totally unreactive towards OH to check our experimental system for unexpected reactions.

Also this series of compounds will represent OH rate constants ranging from the very fast (C_2H_6) to the very slow (CF_2Cl_2). During this study a similar investigation using discharge flow

with resonance fluorescence detection was published (Jeong and Kaufman 1982). This gives an excellent chance for making comparisons.

5.4.2. Experimental

In general, samples of highest commercial purity were used directly. Two commercially available CH_3CCl_3 samples both yield an OH rate constant an order of magnitude greater than generally accepted (Hampson 1980). Gas chromatography analysis after the experiments showed impurities on the percentage level, supposedly olefinic i.e. CH_2CCl_2. This compound reacts two to three orders of magnitude more rapidly with OH so that only a 0.1% admixture can lead to errors up to 100%. CH_3CCl_3 has to be purified by a very extensive procedure (Jeong and Kaufman 1979). This was not done in our investigation and the CH_3CCl_3 results were left out of account. Results for a purified $CHCl_3$ sample were also left out because of remaining impurities.

In all experiments reaction kinetics was studied by monitoring the transient OH-absorption around 3090 Å using an optical path length of 120 cm and a spectral bandpass of 0.8 Å. The Beer law exponent, n, was determined every time the spectrometer setting was changed. Normally n had a value around 0.7.

For most reactions experiments were carried out at 5 different temperatures: 27, 49, 75, 97 and 127 °C. At each temperature the partial pressure of water vapor was kept constant while the partial pressure of the compound, RH, being investigated was varied to promote competition between RH + OH → H_2O + R and the OH decay channels in the pure H_2O-Ar system. Total pressure was kept at 1 atm by backing up with Ar.

Reading partial pressure at elevated temperatures caused a small problem. When a cold gas is admitted to the heated cell a slow rise in partial pressure was observed which must be ascribed to equilibration of gas temperature through wall collisions. Thus, reading of true pressure required an ill-defined delay time on the order of minutes to obtain a stationary pressure. Even a

small leak would give a greater uncertainly in the reading of partial pressure at elevated temperatures. Error limits of ± 0.5 mbar and ± 0.1 mbar were estimated for 127 °C and 27 °C, respectively.

5.4.3. Results and discussions

The order of presentation is chosen to facilitate the understanding.

5.4.3.1. OH + C_2H_6.

A summary of the experimental conditions is given in Table 5.3.

Table 5.3. Summary of experimental conditions in the C_2H_6 experiments.

T in °C	P(H_2O) in mbar	C_2H_6 pressures in mbar	Number of xp.
27	20	0, 3.5, 7.2, 10.4	8
49	50	0, 1.1, 2.1, 5.0, 10.0	18
97	100	0, 2.3, 5.3, 11.0	12
127	200	0, 2.7, 5.0, 9.6	11

From the two curves in Figure 5.3 it is clearly seen that the OH decay in the presence of 2.7 mbar C_2H_6 has changed into pseudo-first-order kinetics, which is further clarified by the linear logarithmic plot shown in the same figure. As discussed in Chapter 5.2, the following two expressions are used to calculate the rate constant:

$$1/\tau = 1/\tau_o + k[C_2H_6]/\ln 2 \qquad (27)$$

and

$$k = (d(d\ln(A))/dt)/d([C_2H_6]) \qquad (40)$$

In Figure 5.5 the experimental curves are shown for the pure system and for 2.7, 5.0, and 9.6 mbar C_2H_6 added. When C_2H_6 is added these experimental curves are fitted with an exponential curve: $A/A_o = \exp(-k \times t)$. For 5.0 and 9.6 mbar C_2H_6 this fitted curve actually crosses the experimental curve having a slightly higher tail-end. The reason for this is that with the short half-lives 9.4 and 5.8 μs the OH formation cannot be considered instantaneous. Therefore, both source and sink terms contribute to the experimental curve shape around the absorption maximum. However, the tail-end is free of interference from OH formation. For a true first-order reaction $t_{1/4} = 2 \times t_{1/2}$, where $t_{1/4}$ is the time when absorption has decreased to one fourth of A_{max}.

In general, we found $t_{1/4} < 2 \times t_{1/2}$ in the presence of C_2H_6. To avoid systematic errors due to OH-formation instead of the first half-life, $t_{1/2}$, $\tau = t_{1/4} - t_{1/2}$ was used in Equation 27. Using Equation 40 seems more reliable since it takes into account the entire experimental curve and allows a clear distinction to be made between first- and second-order kinetics. The experimental results obtained at 127 °C are summarized in Table 5.4.

Table 5.4. Experimental results for C_2H_6 at 127 °C.

$[C_2H_6]$ in M	$t_{1/2}$ in μs	$t_{1/4}$ in μs	$1/\tau$ in s^{-1}	$d(\ln(A))/dt$ in s^{-1}
0	81.5	216	1.5×10^4	
8.24×10^{-5}	15.8	29.5	7.3×10^4	4.37×10^4
1.53×10^{-4}	9.1	16.8	1.3×10^5	8.37×10^4
2.93×10^{-4}	6.1	10.8	2.4×10^5	1.60×10^5

In Figures 5.6 and 5.7 the plots corresponding to Equations 27 and 40 are shown, respectively. From the slopes the identical value of (5.5 × 0.2) × 10^8 $M^{-1}s^{-1}$ was obtained for the OH + C_2H_6 rate constant at 127 °C. The procedures were used in the analysis of experimental results obtained at lower temperatures. In Table 5.5 the results are summarized.

Table 5.5. Rate constants for C_2H_6 at 4 temperatures in $M^{-1}s^{-1}$.

T in °C	k from Equation 20	k from Equation 40
27	1.69 × 10^8	1.95 × 10^8
48	2.46 × 10^8	3.15 × 10^8
100	3.70 × 10^8	3.94 × 10^8
127	5.30 × 10^8	5.40 × 10^8

The rate constants can be expressed in Arrhenius form:

$$k = A \exp(- E_a/RT) \quad (41)$$

and taking the natural logarithm

$$\ln(k) = \ln(A) - 1/T \, (E_a/R) \quad (42)$$

where the Arrhenius parameters A and E_a are normally referred to as the pre-exponential factor and the activation energy, respectively. From Equation 42 it is seen that A and E_a can be found from a linear regression of a ln(k) versus 1/T plot. From the Arrhenius plot, shown in Figure 5.8, A = 9.7 × 10^9 $M^{-1}s^{-1}$ and E_a = 2.33 kcal/mole are obtained with 2.2% and 15% standard deviation (within a 95% confidence limit), respectively.

As Table 5.6 shows, only four other investigations on the OH + C_2H_6 reaction were found in the literature (Greiner 1970; Overend et al. 1975; Gordon and Mulac 1975; Howard and Evenson 1976).

Table 5.6. Comparison of rate parameters for OH + C_2H_6.

Reference	T in K	k in 10^8 $M^{-1}s^{-1}$	A in $M^{-1}s^{-1}$	E_a in kcal/mol
Greiner 1970	300	1.83	1.1×10^{10}	2.45
Overend et al. 1975	295	1.59		
Gordon and Mulac 1975	381	4.00	3.5×10^9	1.64
Howard and Evenson 1976	296	1.75		
This work	300	1.95	9.7×10^9	2.33

Gordon and Mulac (1975) gave no A and E_a values since they were measured only at two different temperatures which would give the A- and E_a-value inserted in Table 5.6 for the sake of completeness.

In view of the differences in techniques and experimental conditions the agreement between our result and those of Greiner (1970) and Howard and Evenson (1976) is quite good.

5.4.3.2. OH + CF_2Cl_2. Because CF_2Cl_2 is completely halogenated it is expected and has been found (Atkinson et al. 1975; Howard and Evenson 1976; Cox et al. 1976; Chang and Kaufman 1977) to be inert toward attack by OH. Abstraction of F or Cl is endothermic due to the larger strength of C-F (108 ± 3 kcal/mole in CH_3F) and C-Cl bonds (73 ± 2 kcal/mole in $CFCl_3$) relative to the strengths of F-OH and Cl-OH (60 ± 3 kcal/mole), respectively. It therefore came as a great surprise that the observed OH half-life decreased with increasing CF_2Cl_2 concentration as exemplified in Figure 5.9. If this were due to a hitherto undiscovered reaction channel this would change the status of CF_2Cl_2 as one of the most critical compounds in assesment of ozone depletion. Four hypothetical reactions can be considered:

$$CF_2Cl_2 + OH \rightarrow CF_2Cl + ClOH \quad (43)$$

$$CF_2Cl_2 + OH \rightarrow CFCl_2 + FOH \quad (44)$$

$$CF_2Cl_2 + OH \rightarrow CF_2ClOH + Cl \quad (45)$$

$$CF_2Cl_2 + OH \rightarrow OCFCl_2 + HF \quad (46)$$

Reactions 43 and 44 can be ruled out for energetic reasons as mentioned above. This is not the case for reactions 45 and 46. However, an OH displacement reaction and a four-center elimination reaction are very unlikely although they be exothermic. For any of these four reactions a sufficient CF_2Cl_2 concentration should cause the OH decay to be of a pseudo-first-order type. However, as it is seen in Figure 5.9 the second-order tail remains even with 50 mbar CF_2Cl_2. This leads to the hypothesis that CF_2Cl_2 acts as a very efficient third body, M, in one of the OH combination reactions:

$$OH + OH + M \rightarrow H_2O_2 + M \quad (18)$$

$$OH + H + M \rightarrow H_2O + M \quad (19)$$

Blak and Porter (1962) have investigated relative third-body efficiencies for reactions 18 and 19 using helium, argon, xenon, nitrogen, oxygen, carbon dioxide, and water as third bodies. CF_2Cl_2 was not included in that investigation. A combination reaction like 18 can be described by a pseudo-second-order rate law in which the second-order rate constant depends on [M]. The low-pressure third-order limit is characterised by a rate constant being proportional to [M]. The high-pressure second-order limit is characterised by k_∞, which is independent of [M]. Assuming that the combination involves collisional stabilisation of an excited H_2O_2 molecule, $H_2O_2^*$,

$$OH + OH \rightarrow H_2O_2^* \quad (47)$$

which can either go through the reverse dissociation

$$H_2O_2^* \rightarrow OH + OH \qquad (48)$$

or be collisionally stabilised

$$H_2O_2^* + M \rightarrow H_2O_2 + M \qquad (49)$$

In the steady-state approximation for $H_2O_2^*$:

$$d[OH]/dt = - 2\, k_{47}[OH]^2\, k_{49}[M]/(k_{48} + k_{49}[M])$$

giving the following expression for the reciprocal half-life:

$$1/\tau = 2\, k_{47}[OH]_o\, k_{49}[M]/(k_{48} - k_{49}[M]) \qquad (51)$$

$$1/\tau = 2\, k_{47}[OH]_o\, (k_{49}[M]/k_{48})/(1 + k_{49}[M]/k_{48}) \qquad (52)$$

which approaches a linear function in the low-pressure limit where $k_{49}[M] \ll k_{48}$ and a constant in the high-pressure limit where $k_{49}[M] \gg k_{48}$. Expression 51 was applied to fit a set of experimental OH half-lives measured at 75°C and with $[CF_2Cl_2]$ up to 1.7×10^{-3} M. The best fit was obtained with $2\, k_{47}[OH]_o = 7.75 \times 10^4$ as the constant for the high-pressure second-order limit and $k_{49}[M]/k_{48} = 0.15 + 380\, [CF_2Cl_2]$ to account for the concentration dependence. The constant term of 0.15 is assigned to the contribution from argon and water as third bodies present in constant co.. ntrations. Figure 5.10 shows the excellent agreement between the experimental and theoretical results obtained using Equation 52. In the same figure results obtained by computer simulations of the complete set of reactions involved are also shown. These computer simulations reproduce not only the experimental half-lives but fit the whole experimented decay curve, as seen in Figure 5.11. This third-body model seems to account for the observed kinetic features and this has some implications. It means that the OH-combination has not reached the high-pressure second-order limit in a system of 45 mbar water backed up with Ar to 1 atm at 75 °C. Gordon and Mulac (1975) reported the OH-recombination rate to be independent of water vapour pressure in the range 67-543 Torr in a similar pulse-radiolysis study of pure water vapour. Using the relative third-

body efficiencies for Ar and H_2O of Blak and Porter (1962) our gas mixture has a third-body efficiency equivalent to 75 torr of pure water. According to Gordon and Mulac (1975) this would be in the second-order region in contrast to our observations. However, if CF_2Cl_2 and H_2O act specifically as a third body in each of the two OH-combination reactions 18 and 19:

$$OH + OH + M = H_2O_2 + M \qquad (18)$$

$$OH + H + M = H_2O + M \qquad (19)$$

our observation can then still be understood in terms of a third-body model. The rate of vibration-vibration transfer between an excited species, i.e. $H_2O_2^*$ and a third body, M, will increase the closer one vibrational frequency in $H_2O_2^*$ will be to a vibrational frequency in M (Callear and Lambert 1969). H_2O will then of course be a very efficient third body in reaction 19. A detail of the infrared spectrum of CF_2Cl_2 was recorded and is shown in Figure 5.12. It is seen that CF_2Cl_2 has a vibrational frequency just below 900 cm^{-1} which is in near resonance with the O-O stretching frequency in H_2O_2, ν = 880 cm^{-1} (Redington et al. 1962). In Figure 5.12 it appears that the vibration below 900 cm^{-1} interacts by Fermi resonance with another CF_2Cl_2 vibration just above 900 cm^{-1}. This may further enhance vibration-vibration transfer from $H_2O_2^*$ to CF_2Cl_2. Thus, it seems possible that H_2O and CF_2Cl_2 each acts exclusively as a third body in the specific reactions 19 and 18, respectively. Two further tests could validate this third-body model. One, studies of the yield of H_2O_2 would serve as an unambiguous test of the model. Two, using some of the many fully halogenated hydrocarbons with and without vibrational frequencies in the 880 cm^{-1} region as a third body would also be a significant test of the model. The first method will be experimentally very difficult but the second will be attempted as soon as the experimental set-up becomes available again.

An alternative mechanism may be considered. The alternative mechanism involves dissociation of CF_2Cl_2 in competition with H_2O dissociation:

$$Ar^* + H_2O \rightarrow Ar + H + OH \quad (53)$$

$$Ar^* + CF_2Cl_2 \rightarrow Ar + CF_2Cl + Cl \quad (54)$$

Asuming $k_{53} \sim k_{54}$ a significant yield from reaction 54 may be expected when the CF_2Cl_2 concentration approaches and exceeds that of water. Both CF_2Cl and Cl may react with OH causing a shorter OH half-life and complex second-order kinetics as observed experimentally. A model for this mechanism was set-up for computer simulations. The model was tuned to fit experimental results for pure H_2O and with 50 mbar CF_2Cl_2 added and then the variation of $1/\tau$ with $[CF_2Cl_2]$ was studied. In Figure 5.13, $1/\tau$ versus $[CF_2Cl_2]$ is plotted for the two models and the experiments. The different curvature of the plot for the alternative mechanism shows that the third-body model is the best interpretation of the experimental results.

This investigation showed that CF_2Cl_2 is completely inert toward attack by OH even at atmospheric pressure. From computer simulations with the third-body model it is estimated that k(OH + CF_2Cl_2) is less than 10^6 $M^{-1}s^{-1}$. A greater value would have had an observable effect on the tail-end of the decay curve. This result is in agreement with previous experimental results obtained with different techniques (Atkinson et al. 1975; Howard and Evenson 1975; Cox et al. 1976; Chang and Kaufman 1977). This means that CF_2Cl_2 and other completely halogenated hydrocarbons must still be considered a potential threat to the stability of stratospheric ozone.

This investigation also had another important implication. When there is the possibility of combination reactions with a third body in a reaction system, one has to be very careful when analysing of the experimental results. In the OH case the IR-spectrum of added substances should be checked for vibrational frequencies around 880 cm^{-1}.

5.4.3.3. OH + CH_4. CH_4 is by far the hydrocarbon released to the atmosphere in the largest amounts. This is due to the biogenic

sources. The biogenic production is about 40 times greater than the anthropogenic production and total annual global release of CH_4 lies between 545×10^{12} and 1035×10^{12} g, not including CH_4 from natural gas wells (Ehhalt 1974). Since OH + CH_4 is a rather slow reaction and very well investigated (Horne and Norrish 1967; Wilson and Westenberg 1967; Greiner 1970; Margiton et al. 1974; Davis et al. 1974; Overend et al. 1975; Gordon and Mulac 1975; Howard and Evenson 1976; Zellner and Steinert 1976; Tully and Ravishankara 1980; Jeong and Kaufman 1982) it serves as reference and test for slow reactions in our experimental system.

For each temperature the rate constant was derived using Equation 40 with $[CH_4]$ instead of $[C_2H_6]$ as the plots of ln(A) versus time were linear in the presence of CH_4. The rate constants obtained are given in Table 5.7.

Table 5.7. OH + CH_4 rate constants at different temperatures.

T in °C	k in 10^7 $M^{-1}s^{-1}$
27	1.9 ± 0.2
48	2.0 ± 0.2
75	2.4 ± 0.2
100	3.0 ± 0.2
127	3.5 ± 0.5

The Arhenius plot is shown in Figure 5.14 giving an activation energy, E_a = 1.52 kcal/mole, which is in serious disagreement with all the previously cited studies with E_a ranging from 5 to 3.4 kcal/mole. There could be two reasons for this disagreement: systematic errors or reactive impurities in the applied CH_4. As stated in Chapter 5.4.2 an impurity that reacts 2 to 3 orders of magnitude faster than the compound being investi-

gated has to be present in only 0.1% admixture to cause a 100% error. A careful gas chromatographic analysis of the applied CH_4 showed a 0.13% C_2H_6 content and a 0.18% C_2H_4 content plus about 0.08% of H_2, N_2, O_2, and Ar. The ethane will cause a 10% increase in the observed OH + CH_4 rate constants. C_2H_4, however, reacts much faster with OH than does C_2H_6. Clearly $k(OH + C_2H_4) = 4.8 \times 10^9$ $M^{-1}s^{-1}$ (Baulch et al. 1982) and a 0.18% C_2H_4 content account for an apparent OH + CH_4 rate constant which is much higher than the well-establisted value of 4.8×10^6 $M^{-1}s^{-1}$ at 25°C (Baulch et al. 1982). The E_a = 0.8 kcal/mol for OH + C_2H_4 (Baulch et al. 1982) also explains the value of 1.52 kcal/mol found in this study.

5.4.3.4. OH + CH_3Cl. Of the 360 kt methyl chloride, CH_3Cl, produced industrially in 1980 approximately 20 kT were emitted to the atmosphere (Edwards et al. 1982). Approximately half of the CH_3Cl produced is used for tetramethyllead production. However, more than 200 times as much, 5 MT, is released annually from other sources: combustion and the oceans (Edwards et al. 1982). The only significant pathway by which CH_3Cl is removed from the atmosphere is by OH attack.

Five earlier measurements of the CH_3Cl + OH rate constant have been found in the literature (Howard and Evenson 1976; Perry et al. 1976; Davis et al. 1976; Paraskevopoulos et al. 1981; Jeong and Kaufman 1982). In Table 5.8 rate parameters are compared with published results, and the Arhenius plot is shown in Figure 5.15.

Table 5.8. OH + CH_3Cl rate parameters.

Reference	T in K	k in 10^7 $M^{-1}s^{-1}$	A in $10^9 M^{-1}s^{-1}$	E_a in kcal/mol
Howard and Evenson 1976	296	2.2		
Perry et al. 1976	298	2.7	2.5	2.70 ± 0.3
Davis et al. 1976	298	2.6	1.1	2.18 ± 0.1
Paraskevopoulos et al. 1981	297	2.5		
Jeong and Kaufman 1982	293	2.4	2.1	2.61 ± 0.1
This work	300	4.3	3.2	2.51 ± 0.1

Because CH_3Cl reacts fairly slowly with OH it was necessary to apply rather high partial pressures of CH_3Cl in order to get a significant change in the OH decay. Under these circumstances there is a risk of direct fragmentation of CH_3Cl following irradiation. If a significant number of such fragments are formed together with OH it becomes very difficult to derive the OH rate constant. This is a problem especially at room temperature where the saturation pressure of water is rather low. Here one may have to consider the following additional reactions:

$$OH + CH_2Cl \rightarrow \text{products} \qquad (55)$$

$$OH + CH_3 + M \rightarrow CH_3OH + M \qquad (56)$$

$$OH + Cl + M \rightarrow HOCl + M \qquad (57)$$

In the experiments at room temperature a significant reduction in the initial OH yield, OH_{max}, was observed. This is taken as evidence for direct fragmentation of CH_3Cl. In the analysis of kinetic results the ln(OH) versus time plots were most often used. Deviations from linearity of these plots are observed when radical-radical reactions like 55-57 influences the OH decay which should be controlled by

$$OH + CH_3Cl \rightarrow H_2O + CH_2Cl \qquad (58)$$

Even when there is no direct fragmentation of CH_3Cl, CH_2Cl is produced in reaction 58 and this makes reaction 55 important. However, for the initial slope at t = 0 $[CH_2Cl] = 0$ and again a simple expression is obtained

$$d(\ln(A)) = (2\,k_{11} + k_{12})\,[OH]_o + k_{58}\,[CH_3Cl]_o \qquad (59)$$

which contains no contribution from consecutive reactions. This procedure was used for CH_3Cl.

The activation energy is in good agreement with the result of Jeong and Kaufman (1982). At higher temperatures our rate constant values are in fair agreement with Jeong and Kaufman. However, at 27 °C our rate constant seems to be overestimated by a factor 1.7 as seen from Table 5.8. As already explained, direct fragmentation and/or the third-body effect from the CF_2Cl_2 case may be the reason for this overestimate.

5.4.3.5. OH + CH_2Cl_2. In 1980 570 kt of methylene chloride, CH_2Cl_2, was produced (Edwards et al. 1982). All methylene chloride produced is eventually released to the atmosphere. World production is expected to increase rapidly. Twenty per cent of the production is used in aerosols. This application may increase and develop a larger market percentage. No natural source of methylene chloride has been identified. The rate-controlling step in the trospospheric oxidation of methylene chloride is

the reaction with OH. Since this reaction is fast, CH_2Cl_2 is not a significant contributer to the stratospheric chlorine budget.

The room temperature measurements have been left out because the measurements of partial pressure had been made too quickly after injection. The Arhenius plot is shown in Figure 5.16 and in Table 5.9 the rate parameters are compared with published results.

Table 5.9. OH + CH_2Cl_2 rate parameters.

Reference	T in K	k in $10^8 M^{-1}s^{-1}$	A in $M^{-1}s^{-1}$	E_a in kcal/mol
Perry et al. 1976	299	0.87		
Davis et al. 1976	298	0.70	2.6×10^9	2.17
Howard and Evenson 1976	296	0.93		
Jeong and Kaufman 1982	292	0.92	3.5×10^9	2.08
This work		0.88	4.1×10^9	2.22

Our results seem to be in good agreement with all previously published data. Only the room temperature value of Davis et al. (1976) seems to be out of range.

5.4.3.6. OH + $CHFCl_2$. $CHFCl_2$, CFC-22, is an important refrigerant and has been recommended as a substitute for CFC-11, CFC-12, and CH_3CCl_3 since it contains only one chlorine atom and reacts with tropospheric OH. However, it reacts only slowly with OH, and $CHFCl_2$ concentrations were found to increase at an exponential rate of 11.7% per year (Khalil and Rasmussen 1981).

The Arhenius plot is shown in Figure 5.17 and our results are compared with 8 earlier investigations of the OH + $CHFCl_2$ reaction in Table 5.10.

Table 5.10. OH + $CHFCl_2$ rate parameters.

Reference	T in K	k in $10^8 M^{-1}s^{-1}$	A in $M^{-1}s^{-1}$	E_a in kcal/mole
Atkinson et al. 1975	297	2.9	7.3×10^8	3.25
Howard and Evenson 1976	296	2.0		
Watson et al. 1977	298	2.9	5.6×10^8	3.13
Chang and Kaufman 1977	296	2.6	7.2×10^8	3.29
Handwerk and Zellner 1979	293	2.8	1.3×10^9	3.54
Clyne and Holt 1979	293	2.0	5.7×10^9	4.6
Paraskevopoulos 1981	297	2.8		
Jeong and Kaufman 1982	298	2.9	7.7×10^8	3.32
This work	300	3.1	1.1×10^9	3.55

The result of Clyne and Holt looks suspect compared with the others, which are all in fair agreement with each other.

5.4.4. Theoretical prediction of OH rate constants

From many points of view it would be attractive to be able to predict accurate values of OH rate constants theoretically. Our material here is too sparse to go through a theoretical discussion of the variations in A and E with halogen substitution as given in the paper by Jeong and Kaufman (1982). However, a short theoretical discussion of the possibilities of prediction of OH-haloalkane rate constants is given below.

It is convenient to distinquish between fully and partially halogenated compounds. For the fully halogenated compound halogen abstraction is endothermic by up to 25 kcal/mole and can therefore be ruled out. The substitution reaction is exothermic but has no simple reaction path and is not taken into account.

For the partially halogenated compounds the reaction proceeds via hydrogen abstraction by OH. Arrhenius's pre-exponential factors can be computed from collision theory. For computation of activation energies only semiemperical methods have been proposed. For a homologous series of reactions:

$$AH + {}^{\bullet}OH \rightarrow {}^{\bullet}A + H_2O \qquad (60)$$

where A represents any group, a simple assumption is that the activation energy is a linear function of the bond dissociation energy, D_{A-H}. As seen in Fig. 5.18 there is a clear trend, but also considerable scatter in the data.

Several investigators (Howard and Evenson 1976; Nip et al. 1979) have correlated rate constants with D_{C-H} for several haloalkanes also taking into account the number of H atoms, n, in the molecule (see Fig. 5.19).

McKean (1978) has correlated C-H stretching frequencies ν_{C-H} with D_{C-H} for a large number of molecules (see Fig. 5.20). As ν_{C-H} values are more easily available and more reliable than bond dissociation energies, rate constants can also be correlated with ν_{C-H} (Nip et al. 1979) (see Fig. 5.21).

In Fig. 5.21 there is a nice linear correlation between log(k) and ν_{C-H} except for CHF_3. From Fig. 5.20 it is seen that some haloalkanes do not follow the linear correlation between D_{C-H} and ν_{C-H}, especially CH_3Cl, CH_2Cl_2, and $CHCl_3$. Using ν_{C-H} to predict rate constants can therefore lead to erroneous predictions. Even the model derived by Heicklen (1981) from correlating a large number of OH H-abstraction rate constants with C-H bond energies encounters difficulties in predicting rate constants for haloalkanes (see Fig. 5.22).

At present, it therefore seems impossible to predict reliable rate constants theoretically for the reaction of OH with partially halogenated alkanes.

5.4.5. Conclusions

In this OH + CFC project, a number of important rate parameters have been derived. Some problems in the use of the pulse-radiolysis technique have been presented. One of the problems is the direct fragmentation of a CFC. However, in a preliminary experiment we have obtained the first absorption spectrum of the CCl_3 radical in the 200-220 nm region. We should be able to obtain spectra of other halogenated alkyl radicals, which will help us to assess direct fragmentation and consecutive reactions.

The OH + CFC reaction is merely the first step in the chain sequence for the atmospheric oxidation of a CFC. No paper in the literature even attempts to give the complete chain sequence for the atmospheric oxidation of a CFC. The statement found in the literature that the ultimate atmospheric oxidation products of CFC's are CO_2, HCl, and H_2O are based on three considerations:

1) an analogy with the CH_4 oxidation system.
2) an examination of the physical and chemical properties of the compounds involved.
3) Laboratory simulations of CFC oxidation.

In the literature two possible routes to start the oxidation of perhaloalkyl radicals are given, normally referred to as route a and b, respectively. In route a the first step is the direct reaction:

$$CX_3 + O_2 \rightarrow CX_2O + XO \qquad (61)$$

which was favoured earlier by Heicklen (1970). In route b the first steps are:

$$CX_3 + O_2 + M \rightarrow CX_3O_2 + M \qquad (62)$$

$$2\ CX_3O_2 \rightarrow 2\ CX_3O + O_2 \qquad (63)$$

$$CX_3O \rightarrow CX_2O + X \qquad (64)$$

This route was later preferred by Heicklen and coworkers (Matias et al. 1974). One recent publication (Suong and Carr 1982) also favours route b, but further studies of the systems are clearly needed. Being able to record spectra of perhaloalkyl radicals we are in a very good position to investigate these systems further, which is our intention.

We have also planned to place our experiments on a more quantitative basis, in the sense that we will determine our initial OH concentration. This can be done in a $CHCl_3$-Ar-H_2O system. The OH will abstract H from $CHCl_3$ to form CCl_3, which will recombine:

$$CCl_3 + CCl_3 \rightarrow C_2Cl_6 \qquad (65)$$

We can follow CCl_3 decay and as k_{65} is well known the CCl_3 concentration equal to the OH concentration can be calculated. It seems that for OH and CFC radicals there are several years of interesting pulse-radiolysis experiments waiting to be done.

6. CHEMICAL KINETICS IN HYDROGEN SULFIDE SYSTEMS

6.1. Introduction

The atmospheric chemistry of sulfur has received considerable attention in recent years. Emissions of sulphur-containing compounds can cause acidification of precipitation with consequent influence on even remote ecosystems. Combustion of fossil fuel introduces about 65×10^{12} g sulfur (Granat et al. 1976) into the atmosphere annually and represents the major source of tropospheric sulfur for the industrialized world. Other sulfur

sources are volcanic eruptions and H_2S and dimethylsulfide produced in the sulfate metabolism under anaerobic conditions. Understanding of the sulfur cycle, illustrated in Figs. 6.1 and 6.2, is still quite unsatisfactory (Sze and Ko 1980). Although a radical like HS is an important precursor for H_2S and SO_2 very little information exists for reactions of this radical. Both McElroy et al. (1980) and Sze and Ko (1980) state that: "More laboratory measurements of HS reactions are required".

The atmospheric source for HS is the reaction of OH with COS and CS_2, present in relatively constant background concentrations in the troposphere:

$$OH + COS \rightarrow HS + CO_2 \quad (66)$$

$$OH + CS_2 \rightarrow COS + HS \quad (67)$$

Production of H_2S takes place through

$$HS + HO_2 \rightarrow H_2S + O_2 \quad (68)$$

$$HS + CH_2O \rightarrow H_2S + HCO \quad (69)$$

$$HS + H_2O_2 \rightarrow H_2S + HO_2 \quad (70)$$

$$HS + CH_3OOH \rightarrow H_2S + CH_3O_2 \quad (71)$$

$$HS + HS \rightarrow \text{products} \quad (72)(33)$$

and removal of H_2S and regeneration of HS is accomplished by

$$OH + H_2S \rightarrow H_2O + HS \quad (73)$$

The last reaction is sufficiently rapid to ensure a lifetime for H_2S on the order of one day (Perry et al. 1976b). No measurements of HS concentrations in the atmosphere have been found in the literature.

Only four gas phase pulse-radiolysis studies on H_2S systems were found in the literature (Willis et al. 1971a; Willis et al. 1971b; Boyd et al. 1973b; Perner and Franken 1969). The three first studies deal with the hydrogen yield, absolute dosimetry, and the effect of SF_6 and sulfur as electron scavengers in the primary ionic processes. Only one gas phase pulse-radiolysis study (Perner and Franken 1969) has dealt with the kinetics of the non-ionic secondary reactions involving radicals, atoms, and molecules. They monitored the transient species HS, HS_2, and S_2 by kinetic absorption spectroscopy and found values of rate constants for reaction 72, $k_{72} = 3.2 \times 10^{10}\ M^{-1}s^{-1}$, and

$$H + H_2S \rightarrow H_2 + HS \qquad (74)(12)$$

$k_{74} = 7.7 \times 10^{8} M^{-1}s^{-1}$. Determining k_{72} requires knowledge of the initial HS concentration just after the pulse. As the extinction coefficient for the observed HS-absorption band is unknown, Perner and Franken's solution of the problem depends on the $G(H_2)$ value. Their $G(H_2)$ value was obtained assuming $G(N_2) = 10.0$ in N_2O. However, at Febetron dose rates $G(N_2)$ and thereby $G(H_2)$ should have been increased (Willis et al. 1971a). With these dubious assumptions their results are probably not very reliable. Perner and Franken (1969) also investigated H_2S-Ar and H_2S-Xe mixtures. As they did not present a complete reaction scheme the investigation presented here is more exhaustive and hopefully more elucidating including experiments on pure H_2S, H_2S-Ar, and H_2S-H_2 mixtures.

As in the H_2O case, the quadratic array shown in Figure 6.3 was set up. In this no imaginable reaction was left out. In Table 6.1 all these reactions are listed. The numbering from this table is used throughout Chapter 6.

6.2. Experimental

Experiments have been carried out only at room temperature. The formation and decay of HS, HS_2, and S_2 were monitored at:

Table 6.1. Considered reactions with standard enthalpy in kcal/mol and the 4 room temperature rate constants given by Hampson (1980).

(11)	$H + H + M$	→	$H_2 + M$	-104.2	1.25×10^8
(12)	$H + H_2S$	→	$H_2 + HS$	- 12.3	4.3×10^8
(13a)	$H + HS + M$	→	$H_2S + M$	- 92.0	
(13b)	$H + HS$	→	$H_2 + S$	- 20.8	1.5×10^{10}
(14a)	$H + H_2S_2$	→	$H_2 + HS_2$	- 33.8	
(14b)		→	$HS + H_2S$	- 25.8	
(15)	$H + S + M$	→	$HS + M$	- 83.4	
(16a)	$H + S_2 + M$	→	$HS_2 + M$	- 60.7	
(16b)	$H + S_2$	→	$HS + S$	+ 18.5	
(17a)	$H + HS_2 + M$	→	$H_2S_2 + M$	- 70.4	
(17b)	$H + HS_2$	→	$H_2 + S_2$	- 43.5	
(17c)		→	$HS + HS$	- 4.2	
(23a)	$H_2S + HS$	→	$H_2 + HS_2$	- 8.0	
(23b)		→	$H_2 + H + S_2$	+ 52.7	
(25a)	$H_2S + S + M$	→	$H_2S_2 + M$	- 57.6	
(25b)	$H_2S + S$	→	$H_2 + S_2$	- 30.7	
(25c)		→	$HS + HS$	+ 8.6	
(25d)		→	$H + HS_2$	+ 12.8	
(33a)	$HS + HS + M$	→	$H_2S_2 + M$	- 66.2	
(33b)	$HS + HS$	→	$H_2S + S$	- 8.6	7.8×10^9
(33c)		→	$H_2 + S_2$	- 39.3	
(33d)		→	$H + HS_2$	+ 4.2	
(34)	$HS + H_2S_2$	→	$H_2S + HS_2$	- 21.6	
(35a)	$HS + S + M$	→	$HS_2 + M$	- 79.2	
(35b)	$HS + S$	→	$H + S_2$	- 18.5	
(36a)	$HS + S_2 + M$	→	$HS_3 + M$	- 40.4	
(36b)	$HS + S_2$	→	$HS_2 + S$	+ 22.7	
(37a)	$HS + HS_2$	→	$H_2S + S_2$	- 31.3	
(37b)	$HS + HS_2$	→	$H_2S_2 + S$	+ 13.0	
(38)	$HS + H_2$	→	$H_2S + H$	+ 12.2	
(45a)	$H_2S_2 + S + M$	→	$H_2S_3 + M$	- 62.7	
(45b)	$H_2S_2 + S$	→	$HS + HS_2$	- 13.0	

Continued

(45c)		→	$S_2 + H_2S$	- 44.3
(55)	$S + S + M$	→	$S_2 + M$	-101.9
(56)	$S + S_2 + M$	→	$c\text{-}S_3 + M$	- 64.5
(57)	$S + HS_2 + M$	→	$HS_3 + M$	- 63.1
(58)	$S + H_2 + M$	→	$H_2S + M$	- 71.2
(66)	$S_2 + S_2 + M$	→	$c\text{-}S_4 + M$	- 30.4
(67)	$S_2 + HS_2 + M$	→	$HS_4 + M$	
(77a)	$HS_2 + HS_2 + M$	→	$H_2S_4 + M$	- 33.6
(77b)	$HS_2 + HS_2 + M$	→	$H_2S_2 + S_2 + M$	- 9.7
(77c)		→	$H_2 + S_2 + S_2$	+ 17.2
(78)	$HS_2 + H_2$	→	$H_2S_2 + H$	+ 33.8

HS; 3242Å, (0,0) $A^2\Sigma^+ - X^2\Pi_{3/2}$ transition

S_2; 2829Å, (9,0) $B^3\Sigma_n^- - X^3\Sigma_g^-$ transition

HS_2; 3408 and 3483Å, in the $\tilde{A}^2A' - X^2A''$ band.

For HS the monitored transition is part of the detail of the HS emission spectrum showed in Figure 6.4 from a recent spectroscopic investigation (Tiee 1981). Since the spectral band pass was smaller than the width of the spectral feature monitored, the exponent, n, in the modified Lambert-Beer law was always equal to 1. Gases of highest commercial purity were used directly.

6.3. Results and discussions

6.3.1. The H_2S-H_2 system.

The reason for starting with this system is that it gives us a chance to determine the extinction coefficent at 3242Å, ε, for HS produced by $H + H_2S \rightarrow H_2 + HS$, because a method for determining H atom concentrations has already been presented in this report.

In H_2S-H_2 mixtures with a partial pressure of H_2S less than 25 torr and backed up with H_2 to 1 atm, more than 75% of the energy deposited during irradiation will be absorbed by H_2, and the primary result is

$$H_2 \rightarrow H + H \qquad (75)$$

The H atoms produced will react first with H_2S

$$H + H_2S \rightarrow H_2 + HS \qquad (12)$$

and further removing HS

$$H + HS \rightarrow H_2 + S \qquad (13b)$$

HS will also be removed by the combination reaction

$$HS + HS \rightarrow H_2S + S \qquad (33b)$$

Using the procedure outlined in Chapter 4 the initial H atom concentration after the pulse with the new field emission tube in the accelerator was determined to be $(4.74 \pm 0.5) \times 10^{-7}$ M. The problem here compared with the H_2-O_2 mixture in Chapter 4, is that the HS source, Reaction 12, is slow compared to the HS-removal Reaction 33b. This means that not all H atoms are converted to HS prior to the start of HS-removal. A computer simulation with sensitivity analysis taking into account the 4 reactions in Table 6.1 with reasonable rate constants has shown that the HS maximum absorbance corresponds to 91% of the H-atom concentration produced when the amount H_2S is 19.7 mbar. In Figure 6.5 maximum HS absorbance versus H_2S partial pressure is plotted. The slowly increasing HS absorbance for H_2S pressures higher than 25 torr can be ascribed to direct radiolysis of H_2S. In Figure 6.6 computer simulations for 5 different H_2S concentrations are shown, with two different models for each H_2S concentration. Using Eq. 15

$$A = \varepsilon \cdot l \cdot c \qquad (15)$$

with A = 0.033, l = 80 cm, and c = 4.32 x 10^{-7} M gives ε = 9.5 x 10^{2} $cm^{-1}M^{-1}$ for HS at 3242Å. In Table 6.2 a set of experimental data for the H_2S-H_2 system is given. A plot of reciprocal formation half-life showed that HS formation did not follow pseudo-first-order kinetics. In Figure 6.7 the derived values of k_{12} assumming pseudo-first-order conditions are plotted. This plot shows that other H and HS reactions should be considered in this H_2S concentration range, and that the "asymptotic" k_{12}-value lies in the range 4-6 x 10^{8} $M^{-1}s^{-1}$. In Table 6.3 this estimate is compared with values found in the literature.

In Figure 6.5 maximum HS absorbance versus H_2S partial pressure is plotted. The slowly increasing HS absorbance for H_2S pressures higher than 25 Torr can be ascribed to direct radiolysis of H_2S.

Table 6.2. Experimental data from the H_2S/H_2system, formation half-life, τ_f, and the derived rate constant

$p(H_2S)$ in Torr	τ_f in μsec	$\ln 2/(\tau_f \cdot c_o)$ in $10^9 M^{-1}s^{-1}$
0.5	13.5	1.87
0.5	14.0	1.80
1.0	6.2	2.00
1.0	6.5	1.95
2.0	5.5	1.15
2.0	5.6	1.13
3.0	5.0	0.84
3.0	4.2	1.00
4.0	4.2	0.75
4.0	3.8	0.83
5.0	3.4	0.74
10.0	2.0	0.63
25.0	1.4	0.36

Table 6.3. Room temperature rate constants for $H + H_2S \rightarrow H_2 + HS$

Reference	k_{12} in $M^{-1}s^{-1}$
Perner and Franken 1969	$(7.7 \pm 1.5) \times 10^8$
Kurylo et al. 1971	$(4.34 \pm 0.3) \times 10^8$
Clyne and Ono 1983	$(4.46 \pm 0.2) \times 10^8$
This work	$4 - 6 \times 10^8$

Table 6.4. Experimental data for the H_2S/H_2-system

$p(H_2S)$ in Torr	Amax	decay half-life in μs	$k_{33} = \frac{\varepsilon \cdot \ell}{2 \cdot \tau_o \cdot A_{max}}$ in $M^{-1}s^{-1}$
5	0.037	83	1.9×10^{10}
10	0.048	64	1.9×10^{10}
10	0.048	70	1.7×10^{10}
15	0.043	64	2.1×10^{10}
20	0.046	63	2.0×10^{10}
20	0.045	64	2.0×10^{10}
25	0.050	56	2.0×10^{10}
25	0.051	64	2.0×10^{10}
50	0.051	57	1.8×10^{10}
50	0.055	58	1.8×10^{10}
100	0.072	45	1.8×10^{10}
100	0.060	50	1.9×10^{10}
		mean	$(1.9 \pm 0.1) \times 10^{10}$

Our estimate favours the results of Kurylo et al. (1971) and Clyne and Ono (1983). In Table 6.4 experimental data concerning HS decay is listed, which takes place according to second-order kinetics. A total Reaction 33

$$HS + HS \rightarrow \text{products} \qquad (33)$$

includs Reactions 33a, 33b, and 33c. For second-order decay $2k_{33} = 1/(\tau_D \cdot [HS]_o)$, where τ_D is the decay half-life and $[HS]_o$ the initial HS concentration, which can be expressed as

$$[HS]_o = A_{max}/(\varepsilon \cdot \ell) \qquad (76)$$

using equation 15, where A_{max} is maximum HS absorbance. The average value of $k_{33} = (1.9 \pm 0.1) \times 10^{10}$ $M^{-1}s^{-1}$ is in fair agreement with $k_{33b} = 7.8 \times 10^9$ reported by Bradley et al. (1973). The difference between 1.9×10^{10} and 7.8×10^9 could be accounted for by Reactions 33a and 33c. At first one would think it would be possible to analyse the H_2S-H_2 system in the same way that the H_2O-Ar system was analysed, as the systems contain analogous initial species H, OH, H_2O, and H,SH, and H_2S. In Table 6.5 tha analogous reactions are listed.

Table 6.5. Analogous reactions i H_2O-Ar and H_2S-H_2 systems

H_2O-Ar		H_2S-H_2
$H + H + M \rightarrow H_2 + M$	(1)	$H + H + M \rightarrow H_2 + M$
$OH + OH + M \rightarrow H_2O_2 + M$	(2)	$HS + HS + M \rightarrow H_2S_2 + M$
$OH + OH \rightarrow H_2O + O$	(3)	$HS + HS \rightarrow H_2S + S$
$H + OH + M \rightarrow H_2O + M$	(4)	$H + HS + M \rightarrow H_2S + M$
$H + H_2O \rightarrow OH + H_2$	(6)	$H + H_2S \rightarrow HS + H_2$

The reason why a better analysis was possible for the OH case was that the high specific third-body efficiency of CF_2Cl_2 made it possible to separate out OH + OH + M → H_2O_2 + M and that most of the relevant rate constants in the H_2O-Ar system had been estimated before. However, one significant observation was that no HS_2 was formed in the H_2S-H_2 system in contrast to the systems below, which we will now deal with.

6.3.2. The pure H_2S system

Very few experiments on pure H_2S were performed. This was due to the destruction of the mirrors in the cell after just one irradiation. Actually only 3 experiments were carried out all on 1 atm H_2S. HS absorption was followed for 20 and 400 μs and HS_2 absorption was followed for 400 μs. The experimental curves are shown in Figures 6.8, 6.9, and 6.10, respectively.

The result of the ionic and the neutralization processes will be (Nielsen 1979):

$$H_2S \rightarrow H + HS \qquad (77)$$

$$H_2S \rightarrow H_2 + S \qquad (78)$$

$$H_2S \rightarrow H + H + S \qquad (79)$$

Processes 77 and 79 have been observed directly in early flash photolysis of H_2S (Porter 1950 and Kurylo et al. 1971). Even though Process 78 is the most favourable energetically, no direct experimental evidence for this process has been found in the literature. However, this is not important for the analysis of the few results on the pure H_2S system. Regardless of Process 78, just after the pulse there will be H and S atoms and HS radicals in an unknown ratio in the 1 atm H_2S. The H atoms will immediately react with H_2S to form H_2 and HS, which is seen in Figure 6.8 where the HS absorption has reached its maximum in about 2 μs. Therefore, the only species present in the 1 atm H_2S 2 μs after the pulse are H_2, HS, and S. The second-order tail of the HS decay in Figure 6.9 indicates pure second-order kinetics.

The ratio $t_{1/4}/t_{1/2}$ = 1.4 (instead of 2 in the case of pure second-order kinetics) and the unsuccessful attempt to fit the data with a simple second-order curve shows that the HS decay must be of mixed order. Table 6.6 gives the exothermic HS removal reactions relevant 2 μs after the pulse in the pure H_2S system.

In principle, all the reactions given in Table 6.6 may all contribute to the removal of HS in the pure H_2S system. Reaction 23a has not been considered elsewhere. The reason is probably because the reaction must proceed through a reaction complex with some very unlikely rearrangements taking place even though it is exothermic. Darwent et al. (1967) have neglected to discuss reaction 33a. As a first approximation we assume that the decay to be of second order and caused by a total reaction:

Table 6.6. Exothermic HS-removal reactions in the pure HS-system.

		ΔH kcal/mol
(23a)	$H_2S + HS \rightarrow H_2 + HS_2$	- 8.0
(33a)	$HS + HS + M \rightarrow H_2S_2$	-66.2
(33b)	$HS + HS \rightarrow H_2S + S$	- 8.6
(33c)	$HS + HS \rightarrow H_2S + HS_2$	-39.3
(34)	$HS + H_2S_2 \rightarrow H_2S + HS_2$	-21.6
(35a)	$HS + S + M \rightarrow HS_2$	-79.2
(35b)	$HS + S \rightarrow H + S_2$	-18.5
(36a)	$HS + S_2 + M \rightarrow HS_3$	-40.4
(37a)	$HS + HS_2 \rightarrow H_2S + S_2$	-31.3

$$HS + HS \rightarrow \text{products.} \qquad (33)$$

Determination of k_{33} involves the usual problem of estimating $[HS]_o$. However, the extinction coeficient for HS derived earlier in this report here comes as a convenient help. The

measured A_{max} = 0.1 together with ϵ = 950 $cm^{-1}M^{-1}$ and l = 120 cm gives $[HS]_o$ = 8.8 × 10^{-7} M. For a pure second-order decay the half-life, $t_{1/2}$, is given by:

$$t_{1/2} = \frac{1}{c_o \cdot k} \qquad (79)$$

which, with the experimental $t_{1/2}$ = 28 μs, gives k_{33} = 4.1 × 10^{10} $M^{-1}s^{-1}$. This is 28% higher than the value of 3.2 × 10^{10} $M^{-1}s^{-1}$ published by Perner and Franken (1969). There is no immediate explanation for this difference. Bradley et al. (1973) have published a value for Reaction 33b of k_{33b} = 7.8 × 10^{9} $M^{-1}s^{-1}$.

In Figure 6.10 it is seen that HS_2 is formed so fast that it considered to be almost prompt. It has not been possible to explain the difference in HS_2 formation in 1 atm H_2S in these experiments and in those of Perner and Franken (1969) shown in Figure 6.11. In Table 6.7 the exothermic HS_2 source reactions are given. The prompt formation of HS_2 and the absence of HS_2 in the H_2-H_2S system will leave only the unlikely Reaction 23a and Reaction 35a as possible sources for HS_2. In this case the formation half-life of HS_2 increases with increasing concentrations of H_2S. This will be dealt with in the H_2S-Ar system.

Table 6.7. Exothermic HS source reaction

(14a)	$H + H_2S_2$	$\rightarrow HS_2 + H_2$
(16a)	$H + S_2 + M$	$\rightarrow HS_2 + M$
(23a)	$HS + H_2S$	$\rightarrow HS_2 + H_2$
(34)	$HS + H_2S_2$	$\rightarrow HS_2 + H_2S$
(35a)	$HS + S + M$	$\rightarrow HS_2 + M$
(45b)	$H_2S_2 + S$	$\rightarrow HS_2 + HS$

The experimental data on the pure H_2S system is too sparse to establish a kinetic model with any validity.

6.3.3. The H_2S-Ar system.

In the pulse radiolysis of H_2S-Ar mixtures, energy will be absorbed by H_2S and Ar according to the relative stopping powers and relative concentrations. Rare-gas-sensitized radiolysis has been investgated in detail (Jowko et al. 1977; Forys et al. 1976: Ahmad et al. 1972; Jezierska and Forys 1972; Jerzierska 1971). As in the pure H_2S system the species present in the Ar after the pulse are H, HS, S, and H_2S. In this system, in contrast to the pure H_2S system, Reaction 12

$$H + H_2S \rightarrow H_2 + HS \qquad (12)$$

will remove H atoms and produce HS more slowly because of the smaller H_2S concentration, which is seen when comparing Figure 6.12 and 6.8. On neglecting HS removal in the beginning, the HS formation should consist of an almost prompt component from Reaction 76 and a slower rising component from Reaction 12. Figure 6.12 could be interpreted in this way. However, the quality of plots of experiments with H_2S partial pressures from 1 to 10 torr allows only a rough estimate of the ratio of the prompt Reaction 76 to the slower Reaction 12 to be around 1:1. The increasing HS yield with increasing H_2S partial pressure shown in Figure 6.13 should cause HS to be removed faster by Reaction 33b, which is also observed experimentally.

Earlier in this report it has been shown that either Reaction 23a or 35a:

$$HS + H_2S \rightarrow HS_2 + H \qquad (23a)$$

$$HS + S + M \rightarrow HS_2 + M \qquad (35a)$$

is the HS_2 source reaction. Experimentally it is found that the HS_2 formation half-life and the yield of HS_2 are independent of the H_2S partial pressures above 2 Torr, as shown in Figures 6.14 and 6.15. On this basis, it is concluded the Reaction 35a is the major HS_2 source, while Reaction 23a contributes only to a very minor extent, if at all, to the formation of HS_2. As a consequence, it was attempted to establish a model that would account for the observed HS and HS_2 experimental data.

The prompt part of the HS formation is not 100% prompt, because Reaction 77 is one between excited Ar atoms, Ar*, and H_2S:

$$Ar^* + H_2S \rightarrow H + HS + Ar \qquad (81)$$

and this is also the case for Reaction 79:

$$Ar^* + H_2S \rightarrow H + H + S + Ar \qquad (82)$$

The excited Ar atoms decay by emission of light

$$Ar^* \rightarrow Ar + h\nu \qquad (83)$$

The term k_{83} is given by Sauer (1976) as $5 \times 10^5\ s^{-1}$. Relative values of k_{81}, k_{82}, and G(Ar*) can be determined from computer simulations to fit HS formation and maximum HS concentration $k_{81} = (6 \pm 4) \times 10^9\ M^{-1}s^{-1}$, $k_{82} = (5 \pm 3) \times 10^9\ M^{-1}s^{-1}$, and G(Ar*) = 22.5 was determined. Besides Reactions 81 and 82 the model consisted of the following reactions:

$H + H + M \rightarrow$	$H_2 + M$	(11)
$H + H_2S \rightarrow$	$H_2 + HS$	(12)
$H + HS \rightarrow$	$H_2 + S$	(13b)
$HS + HS \rightarrow$	products	(33)
$HS + HS \rightarrow$	$H_2S + S$	(33b)
$HS + S + M \rightarrow$	$HS_2 + M$	(35a)
$HS_2 + HS_2 + M \rightarrow$	$H_2S_4 + M$	(77a)

For 5 of these 8 reactions reliable rate constants exists, $k_{11} = 1.25 \times 10^8\ M^{-1}s^{-1}$ (Hampson 1980), $k_{12} = 4.35 \times 10^8\ M^{-1}s^{-1}$ (Kurylo 1971), $k_{13b} = 1.4 \times 10^{10}\ M^{-1}s^{-1}$ (Bradley et al. 1973), $K_{33b} = 7.8 \times 10^9\ M^{-1}$ (Bradley et al. 1973), $k_{33} = 3.2 \times 10^{10}\ M^{-1}s^{-1}$ (Perner and Franken1969). From the computer simulations k_{35a} and k_{77a} were determined, $k_{35a} = (2.5 \pm 1) \times 10^{10}\ M^{-1}s^{-1}$ and $k_{77a} = (8.5 \pm 3) \times 10^{10} M^{-1}s^{-1}$, which are realistic values for radical-radical reactions. The model was insensitive to Reactions 37a and 55:

$$HS + HS_2 \rightarrow H_2S + S_2 \quad (37a)$$

$$S + S + M \rightarrow S_2 + M \quad (55)$$

hence k_{37a} and k_{55} could not be determined and these two reactions were not included in the model. The final model is also in agreement with the absense of any HS_2 in the H_2S-H_2 system. In Figures 6.16 and 6.17 the model and experimental curves for HS and HS_2, respectively, are shown.

7. CONCLUSION

The work described in this report confirms that pulse radiolysis of gases can yield valuable information about reactions and transient species. The experiments presented here have been of both fundamental and environmental interest. Still some work remains to be done on the "third-body model" for the OH + CF_2Cl_2 reaction. The use of computer simulations have been demonstrated and described. Suggestions for further research have been given.

REFERENCES

AHUMADA, J.J., MICHAEL, J.K., and OSBORNE, D.T. (1972). J. Chem. Phys. 57, 3736.

AMAD, M., D.W. and WOODWARD, T.W. (1972). J.C.S. Faraday Trans. 1972, 1857-1865.

ARMSTRONG, D.A. and WILLIS, C (1976). Int. J. Radiat. Phys. Chem. 8, 221.

ATKINSON, R. DARNALL, K.R. LLOYD, A.C., WINER, A.M., and PITTS, Jr.J.N. (1979). Adv. Photochem. 11, 375.

ATKINSON, R., HANSEN, D.A., and PITTS, Jr. J.N.(1975). J. Chem. Phys. 63, 1703.

BALLASH, N.M. and ARMSTRONG, D.A. (1974). Spectrochim Acta A30, 941.

BAULCH, D.L. and CAMPBELL, I.M. (1981). Gas Kinetics and Energy Transfer 4, 137.

BAULCH, D.L., COX, R.A., CRUTZEN, P.J., and HAMPSON Jr., R.F., KERR, J.A., TROE, J., and WATSON, R.T. (1982). J. Phys. Ref. Data 11, 327.

BAULCH, D.L., COX, R.A., HAMPSON, R.F. KERR, J.R., TROE, J., and WATSON, R.T. (1980) J. Phys. Chem. Ref. Data 9, 295.

BAUM, R.M. (1982). Chem. Eng. News 60, (37) 21.

BEIJER, K. and JERNLOV, A. (1982). To be publisheds in: Biological effect of organolead compounds, Ed. by Grandjean, P., CRC Press, Cleveland, Ohio.

BISHOP, W.P. and DORFMAN, L.M. (1970). J.Chem. Phys. 52, 3210.

BJARNOV, E., MUNK, J., NIELSEN, O.J., PAGSBERG, P., and SILLESEN, A. (1983). Risø-M-2366.

BLAK, G. and PORTER, G. (1962). Proc. Roy. Soc. A266, 185.

BONHOEFFER K.F. and REICHARDT, H. (1928). Z. Physik. Chem. 139, 75.

BOURENE, M., DUTUIT, O., and LE CALVE, J. (1974). CEA-N-1758.

BOYD, A.W., WILLIS, C., CYR, R., and ARMSTRONG, D.A. (1969). Can. J. Chem. 47, 4715.

BOYD, A.W., WILLIS, C., and MILLER, D.A. (1973). Can. J. Chem. 51, 4048.

BOYD, A.W., WILLIS, C., and MILLER, O.A. (1973b). Can. J. Phys. 51, 1228.

BRADLEY, J.N., TRUEMAN, S.P., WHYTOCK, D.A., and ZALESKI, T.A. (1973). J.C.S. Faraday I 69, 416.

BUCHARDT, O. (1981). Possible effects of present and future propellants for aerosol cans. Report 35 of the Danish Environmental Protection Agency (in Danish).

CALDWELL, J. and BACK, R.A. (1965). Trans. Faraday Soc. 61, 1939.

CALLEAR, A.B. and TYERMAN, W.J. (1966). Trans. Faraday Soc. 64, 677.

CALLEAR, A.B. and LAMBERT, J.D. (1969) in "Comprehensive Chemical Kinetics" 3, 182. Bamford, C.H. and Tipper, C.F.H. (Eds.). Elsevier, New York.

CHAMEIDES, W.L. and DAVIS, D.D. (1982). Chem. Eng. News 60, (40)38.

CHARBONNIER, F.M., BARBOUR, J.P., and BREWSTER, J.L. (1975). in "Fast processes in radiation chemistry and biology." ADAMS, G.E., FIELDEN, E.M., and MICHAEL, B.D. (Eds.). Wiley and Sons, New York.

CHAMEIDES, W.L. and TAN, A. (1981). J. Geophys. Res. C, 86, 5209.

CHANG, J.S. and KAUFMAN, F. (1977). Geophys. Res. Lett. 4, 192.

CHAU, Y.K. and WONG P.T.S. (1982). To be published in: Biological effects of organolead compounds, Ed. by Grandjean, P., CRC Press, Cleveland, Ohio.

CHAUDHURY, A.U. and GOWENLOCK, B.G. (1969). J. Organometal. Chem. 16, 221.

CLYNE, M.A.A: and HOLT, P.M. (1979). J. Chem. Soc. Faraday Trans. II 75, 582.

CLYNE, M.A.A. and ONO, Y. (1983). Chem. Phys. Lett. 94, 597.

COX, R.A., DERWENT, R.G., and EGGLETON, A.E.J. (1976). Atmos. Environ. 10, 305.

DARWENT, B.deB. WADLINGER, R.L., and ALLARD, M.J. (1967). J. Phys. Chem. 71, 2346.

DAVIS, D.D., FISHER, S., and SCHIFF, R. (1974). J. Chem. Phys. 61, 2213.

DAVIS, D.D., HEAPS, W., PHILEN, D., and McGEE, T. (1979). Atmos. Environ. 13, 1197.

DAVIS, D.D. MACHADO, G., CONAWAY, B., Oh. Y., and WATSON, R.T. (1976). J. Chem. Phys. 65, 1268.

DERWENT, R.G. and EGGLETON, A.E.J. (1981). Nature 293, 387.

DIEKE, G.H. and CROSSWHITE, H.M. (1962). J.QUANT. Spectrosc. Radiat. Trans. 2, 97.

DIXON, P.S. (9170). Radiation Res. Rev. 2, 237.

DOYEL, J.D., LLOYD, A.C., DARNALL, K.R., WINER, A.M., and PITTS, J.N., (1975). Environ. Sci. Technol. 9, 237.

DRYSDALE, D.D. and LLOYD, A.C. (1970). Oxidation Combust. Rev. 4, 157.

DUNN, M.R. SUTTON, M.M. FREEMAN, C.G., McEWAN, M.J., and PHILLIPS, L.F. (1971). J. Phys. Chem. 75, 722.

EDWARDS, P.R., CAPBELL, I., and MILUE, G.S. (1982). Chem. Ind. (1982), 619.

EHHALT, D.H. (1974). Tellus 26, 65.

FORYS, M., JOWKO, A. and SZAMREJ, I. (1976). J. Phys. Chem. 80, 1035-1041.

GHORMLY, J.A., HOCHANDEL, C.J., and BOYLE, J.W. (1969). J. Chem. Phys. 50, 419.

GORDON, S., MULAC, W., and NANGIA, J. (1971). J. Phys. Chem. 75, 2087.

GORDON, S: and MULAC, W. (1975). Int. J. Chem. Kinet. Symp. 1, 289.

GRAEDEL, T.E., FARROW, L.A., and WEBER, T:A: (1976). Atmos. Environ. 10, 1095.

GRANAT, L., ROHDE, H, and HALBERG, K.O. (1976) SCOPE report No. 7.

GRANDJEAN, P., and NIELSEN, T. (1977). SNV PM 879, Swedish Environmetal Protection Agency, Stockholm. 78 pp. (In Danish).

GRANDJEAN, P. and NIELSEN, T. (1979). Environmetal health aspects. Res. Reviews, 72, 97.

GREINER, N.R. (1970). J. Chem. Phys. 53, 1070.

HAMILTON, Jr. E.J. (1975). J. Chem. Phys. 63, 3682.

HAMILTON, Jr. E.J. and LII, R.-R. (1977) Int. Chem. Kinet. 9, 875.

HAMPSON, R.F. (1980). Federal Aviation Administration, Report No FAA-EE-80-17.

HANDWERK, V. and ZELLNER, R. (1979). Ber. Bunsenges: Phys. Chem. 82, 1161.

HANSEN, K.B., WILBRANDT, R., PAGSBERG, P. (1979). Rev. Sci. Instrum. 50, 1532.

HARRISON, R.M., and LAXEN, D.P.H. (1978). Environ. Sci. Technol. 12, 1384.

HEICKLEN, J. (1970). Adv. Photochem. 7, 57.

HOCHANADEL, C.J., GHORMLY, J.A., and OGREN, P.J. (1972). J. Chem. Phys. 56, 4426.

HORNE, D.G: and NORRISH, R.G.W. (1967). Nature 215, 1373.

HOV, Ø., ISAKSEN, I.S.A., and HESSTVEDT, E. (1978). Atmos. Environ. 12, 2469.

HOWARD, C.J., and EVENSON, K.M. (1976). J. Chem. Phys. 64, 4303.

HOWARD, C.J., and EVENSON. K.M. (1976). J. Chem. Phys. 64, 197.

HUEBERT, B.J. and MARTIN, R.M. (1968). J. Phys. Chem. 72, 3046.

HUYTON, D.W: and WOODWARD, T.W. (1970). Radiat. Res. 2, 205.

ILLIES, A.J. and TAKAES, G.A. (1976). J. Photochem. 6, 35.

INN, E.C.Y. and TANAKA, Y. (1953). J. Opt. Soc. Am. 43, 870.

JEONG, K. and KAUFMAN, F. (1982). J.Phys. Chem. 86, 1808.

JEONG, K. and KAUFMAN, F. (1979). Geophys. Res. Lett. 6, 757.

JEZIERSKA, K. and FORYS, M. (1972). Nukleonika 17, 23_29.

JOHNSON, G.R.A. and WILKEY, D.D. (1969). J. Chem. Soc. D, 1969, 1455.

JONGHE, W.R.A. de, CHAKRABORTI, D., and ADAMS, F.C. (1981). Environ. Sci. Technol. 15, 1217.

JOWKO, A., SZAMREJ, I. and FORYS, M. (1977). J. Phys. Chem. 81, 1537-1543.

KERR, J.A., and TIMLIN, D. (1969). J. Chem. Soc. A, 1241

KHALIT, M.A.K. and RASMUSSEN, R.A. (1981). Nature 292, 823.

KURYLO, M.J., PETERSON, N.C. and BRAUN, W. (1971). J. Chem. Phys. 54, 943.

LAVESKOG, A. (1972). TPM-BIL-64, AB Atomenergy, Stockholm.

LEIGHTON, D.A. (1961). "Photochemistry of Air Pollution", Academic Press, N.Y.

LII, R.-R. GORSE, Jr.R.A. SAUER, Jr. M.C. and GORDON, S. (1979). J. Phys. Chem. 83, 1803.

LIU, S.C. (1977). Geophys. Res. Lett. 4, 325.

LLOYD, A.C., DARNALL, K.R., WINER, A.M. and PITTS, J.N., Jr. (1976). J. Phys. Chem. 80, 789.

LORENZ, K., WAGNER, H.G., and ZELLNER, R. (1979). Ber. Bunsenges. Phys. Chem. 83, 556.

LOVELOCK, J.E. (1977). Nature 267, 32.

MARGITAN, J.J., KAUFMANN, F, and ANDERSON, J.G. (1974). Geophys. Res. Lett. 1, 80.

MATHESON, M.S. and DORFMAN, L.M. (1960). J. Chem. Phys. 32, 1870.

MATIAS, E., SANHWEZA, E., HISATSUNE, I.C. and HEICKLEEN, J. (1974). Can. J. Chem. 52, 3852.

McELROY, M.B., WOPSY, S.C., and Sze, N.O. (1980). Atmos. Environ. 14, 159.

McKEAN, D.C., DUNCAN, J.L., and BATT, L. (1972). Spectrochim. Acta A, 29, 1037.

MOLINA, M.J. and ROWLAND F.S. (1974). Nature 249, 810.

NATIONAL ACADEMY OF SCIENCES (1972). Lead Airborne lead in perspective. (National Academy Press, Washington D.C.).

NATIONAL RESEARCH COUNSIL (1982). Causes and effects of stratospheric ozone reduction: An update. (National Academy Press, Washington D.C.).

NIELSEN, O.J. (1979). Risø-M-2216.

NIELSEN, O.J., BJARNOV, E., PAGSBERG, P., and SILLESEN, A. (1982). Risø-M-2337 (in Danish).

NIELSEN, O.J. SILLESEN, A., LUTHER, K., and TROE, J (1982). J. Phys. Chem. 86, 2929.

NIELSEN, T. (1982). To be published in: Biological effects of organolead compounds, Ed.by Grandjean, P., CRC Press, Cleveland, Ohio.

NIELSEN, T. EGSGAARD, H., LARSEN, E., and SCHROLL, G. (1981). Analyt. Chim. Acta 124, 1.

OLDENBURG, O. (1935). J. Chem. Phys. 3, 266.

OVEREND, R.P., PARASKEVOPOULOS, G., and CVETANOVIC, R.J. (1975). Can. J. Chem. 53, 3374.

PARASKEVOPOULOS, G. SINGLETON, D.L. and IRWIN, R.S. (1981). J. Phys. Chem. 85, 561.

PAUKERT, T.T. and JOHNSTON H.S. (1972). J. Chem. Phys. 56, 2824.

PENNER, J.E. (1982). Atmos. Environ. 16, 1109.

PERNER, D., EHHALT, D.H., PATZ, H.W., PLATT, U., ROTH, E.P., and VOLZ, A. (1976) Geophys. Res. Lett. 3, 466.

PERNER, D., EHHALT, D.H., PATZ, H.W., PLATT, U., ROTH, E.P., and VOLZ, A. (1981). J. Geophys. Res. C 86, 12, 155.

PERNER, D. and FRANKEN, T. (1969). Ber, Bunsenges. Physik. Chem. 73, 897.

PERRY, R.A. ATKINSON, R. and PITTS, Jr. R.N. (1976) J.Chem. Phys. 64, 1618.

PERRY, R.A., ATKINSON, R., and PITTS, Jr. R.N. (1976b.). J. Chem. Phys. 64, 3237.

PORTER, G. (1950). Discuss. Faraday Soc. 9, 60.

PUBLIC HEALTH SERVICE (1970). Survey of lead in the atmosphere of three urban communities by the working group on lead contamination. No. 999-Ap-12, Public Health Service Publication.

RADZIUK, B., THOMASSEN, Y., BUTLER, L.R.P., LOON, van J.C., CHAU, Y.K. (1979). Analyt. Chem. Acta 105, 255.

RASMUSSEN, O.L. (1983). Risø-R-395. To be published.

REDINGTON, R.L., OLSON, W.B., and CROSS, P.C. (1962). J. Chem. Phys. 36, 1311.

ROBINSON, J.W. (1975). Analyt. Chem. 78, 474.

SAUER, Jr. M.C. and DORFMAN, L.M. (1964). J. Am. Chem. Soc. 86, 4218

SAUER, Jr. M.C. (1976). Adv. Rad. Chem. 5, 97.

SAUER, Jr. M.C. (1982). in "The study of fast processes and transient species by electron pulse radiolysis". BAXENDALE, J.H. and BUSI, F. (Eds). Reidel Publishing Company, Holland.

SAUER, Jr. M.C. (1967). J. Phys. Chem. 71, 3971.

SHAPIRO, H., and FREY, J.W. (1968). The organic compounds of lead. Interrscience Publ., New York.

SNYDER, L.J. (1967). Anal. Chem. 39, 591.

SZE, N.D. and KO, M.K.W. (1980). Atmos. Environ. 14, 1223.

SUONG, J.Y. and CARR, Jr. R.W. (1982). J. Photochem. 19, 295.

SYMPOSIUM ON REACTION MECHANISMS, MODELS, AND COMPUTERS (1977). J. Phys. Chem. 81, 2309.

TELLINGHUESEN, J.B. (1973). J. Chem. Phys. 58, 2821.

TULLY, F.P. and RAVISHANKARA, A.R. (1980). J. Chem. Phys. Lett. 82, 80.

WAGNER, H.G., WELZBACHER, V., and ZELLNER, R. (1976). Ber. Bunsenges. Phys. Chem. 80, 1023.

VAN den BERGH, H. and TROE, J. (1975). Chem. Phys. Lett. 31, 351.

VAN den BERGH, H. and TROE, J. (1976). J. Chem. Phys. 64, 736.

VAN den BERGH, H., BENOIT-GUYOT, N., and TROE, J. (1977). Int. J. Chem. Kinet. 9, 223.

WANG, C.C., DAVIS, L.I., Jr., WU, C.H. JAPAR, S. NIKI, H., and WEINSTOCK, B. (1975). Science, 189, 797.

WANG, C.C., DAVIS, L.I. Jr., SELZER, P.M., and MUNOZ, R. (1981). J. Geophys. Res. C 86, 1181 and 12, 156.

WARNECK, P. (1974). Tellus, 26, 39.

WATSON, W.W. (1924). Astrophys. J. 60, 145.

WATSON, R. (1982). Personal Communication.

WATSON, R.T., MACHADO, G., CONAWAY, B., WAGNER, S., and DAVIS, D.D. (1977). J. Phys. Chem. 81, 256.

WELGE, K.H. and STUHL, F. (1967). J. Chem. Phys. 46, 2440.

WHITE, J.U. (1942). J. Opt. Soc. Am. 32, 285.

WILLIS, C., BOYD, A.W., YOUNG, M.J. and ARMSTRONG, D.A. 1970). Can. J. Chem. 48, 1505.

WILLIS, C., BOYD, A.W., and MILLER, O.A. (1971a) Radiat. Res. 46, 428.

WILLIS, C., BOYD, A.W., and MILLER, O.A. (1971b). Can. J. Chem. 49, 1677.

WILSON, W.E. and WESTENBERG, A.A. (1976). Int. Symp. Combust. Proc. 11, 1143.

VOLZ, A., EHHALT, D.H., and DERWENT, R.G. (1981). J. Geophys. Res. C 86, 5163.

WONG, W. and DAVIES, D.D. (1974). Int. J. Chem. Kinet. 6, 401.

ZELLNER, R. and STEINERT, W. (1976). Int. J. Chem. Kinet. 8, 397.

APPENDIX I

COMPUTER SIMULATION

Computer modelling equivalent to computer simulation is now used in many research areas to explore connections between an assumed model and real-world observations. There are probably two general reasons for the increased use of computer modelling. One is the improvement of speed and flexibility of computers and programs. The other is that in dealing with the increasing complexity of problems call for computer modelling to actually see and understand connections.

In the more recent gas kinetic literature computer modelling is very often used not only for the design experiments and predictions but also for mechanism development and derivation of rate constant expressions for elementary reactions. One often omitted aspect is how to evaluate results derived from computer simulations.

Computer simulation of a complex chemical reaction system is based upon numerical integration of a set of coupled differential equations. The single independent variable is usually time. The dependent variables in our case are most often only concentrations of species that will influence the reaction system. Also pressure and temperature are examples of dependent variables. A detailed description of mathematical and other aspects of computer modelling may be found in the literature (Symposium 1977).

For us as experimentalists, a typical procedure will be as follows: First, a reaction system as complete as possible is set up. For some of the reactions in this system there will be experimental rate constants upon which we rely, for others we have to begin with estimates. Simulations with this initial set of

rate constants provide guidance for experimental design. Second, we perform the experiments and accumulate data. Third, the concluding round of computer simulations takes place. In early applications of computer modelling computed profiles were just visually compared with experimental profiles, which is not a sufficient way to show that one's final model is unambigous and to say anything about accuracy of derived rate constants. Therefore, another approach must be taken.

A single kinetic experiment involves observing a smooth change of concentration of a species with time. Since in only rare cases are more than two data values required to characterize the shape of the observed change, each experiment therefore provides just a single datum. A kinetic study may be regarded as consisting of accumulating enough such data to provide a scientific description of how the observed change depends upon changing variables. These data (formation half-life, decay half-life, maximum absorbance, etc.) may be regarded as constructing a surface in hyperspace. This surface can be characterized by a data set $[D_i^e]$ of values of experimentally measured quantities. The quality of the final model is assessed by comparing computed set of data $[D_i^m]$ with $[D_i^e]$. A model is improved by adjusting rate constants until a satisfactory agreement between $[D_i^m]$ and $[D_i^e]$ is obtained.

Let us say that the only adjustable parameters in the model are the rate constants k_j for some of the reactions. These k_j's have many constraints on them imposed by the physical meaning. We have the mathematical problem of finding the best set $[k_j]$, which would normally have to be determined by minimizing $\Sigma(D_i^e - D_i^m)^2$. This could be done by numerical differentiation:

$$\frac{\Delta D_i^m}{\Delta k_j} = S_{ij}$$

and integration, where S_{ij} are the sensitivity coefficients. Such an optimization procedure, though computationally possible, is not used in practice. Instead a sequence of trial-and-error computations involving only the significant S_{ij} elements are

performed. Chemical understanding rather than blind numerical pathfinding is used to improve the model until further fine-tuning is unjustified by the quality of $[D_i^e]$.

Once the optimum $[k_j]$ has been determined, one measure of the quality of this set is immediately available through inspection of the sensitivity coefficients, S_{ij}. We calculate these coefficients as follows:

$$S_{ij} = ((D_{i+}^m - D_{i-}^m)/D_i^m)/((k_{j+}-k_{j-})/k_j)$$

where D_{i+}^m = prediction with k_j increased by P%
D_{i-}^m = prediction with k_j decreased by P%
D_i^m = prediction with nominal k_j
k_{j+} = k_j increased by P%
k_{j-} = k_j decreased by P%
P = percentage parameter variation

$$S_j = \Sigma_i |S_{ij}|.$$

The greater the effect of k_j on the predicted D_i^m the greater the value of S_j. And as a rule, the greater is S_j the smaller is the expected uncertainty in k_j.

This method has two problems which are normally ignored. First, the nonlinear relationships between input and output can cause misleading S_j's. The variability among the coefficients with P can be used to estimate the magnitude of this problem. Second, the correlation between various input parameters can be taken into account only if the parameter values are varied simultaneously. It is important to realize that S_j gives a relative not an absolute measure of the importance of k_j's. Clearly k_j's with $S_j = 0$ cannot be determined in a computer simulation.

A simple test for accuracy is performed for a k_j by increasing and decreasing k_j so that $[D_i^m]$ differs from $[D_i^e]$ by more than the experimental uncertainties, noise, etc.

APPENDIX II

ABBREVIATIONS, SYMBOLS, AND UNITS

atm:	atmosphere, unit of pressure (= 101325 N m^{-2})
A:	symbol for absorbance
A:	pre-exponential factor in the Arrhenius expression
bar:	bar, unit of pressure (= 10^5 N m^{-1})
c:	symbol for concentration
^oC:	degrees centigrade, unit of temperature
cal:	calorie, unit of energy
CFC:	chlorofluorocarbon
D_{298}:	*bond dissociation enthalpy* at 298 K
eV:	electronvolt, unit of energy (= 1.6×10^{-19} J)
E or E_a:	symbol for activation energy
g:	gramme, unit of weight
h:	hour, unit of time
H:	symbol for standard enthalpy
k:	kilo, 10^3
K:	kelvin, unit of temperature
l:	symbol for length
l:	litre, unit of volume
m:	milli, 10^{-3}
m:	metre, unit of length
mol:	mole, unit of amount of substance
M:	molar, unit of concentration = mol dm^{-3}
M:	mega, 10^6
M:	symbol for third body molecule
n:	nano, 10^{-9}
p:	symbol for pressure
ppm:	part per million, unit of concentration
R:	gas constant (= 8.3 J K^{-1} mol^{-1})
s or sec:	second, unit of time
t:	symbol for time
T:	symbol for temperature

Torr:	torr, unit of pressure (= 133.3 N m^{-2})
$t_{1/2}$:	symbol for half-life
Å:	ångstrøm, unit of length (= 10^{-10} m)
ε:	symbol for molar extinction coefficient
λ:	symbol for wavelength
μ:	micro, 10^{-6}
ν:	symbol for vibrational frequency or wavenumber
τ:	symbol for half-life
τ_f	symbol for formation half-life
τ_d	symbol for decay half-life

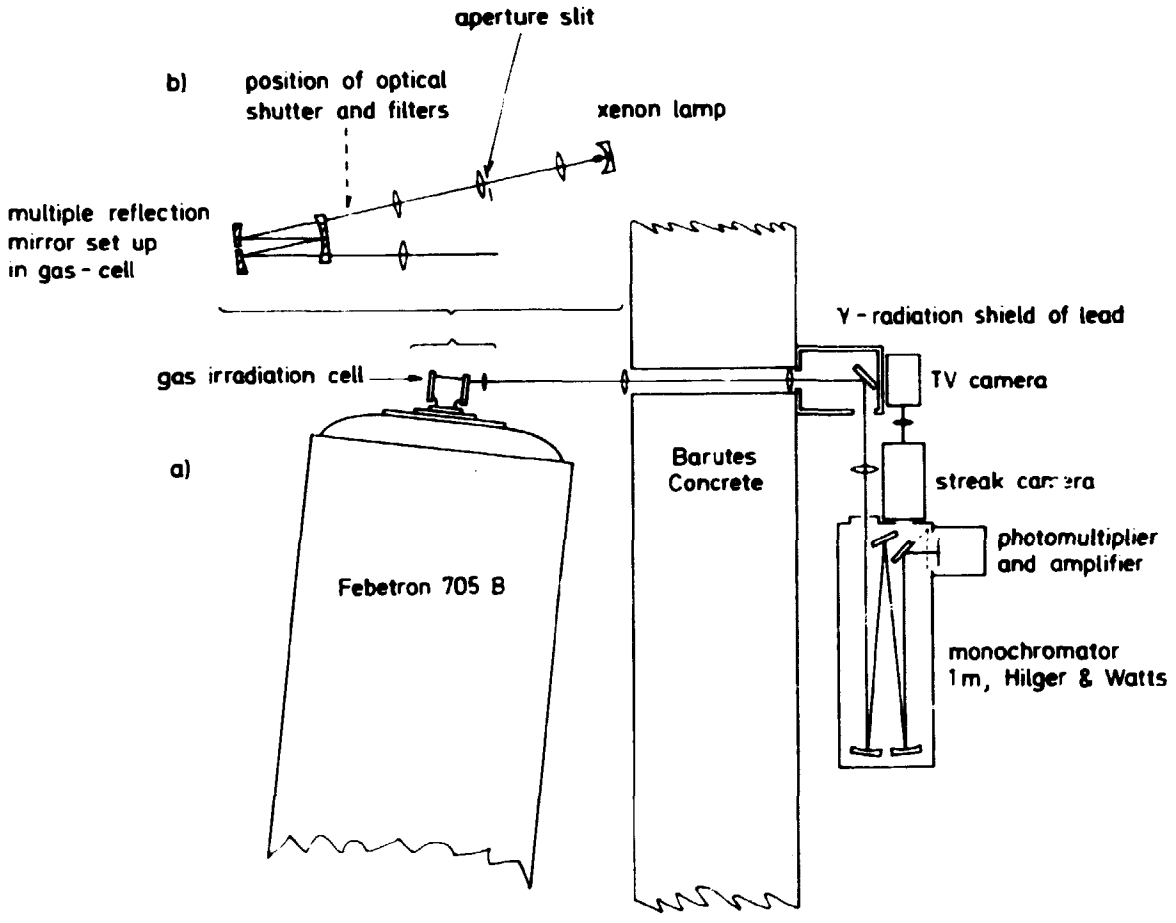

Figure 3.1. Schematic diagram of the experimental gas phase pulse radiolysis set-up. a) Lay-out in the horizontal plane. b) Enlarged vertical cut showing the optics handling the analyzing light beam from the xenon lamp and though the irradiation cell. More details in Fig. 3.3.

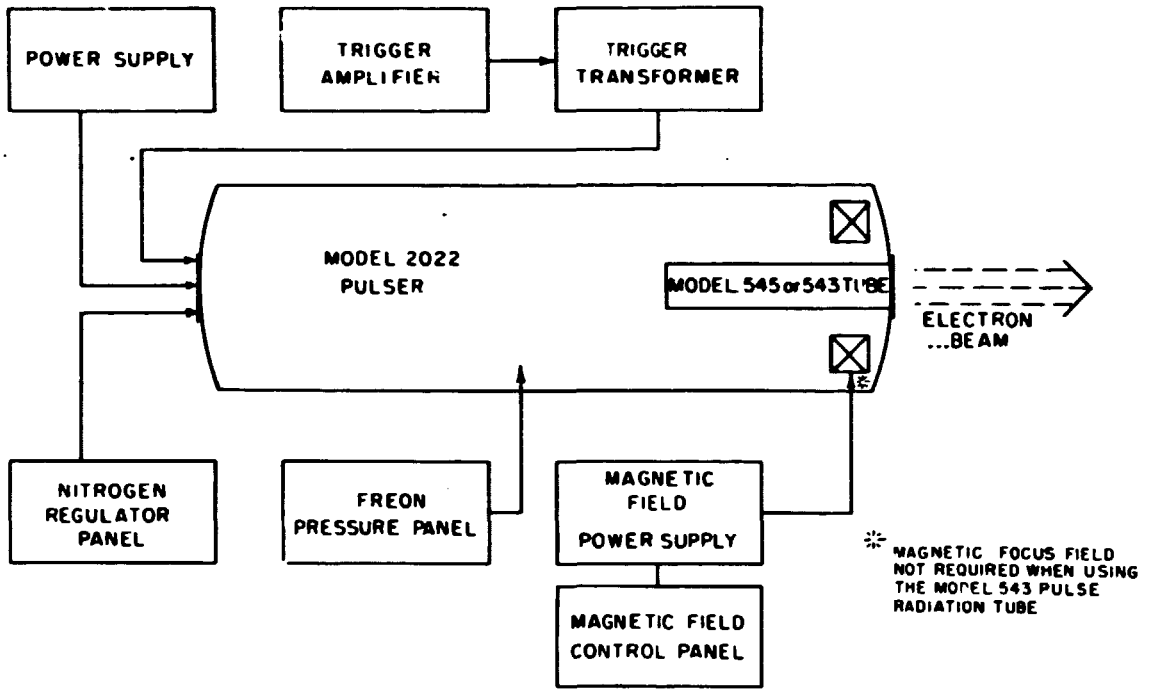

Figure 3.2. Schematic diagram of the Febetron accelerator.

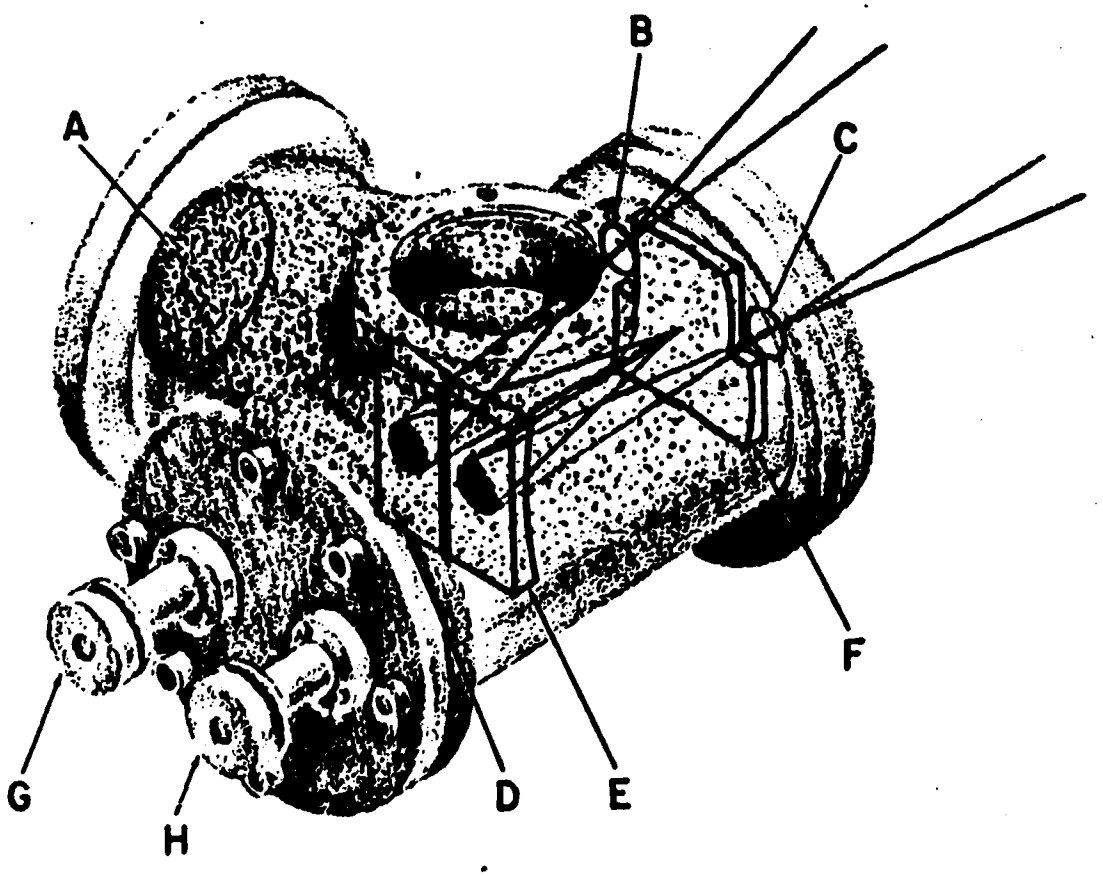

Figure 3.3. Variable path irradiation cell made of stainless steel: A, entrance for electrons; B and C, entrance and exit windows for the analyzing light; D, E and F, spherical mirrors (D and E are externally adjustable by controls G and H).

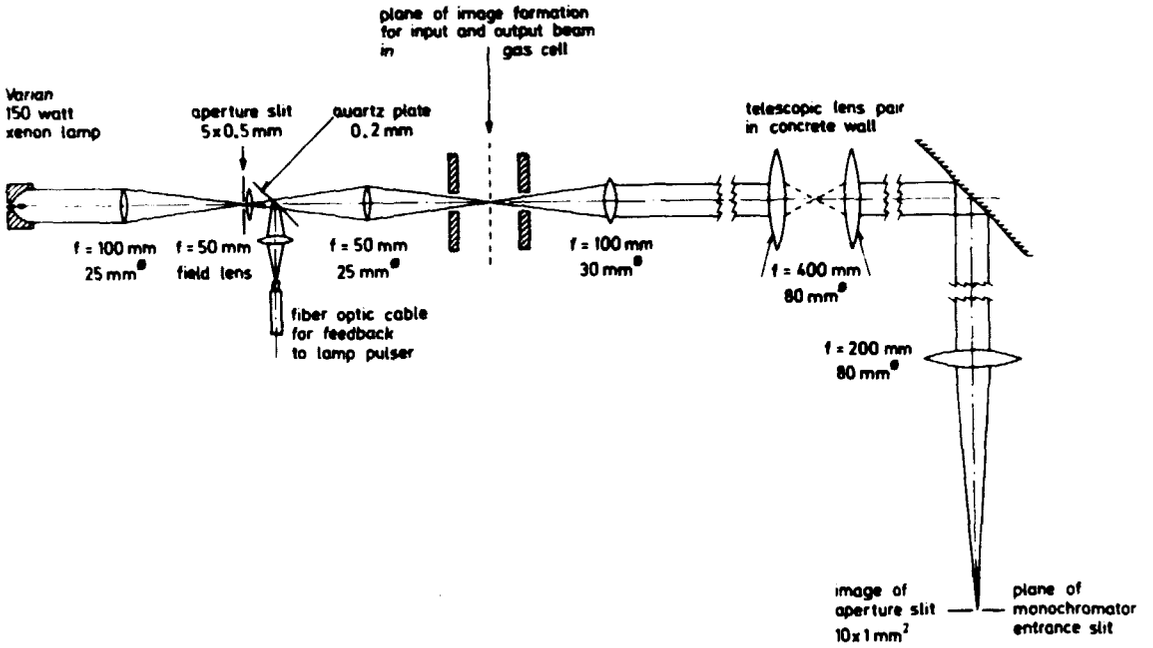

Figure 3.4. The basic components of the pulse radiolysis optical system. For the sake of simplicity, the set of conjugate mirrors in the irradiation cell has been omitted by letting the plane of image formation for input and output beams in the irradiation cell coincide.

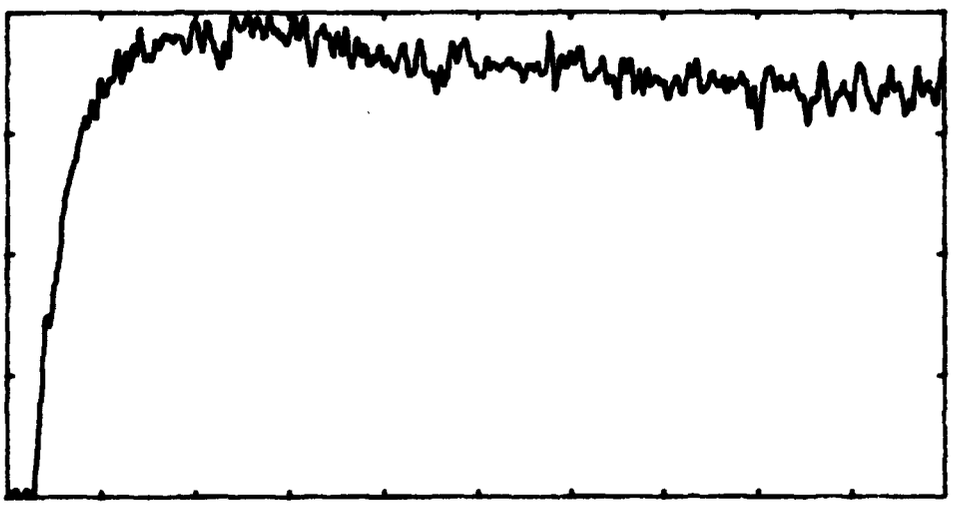

Figure 4.1. Experimental formation and decay of HO_2 in 5 mbar O_2 and H_2 to 1 atm monitored at 2300 Å. T = 298±1 K. Abscissa is time, full timescale = 100 μs, and ordinate is normalized absorbance.

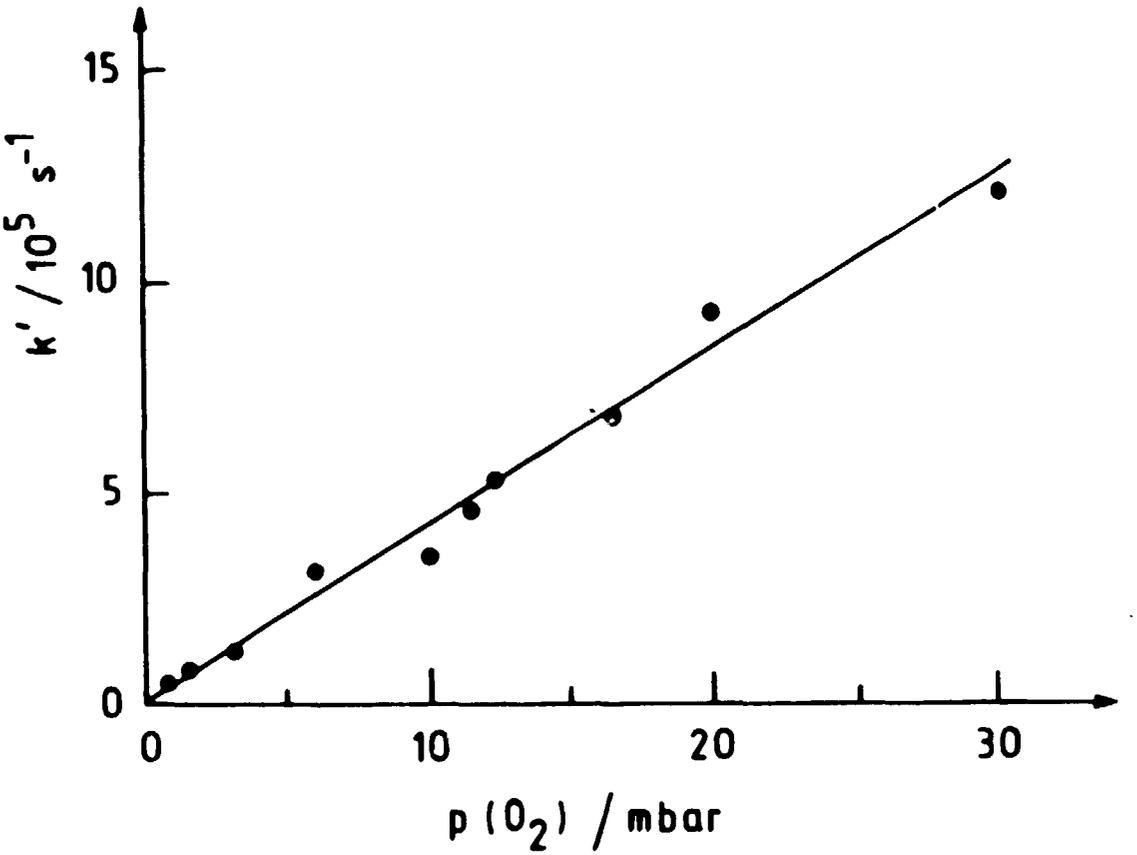

Figure 4.2. Pseudo-first-order rate constants for HO_2 formation in H_2 via $H + O_2 + H_2 \rightarrow HO_2 + H_2$. $k_1' = (d[HO_2]/dt)/([HO_2]_{t=0} - [HO_2]_t)$.

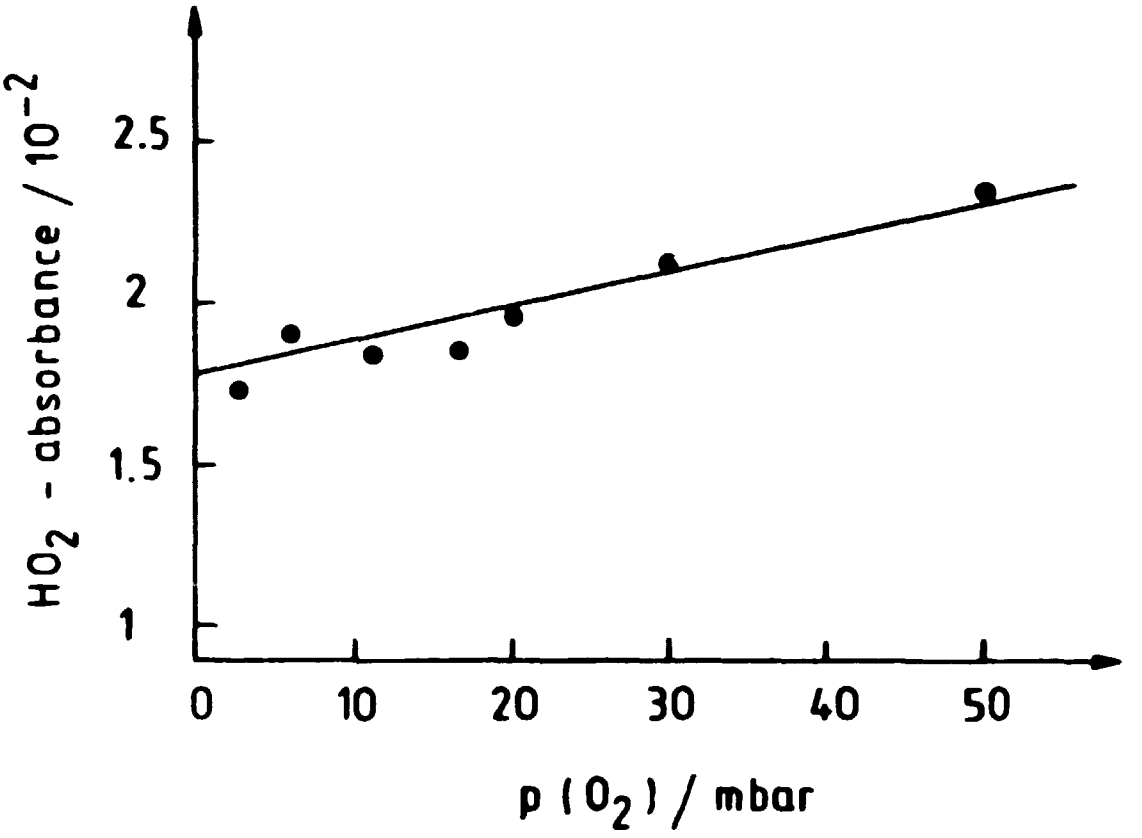

Figure 4.3. HO_2 yield in the pulse radiolysis of H_2 with various pressures of added O_2. Total pressure is 1 atm.

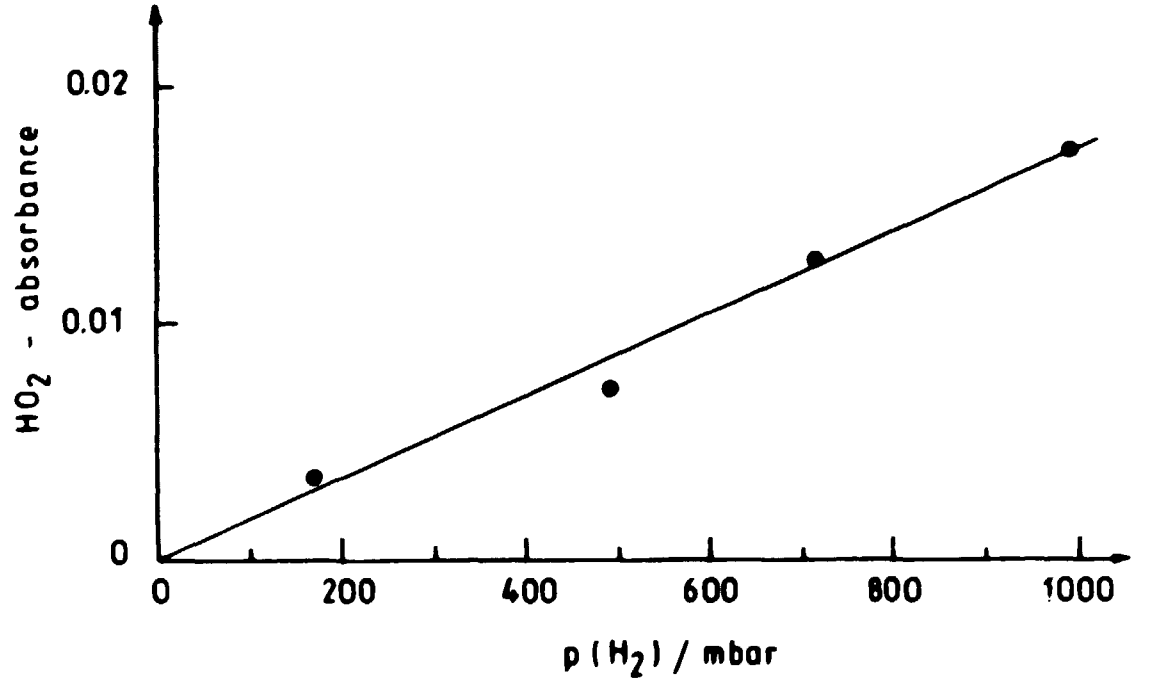

Figure 4.4. HO_2 yield in the pulse radiolysis at various H_2 pressures. O_2 partial pressure is 6 mbar.

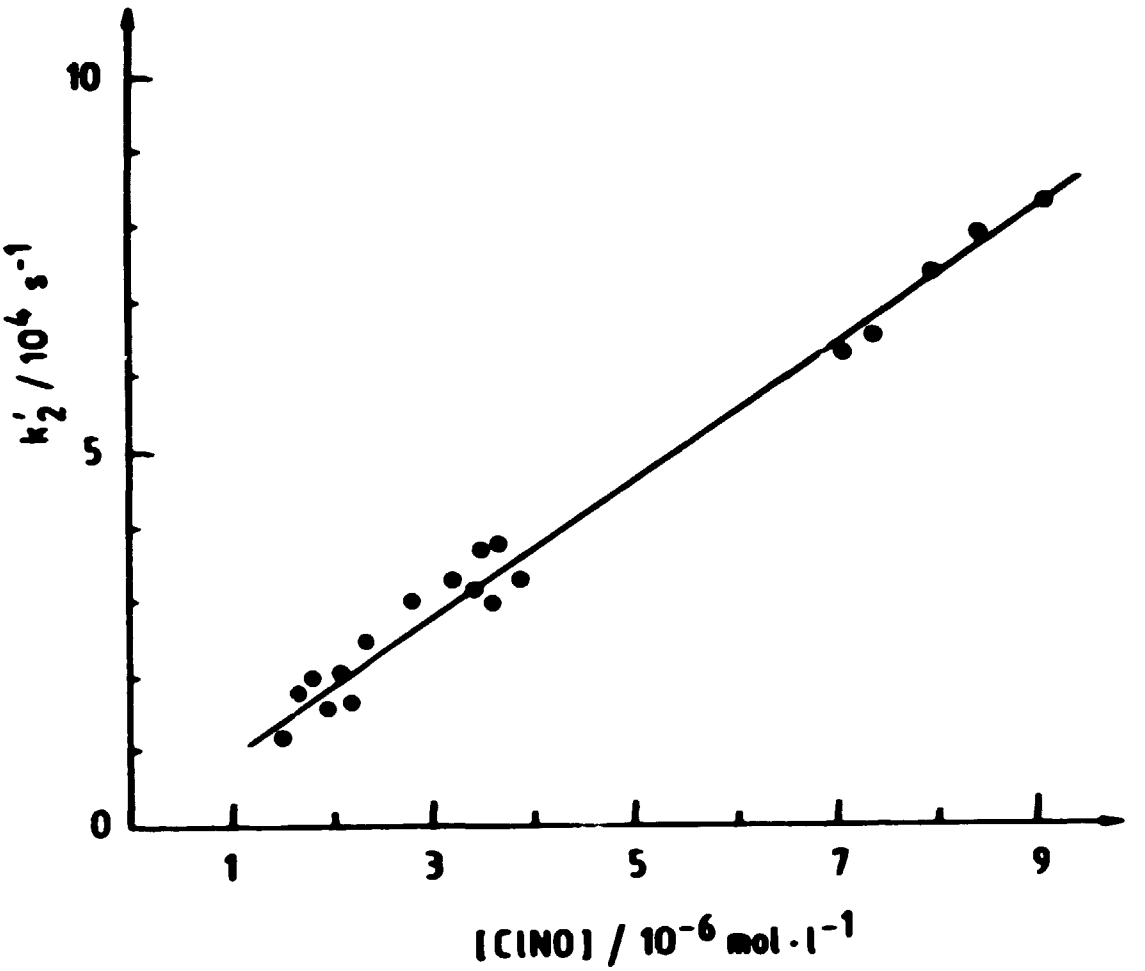

Figure 4.5. Pseudo-first-order rate constant for ClNO disappearance due to H + ClNO → HCl + NO.
$k_2' = -(d[ClNO]/dt)/([ClNO]_t - [ClNO]_{t=\infty})$.

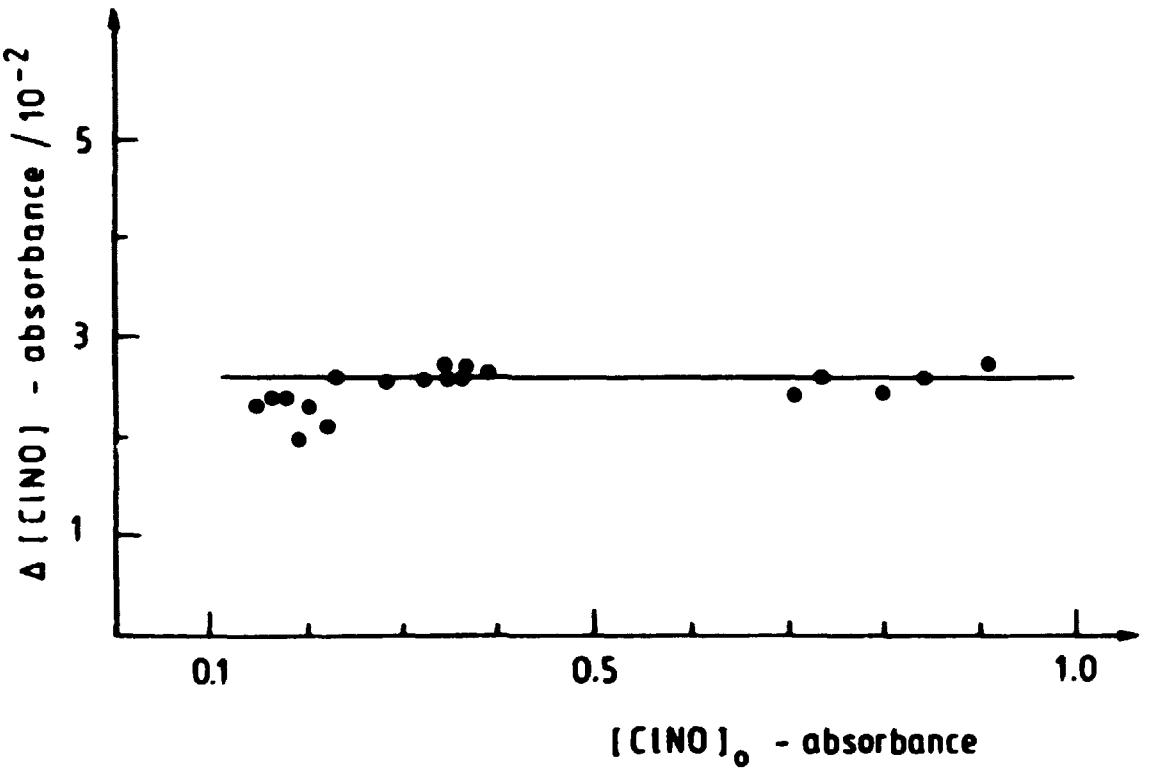

Figure 4.6. Change in ClNO absorbance after pulse radiolysis of H_2/ClNO mixtures (total pressure 1 atm) at various initial ClNO concentrations.

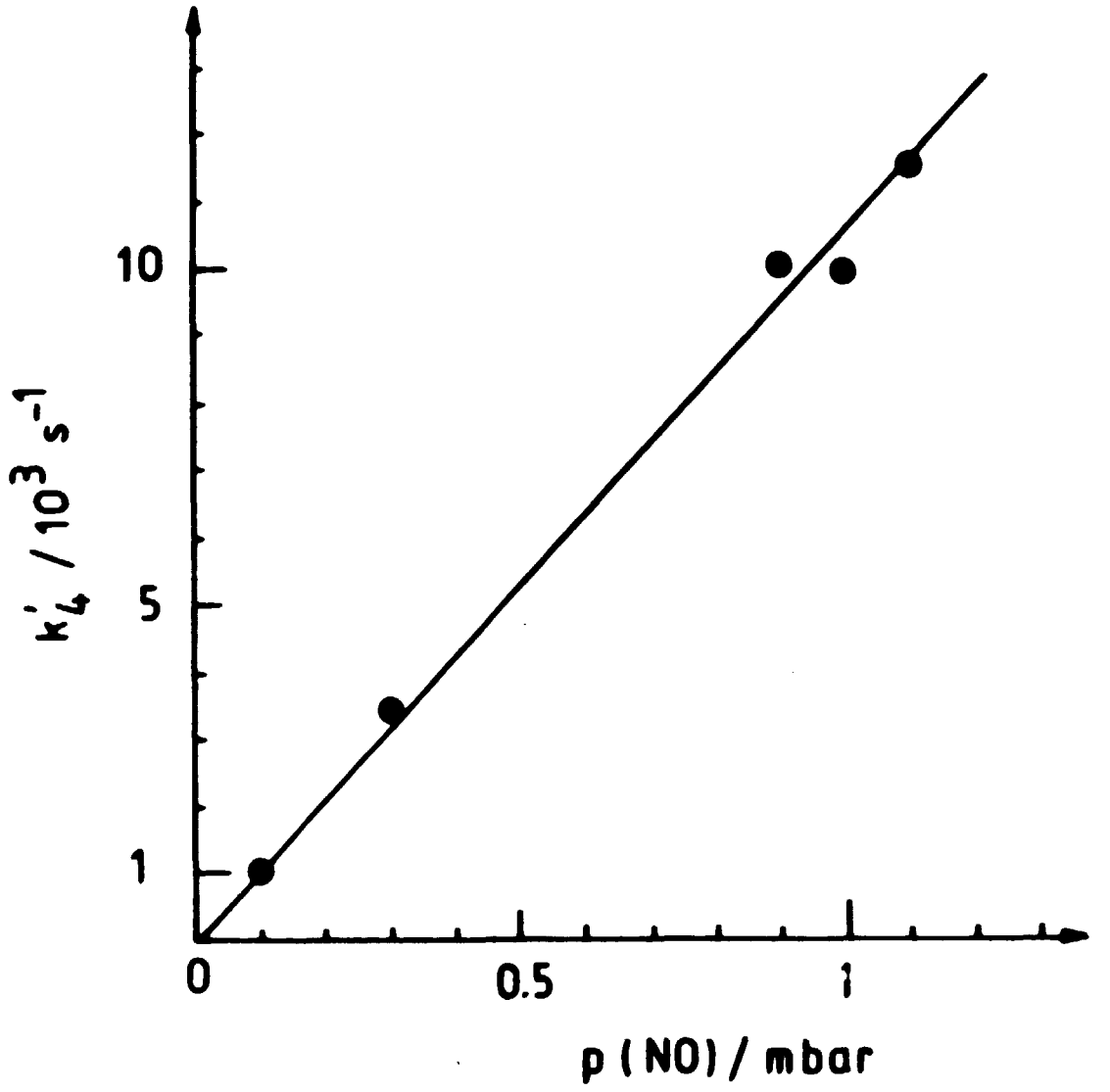

Figure 4.7. Pseudo-first-order rate constant for I_2 formation in the pulse radiolysis of H_2-HI-NO mixtures at various NO partial pressures (total pressure 1 atm). $k'_4 = (d[I_2]/dt)/([I_2]_{t=\infty} - [I_2]_t)$.

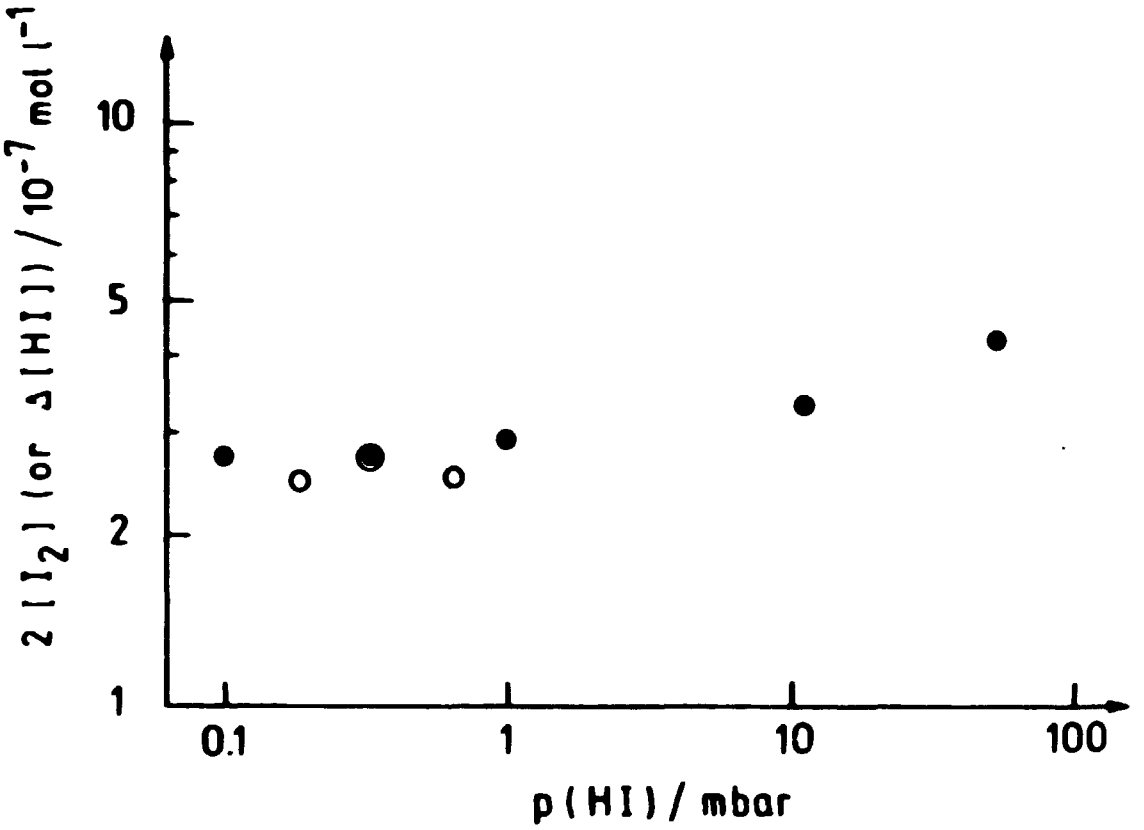

Figure 4.7. Pseudo-first-order rate constant for I_2 formation in the pulse radiolysis of H_2-HI-NO mixtures at various NO partial pressures (total pressure 1 atm). $k_4' = (d[I_2]/dt)/([I_2]_{t=\infty} - [I_2]_t)$.

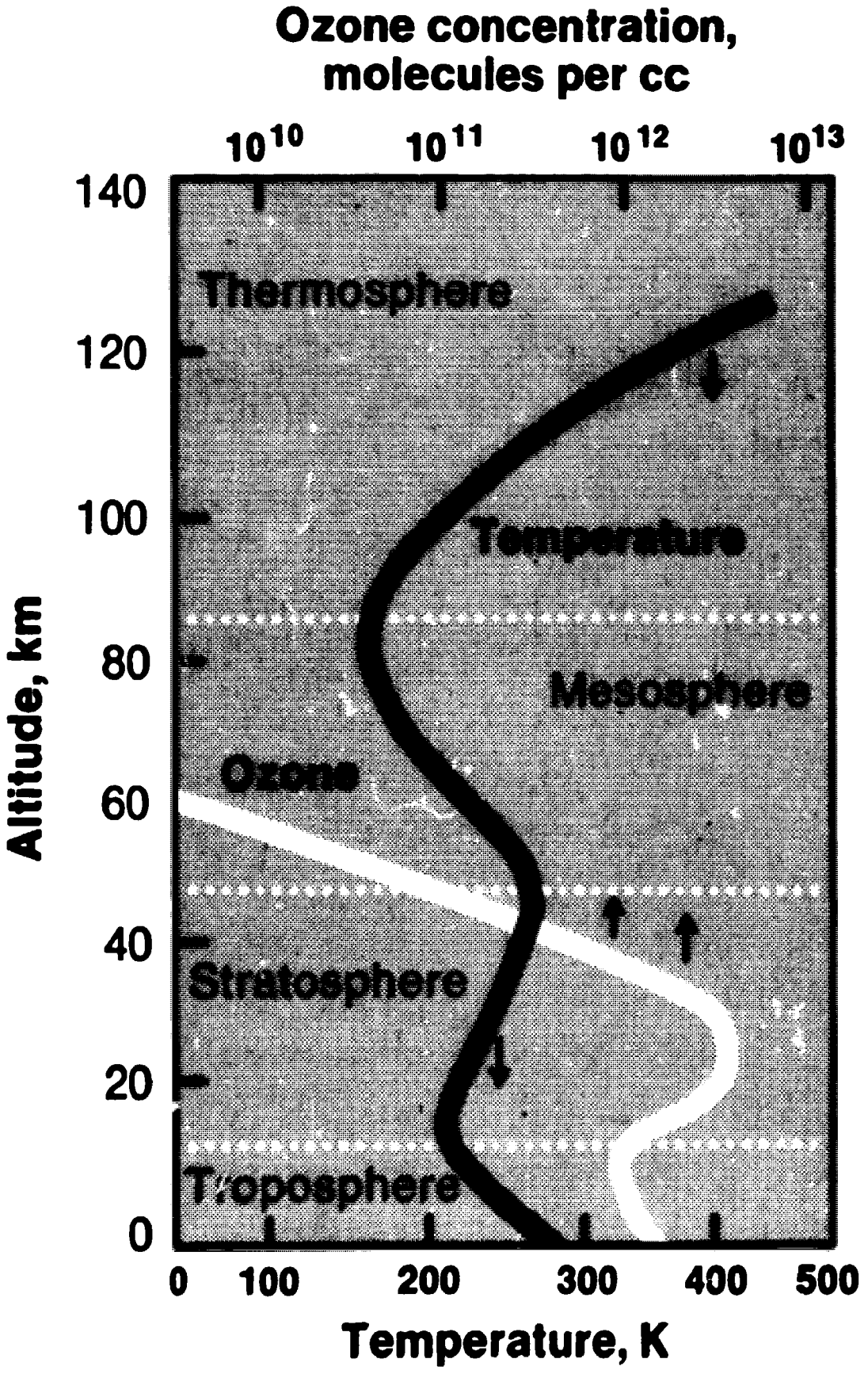

Figure 5.1. Ozone concentration and temperature variation with height in the atmosphere.

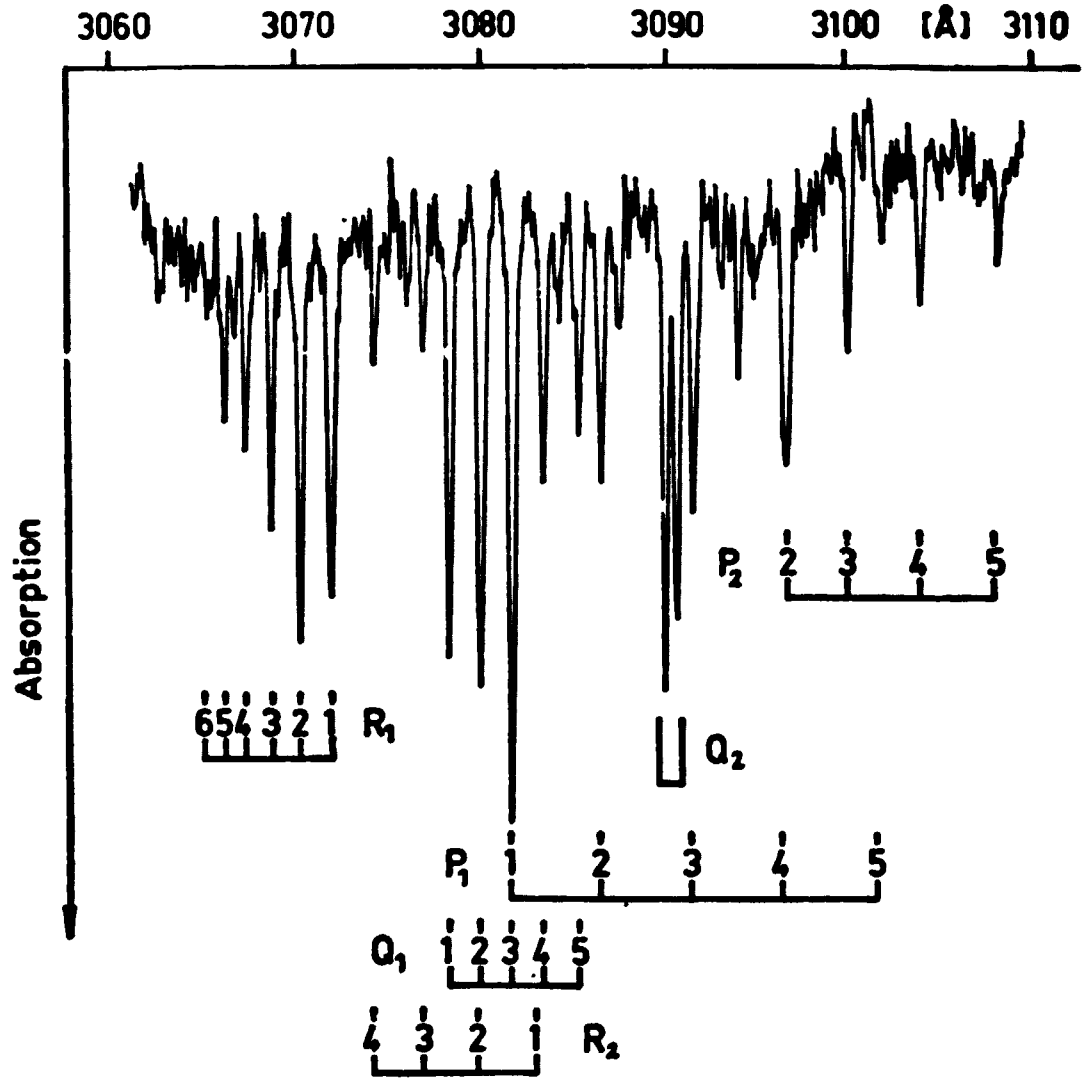

Figure 5.2. OH (0,0; $A^2\Sigma^+ \leftarrow X^2\Pi$) absorption band. (From Welge and Stuhl, 1967).

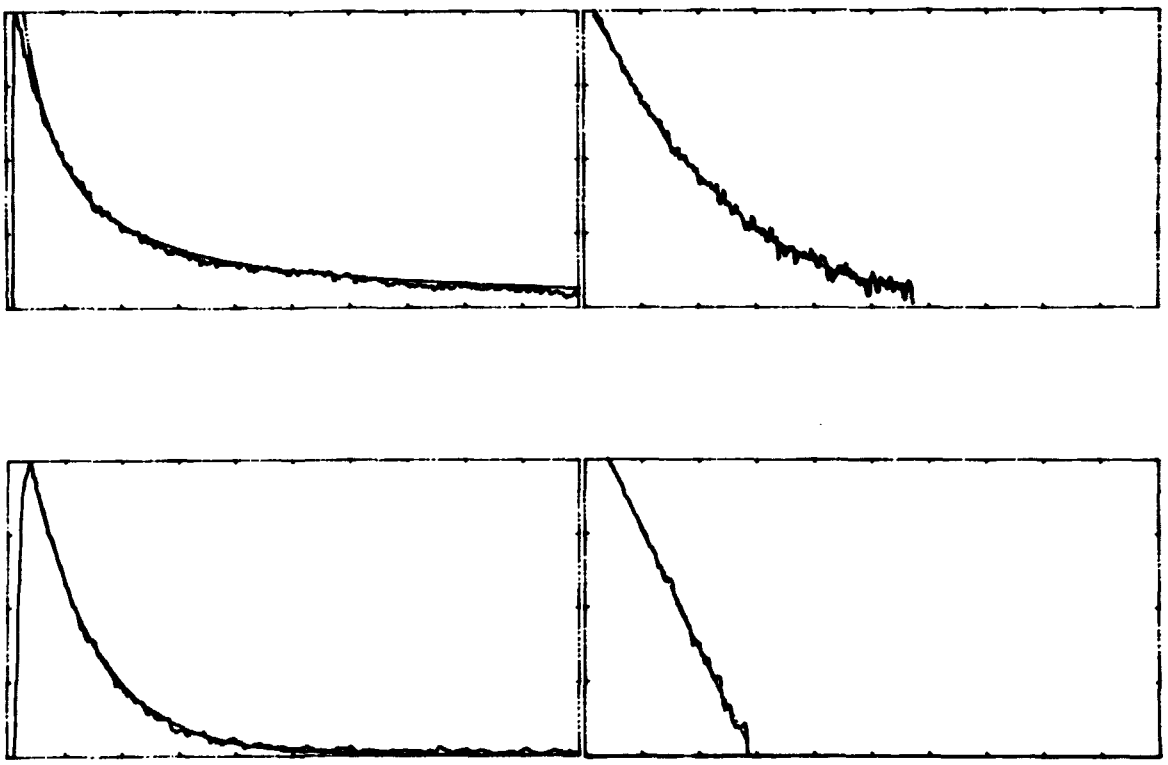

Figure 5.3. OH-kinetics in pulse radiolysis without and with a reactive substance added at a temperature of 400 K. Upper left: 200 mbar H_2O with Ar to 1 atm. Full timescale = 1000 μsec. Lower left: as upper left, but with 2.7 mbar C_2H_6 added and full timescale = 200 μsec. Upper right and lower right: logarithmic plots of the left side curves.

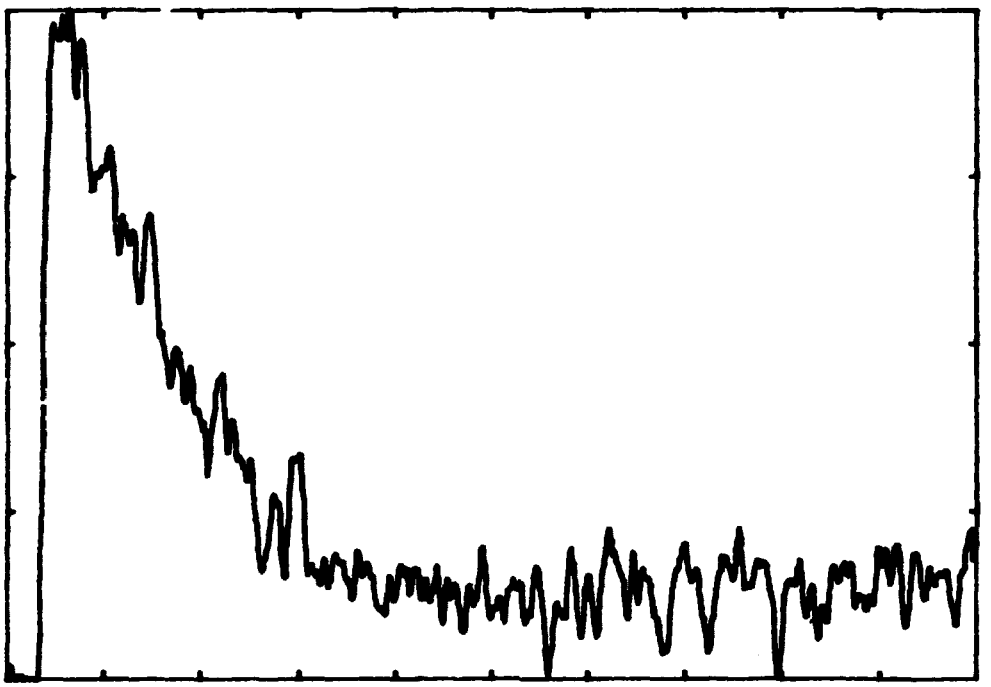

Figure 5.4. OH-decay in pulse radiolysis with 7.5 μmol tetramethyllead added to 20 mbar H_2O + Ar to 1 atm. Monitored at 3090 Å and T = 298±1 K. Abscissa is time, full timescale = 200 μs, and ordinate is normalized absorbance.

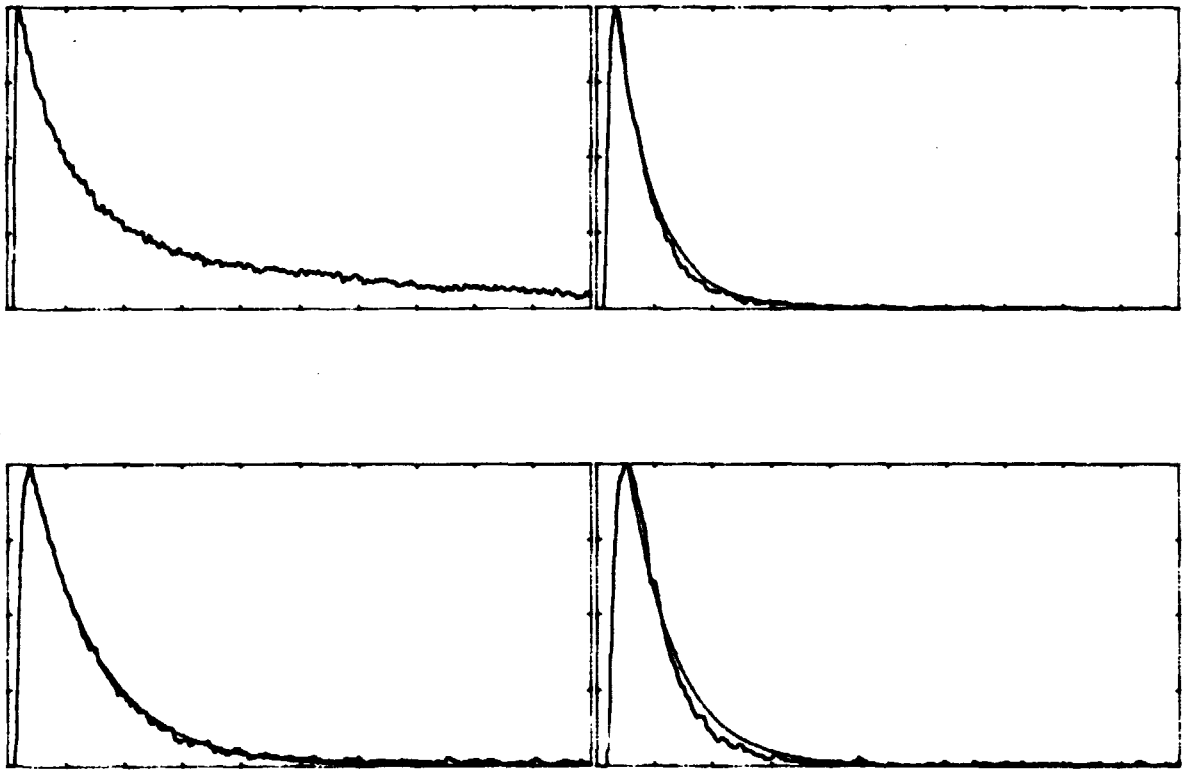

Figure 5.5. OH-decay in pulse radiolysis at 400 K. Upper left: 200 mbar H_2O + Ar to 1 atm. Full timescale = 1000 μsec. Lower left: with 2.7 mbar C_2H_6 added and full timescale = 200 μsec. Upper right: with 5.0 mbar C_2H_6 added and full timescale = 200 μsec. Lower right: with 9.6 mbar C_2H_6 added and full timescale = 100 μsec.

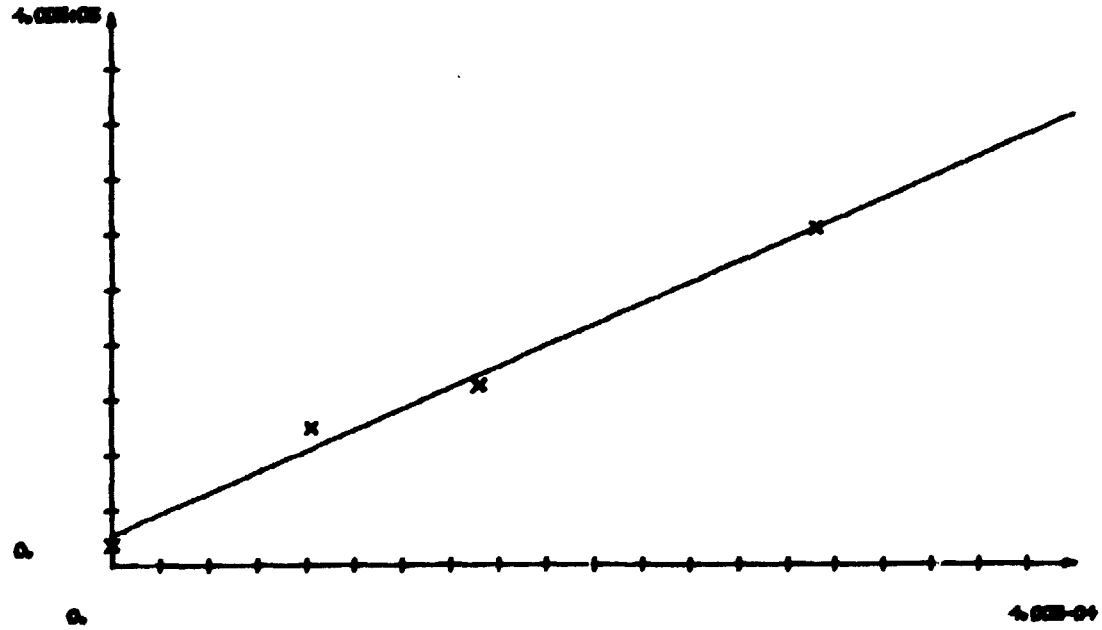

Figure 5.6. OH-reciprocal half-life in s^{-1} vs. C_2H_6 concentration in moles at 400 K.

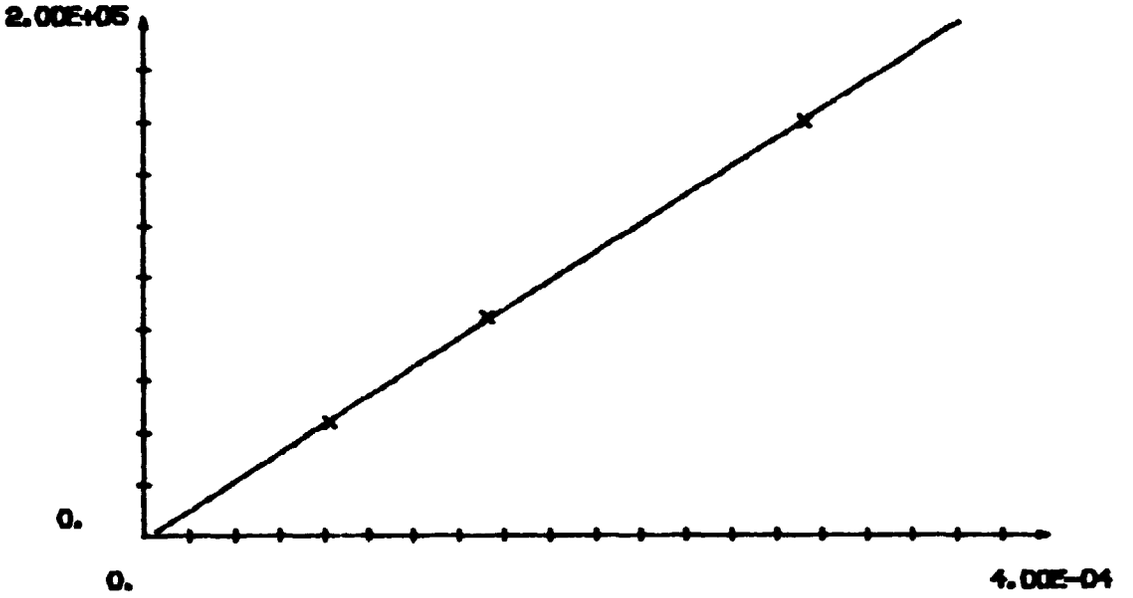

Figure 5.7. d(ln[OH])/dt vs. C_2H_6 concentration in moles at 400 K.

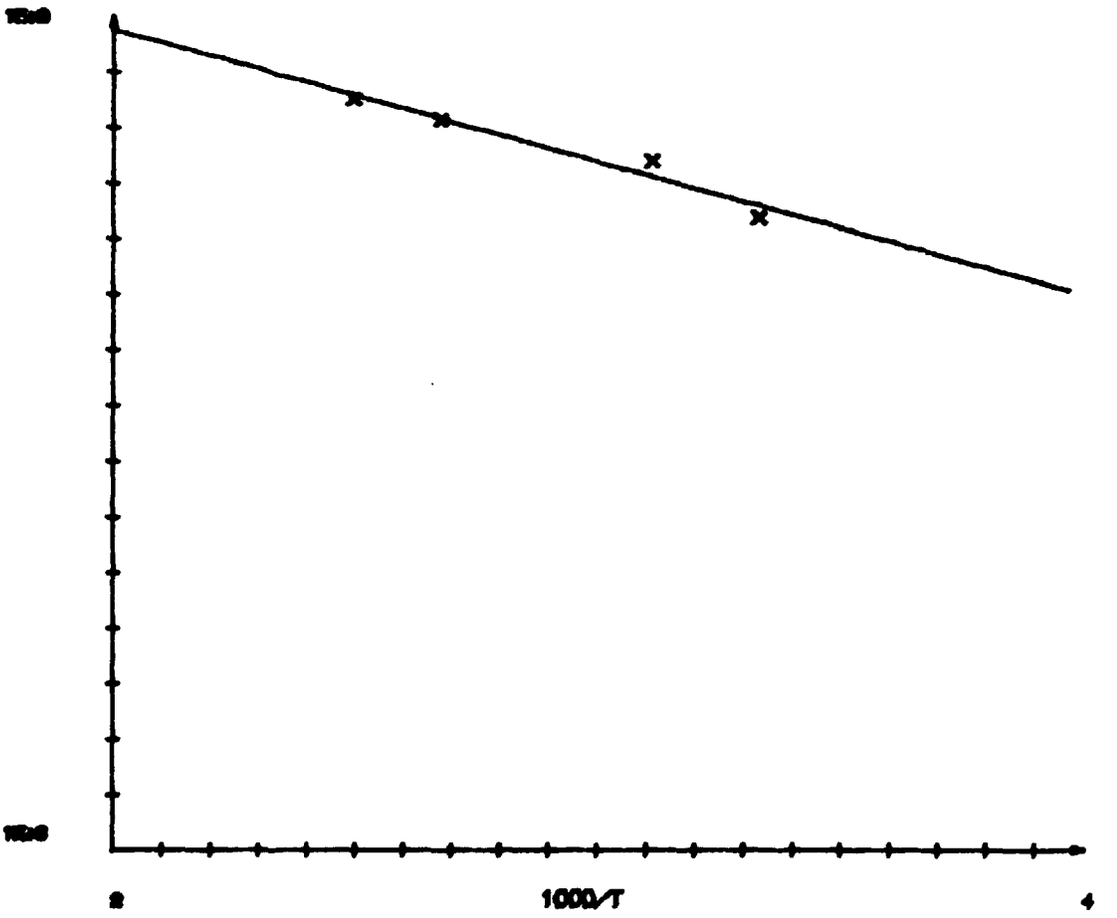

Figure 5.8. Arrhenius plot, k(OH + C_2H_6) in $M^{-1}s^{-1}$ vs. 1000/T in K^{-1}.

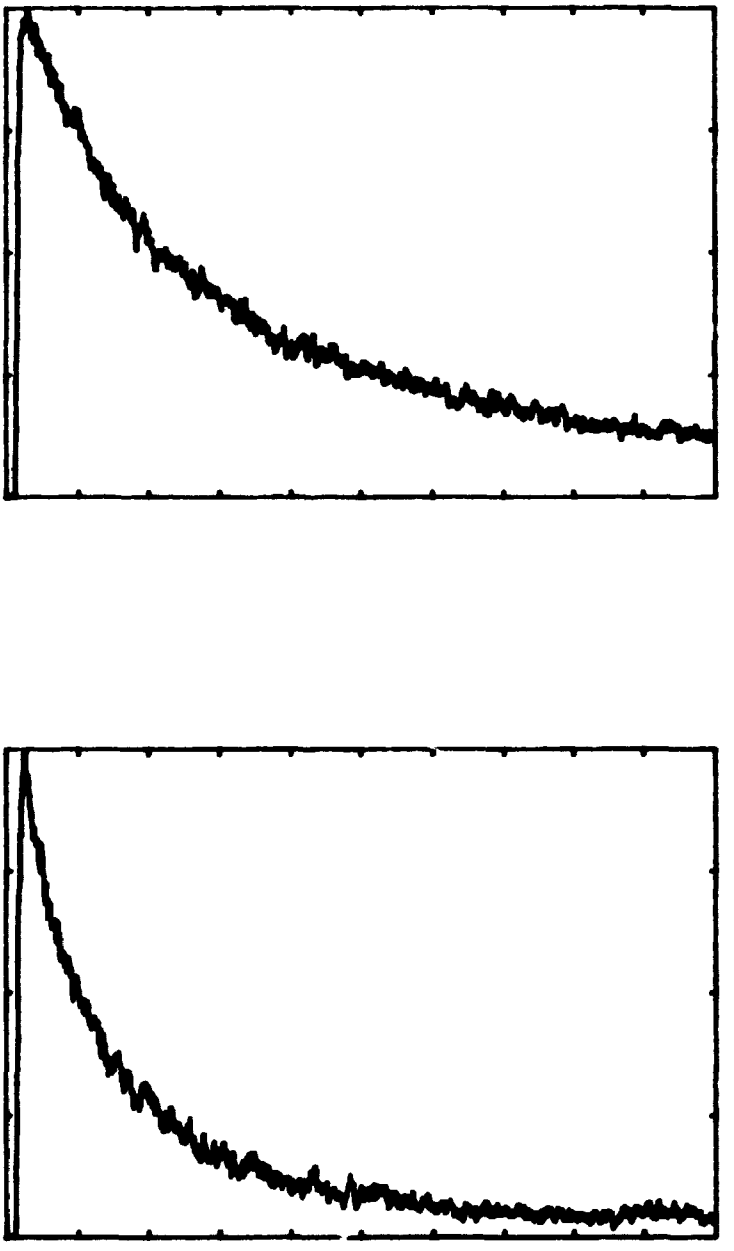

Figure 5.9. Top: OH-decay in 45 mbar H_2O + Ar to 1 atm at 348 K. Bottom: OH-decay in 50 mbar CF_2Cl_2 + 45 mbar H_2O + Ar to 1 atm at 348 K. full timescale = 400 μsec in both cases.

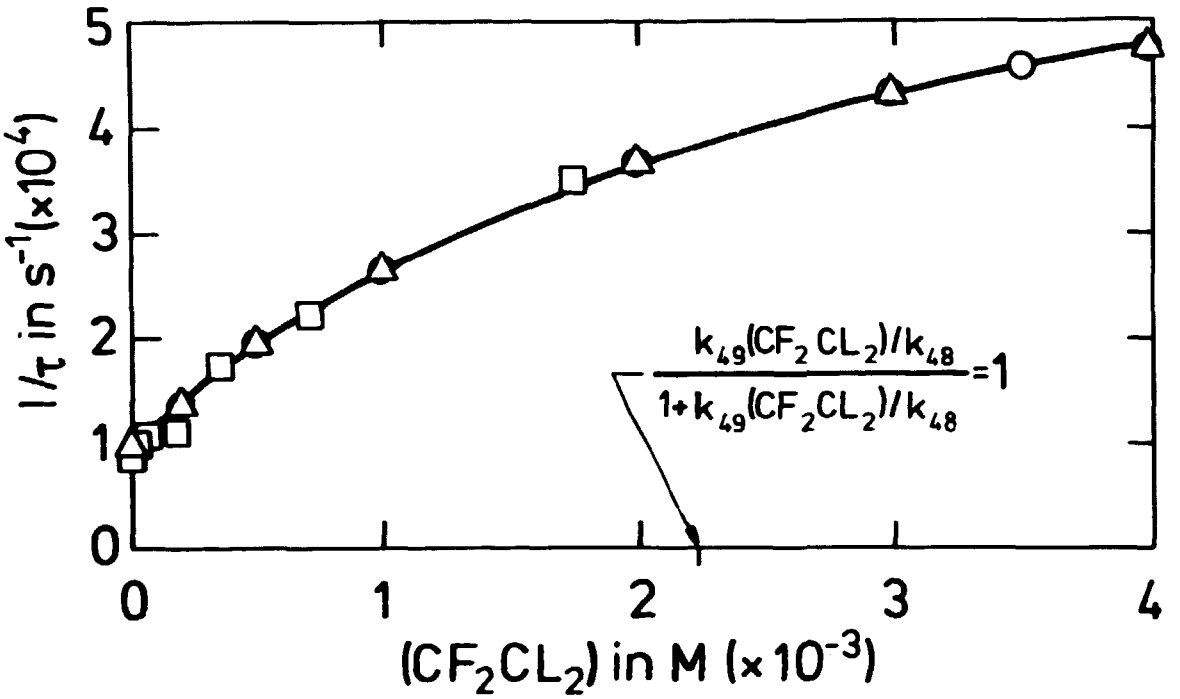

Figure 5.10. Reciprocal OH-halflife in $s^{-1}x10^4$ vs. CF_2Cl_2 concentration in $Mx10^{-3}$ at 348 K. (□): experimental values, (o): results from a computer simulation, (Δ): results from the analytical expression.

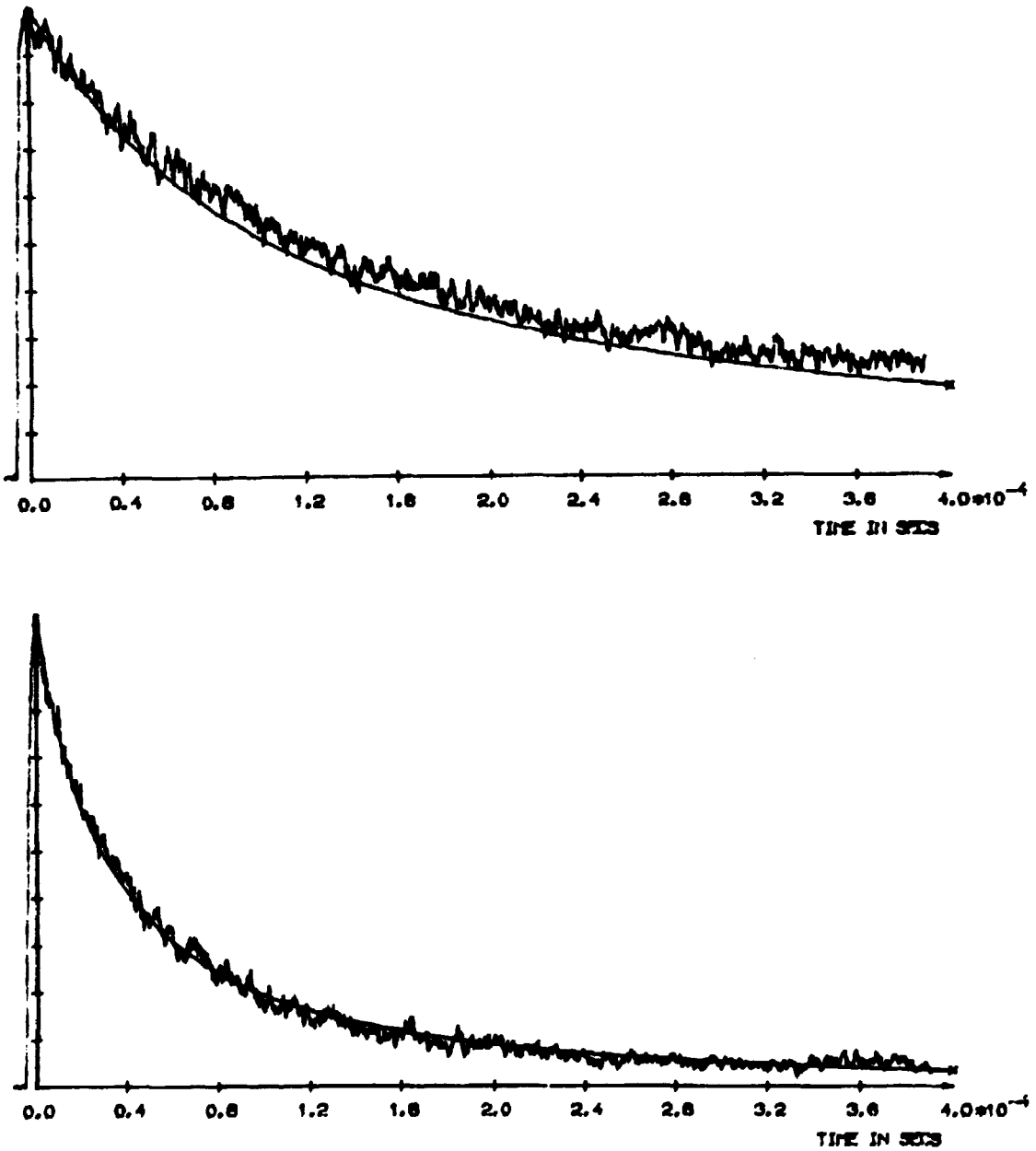

Figure 5.11. Third body effect on the combination reaction, OH + OH + CF_2Cl_2 → H_2O_2 + CF_2Cl_2. Top: OH-decay without CF_2Cl_2 at 348 K. Bottom: OH-decay in the presence of 50 mbar CF_2Cl_2. Computer simulation curve on top of the experimental curve in both cases.

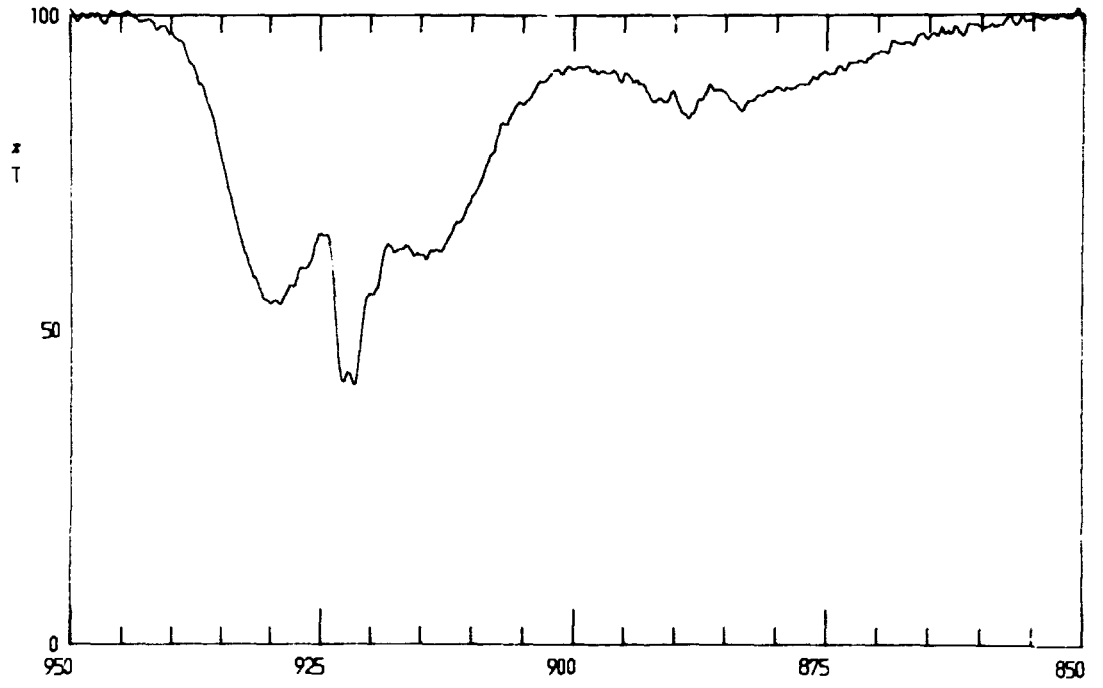

Figure 5.12. Detail of the CF_2Cl_2 IR-spectrum. Abscissa is wavenumber in cm^{-1} and ordinate is %-transmittance.

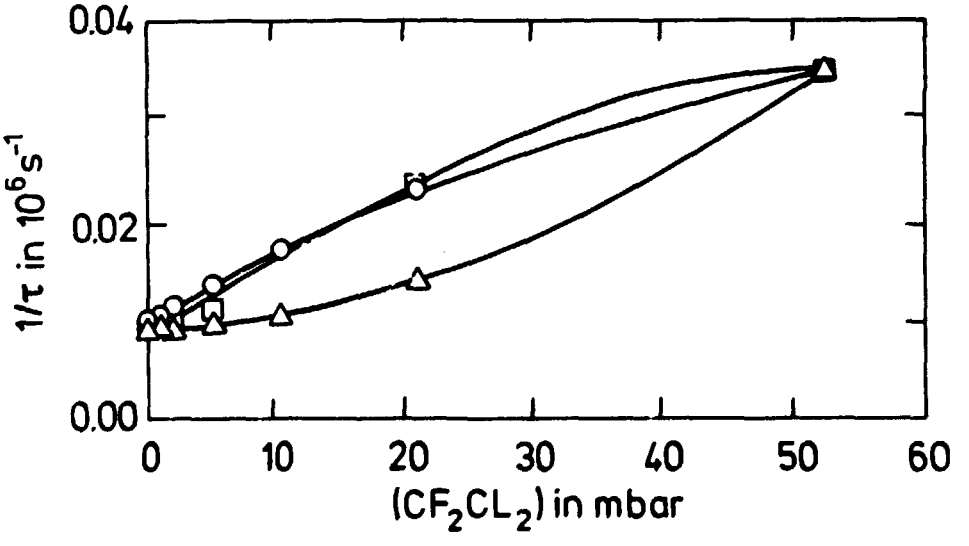

Figure 5.13. Comparison of experimental (□) reciprocal OH-halflives in $s^{-1}x10^{-6}$ vs. partial pressures of CF_2Cl_2 concentrations in mbar with the results of two computer simulations: (o) the third body model and (Δ) the direct fragmentation model.

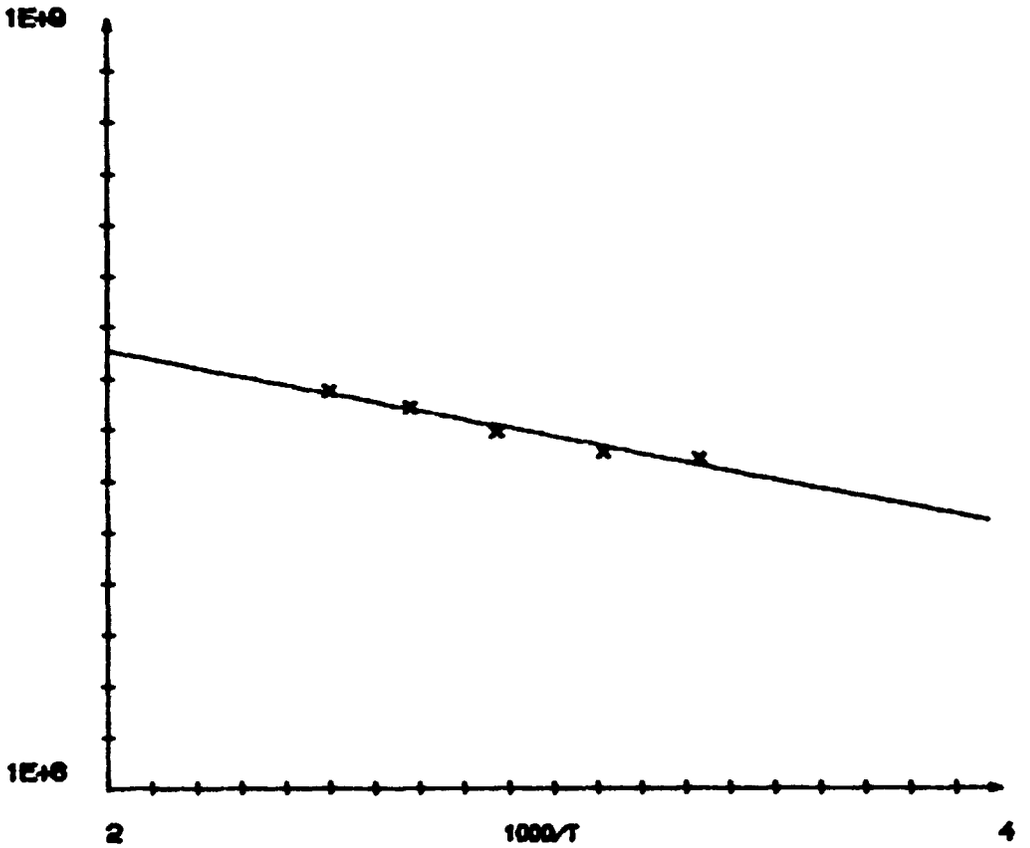

Figure 5.14. Arrhenius plot, k(OH + CH_4) in $M^{-1}s^{-1}$ vs. 1000/T in K^{-1}.

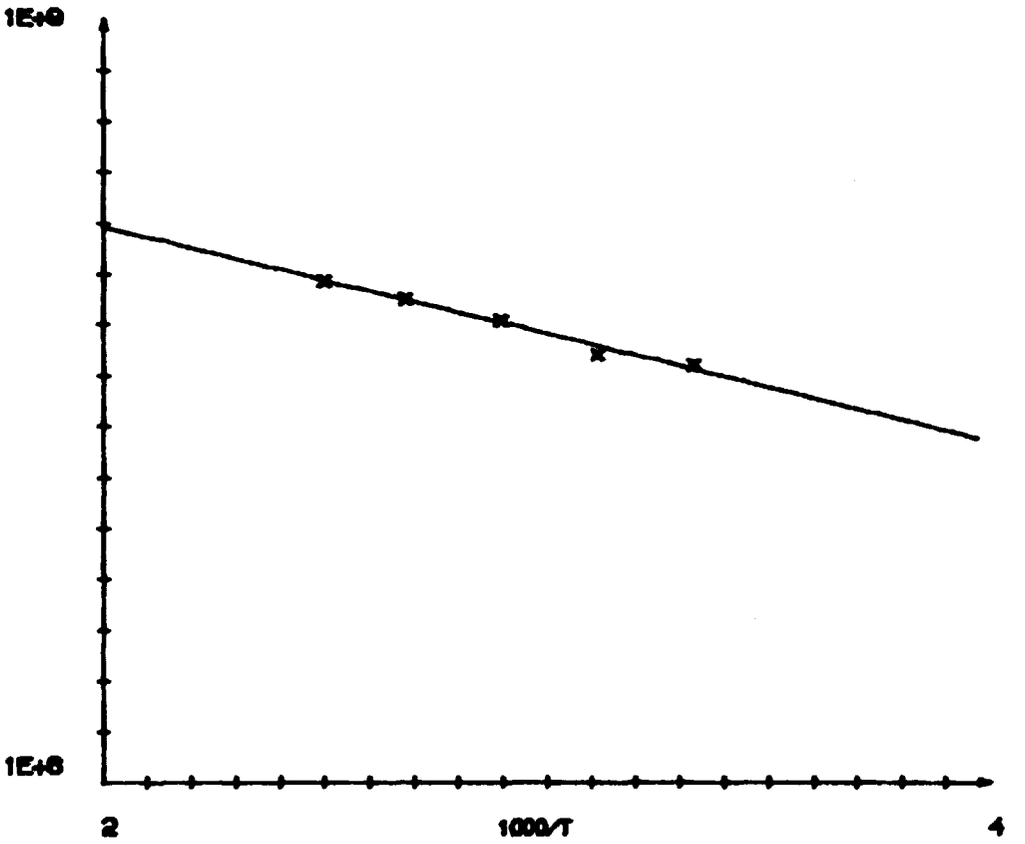

Figure 5.15. Arrhenius plot, k(OH + CH_3Cl) in $M^{-1}s^{-1}$ vs. 1000/T in K^{-1}.

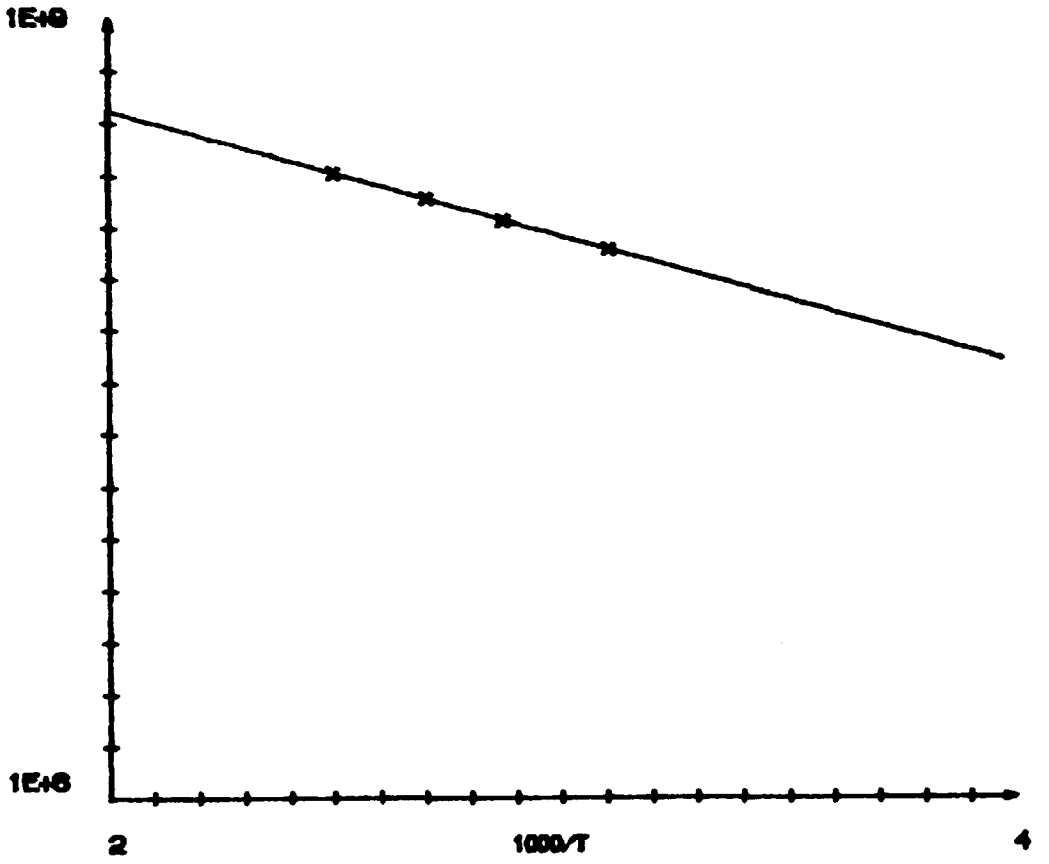

Figure 5.16. Arrhenius plot, k(OH + CH_2Cl_2) in $M^{-1}s^{-1}$ vs. 1000/T in K^{-1}.

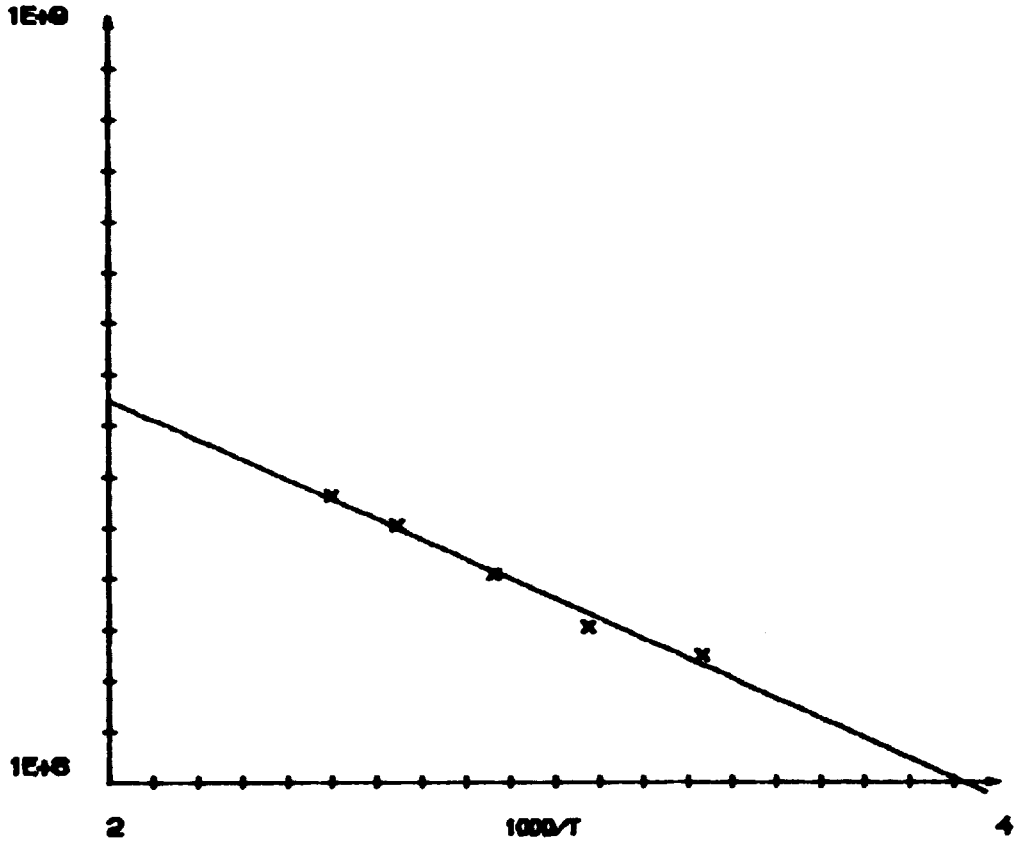

Figure 5.17. Arrhenius plot, k(OH + $CHClF_2$) in $M^{-1}s^{-1}$ vs. 1000/T in K^{-1}.

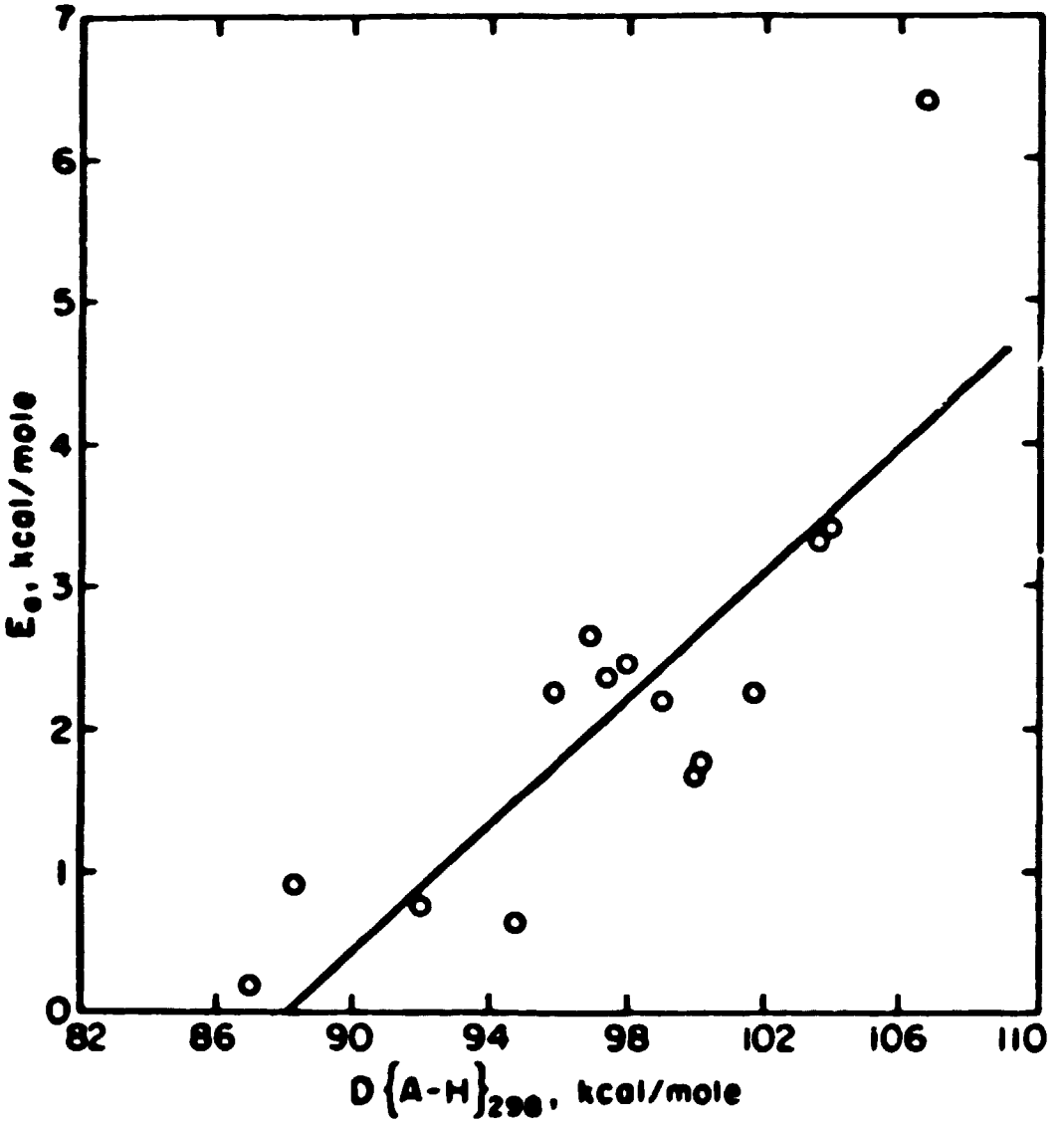

Figure 5.18. Plot of observed activation energy for H abstraction reactions by OH radicals vs. bond dissociation enthalpy at 298 K for compounds with equivalent reacting H-atoms. (Heicklen, 1981).

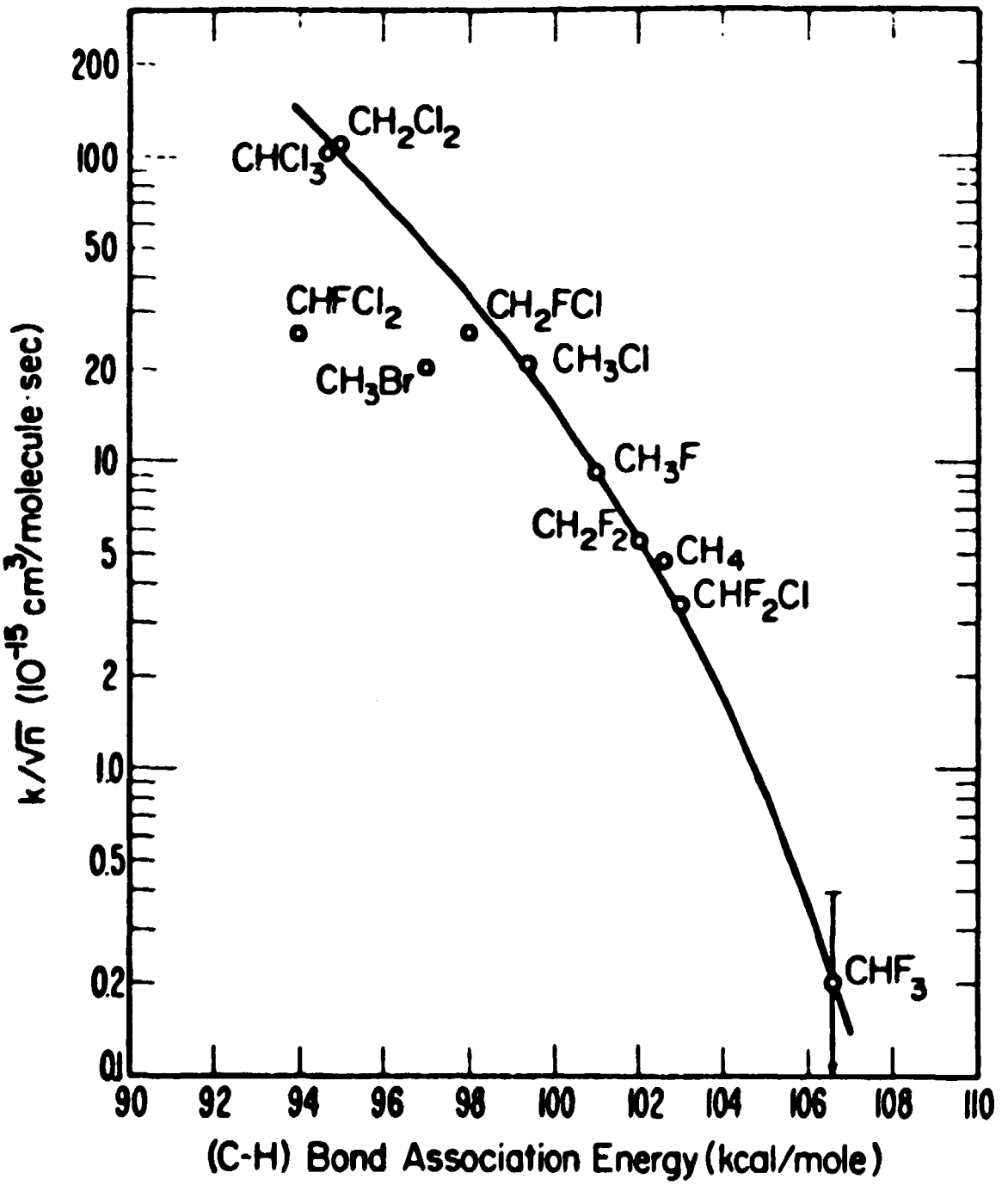

Figure 5.19. Semilog plot of measured rate constants for H-abstraction by OH-radicals divided by $\sqrt{n}$ (where n is the number of H-atoms in the molecule) vs. the C-H bond energy. (Howard and Evenson, 1976).

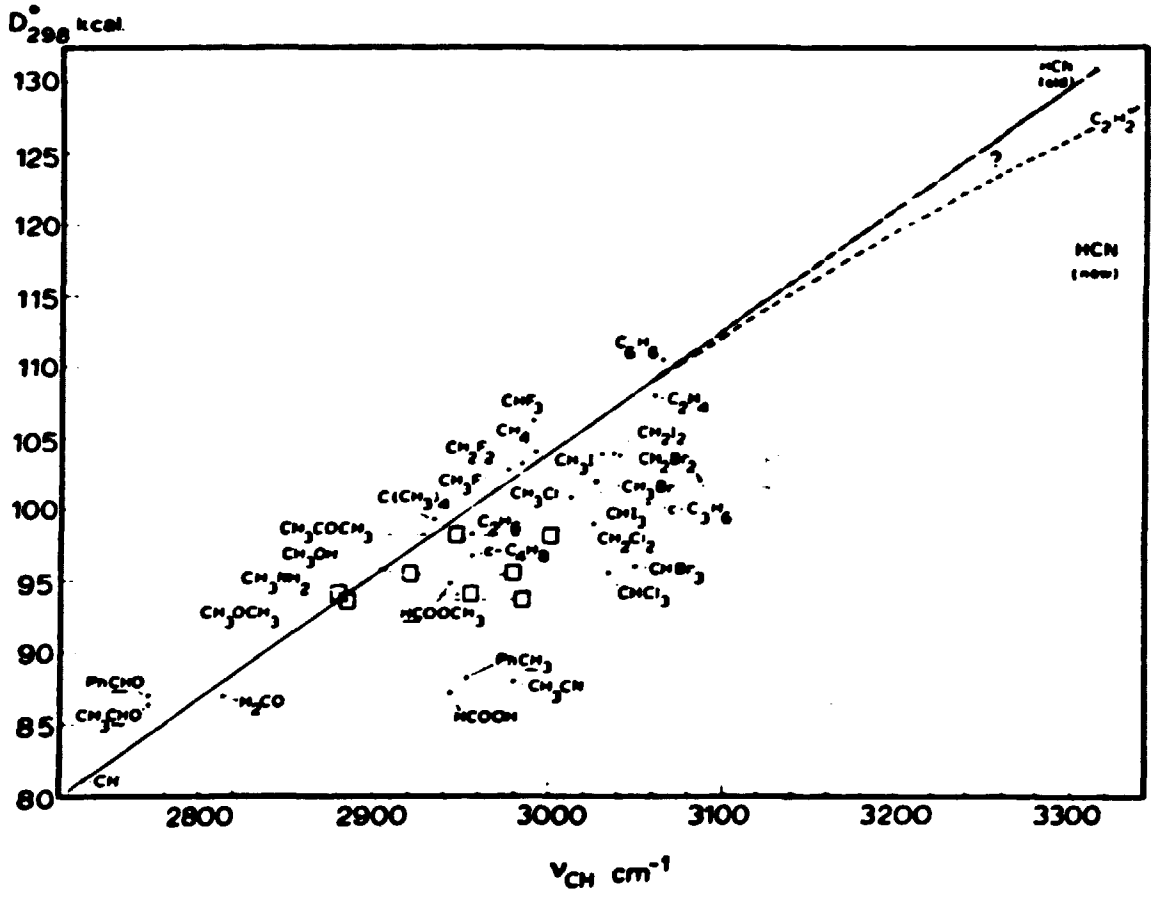

Figure 5.20. Correlation between ν(CH) stretching wavenumbers and D°_{298} dissociation energy. (McKean, 1978).

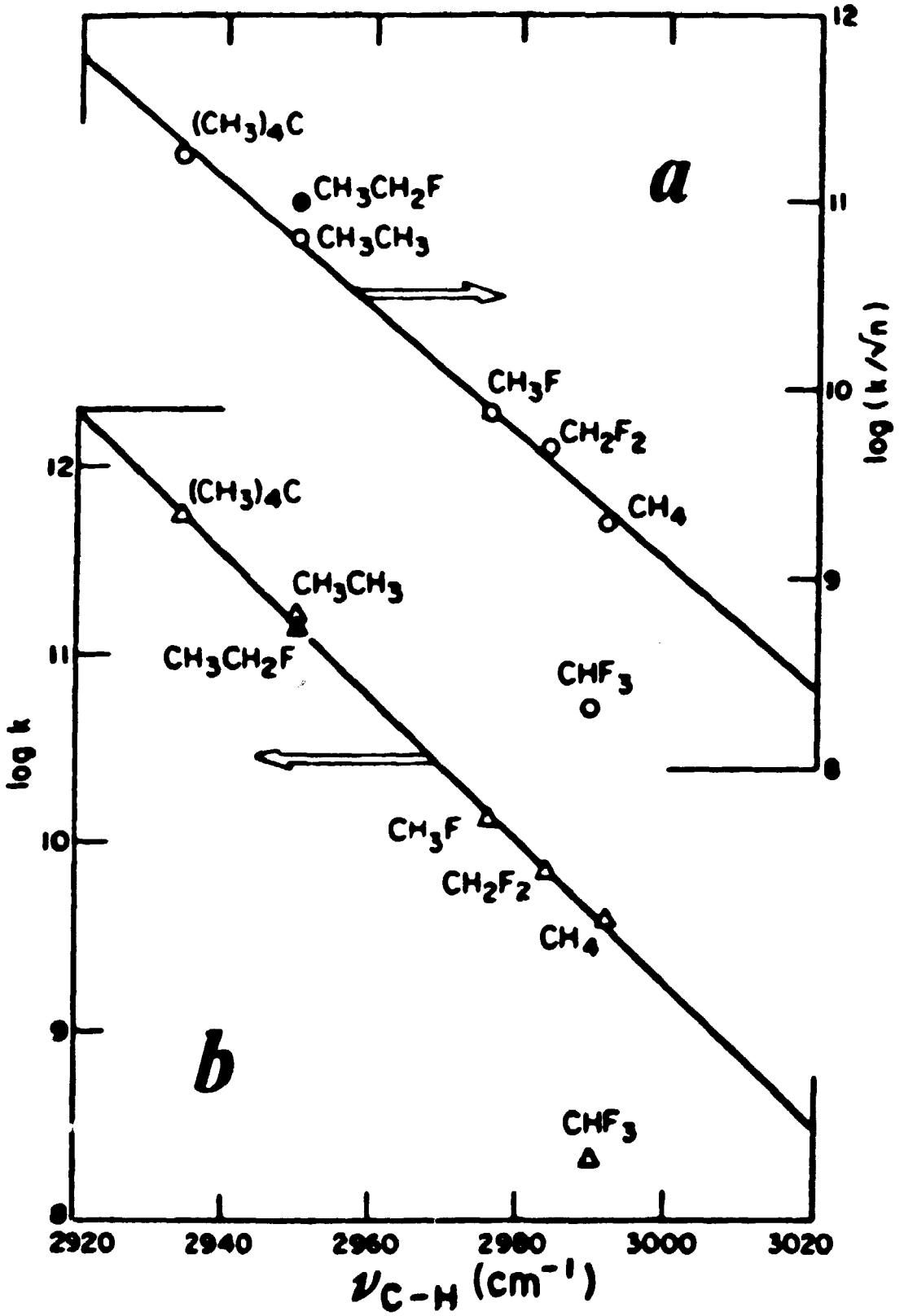

Figure 5.21. (a) Correlation of log(k/√n) with the stretching wavenumber ν(CH); (b) correlation of log(k) with the stretching wavenumber ν(CH); where k is the OH rate constant and n the number of H-atoms in the molecule. (Nip et al., 1979).

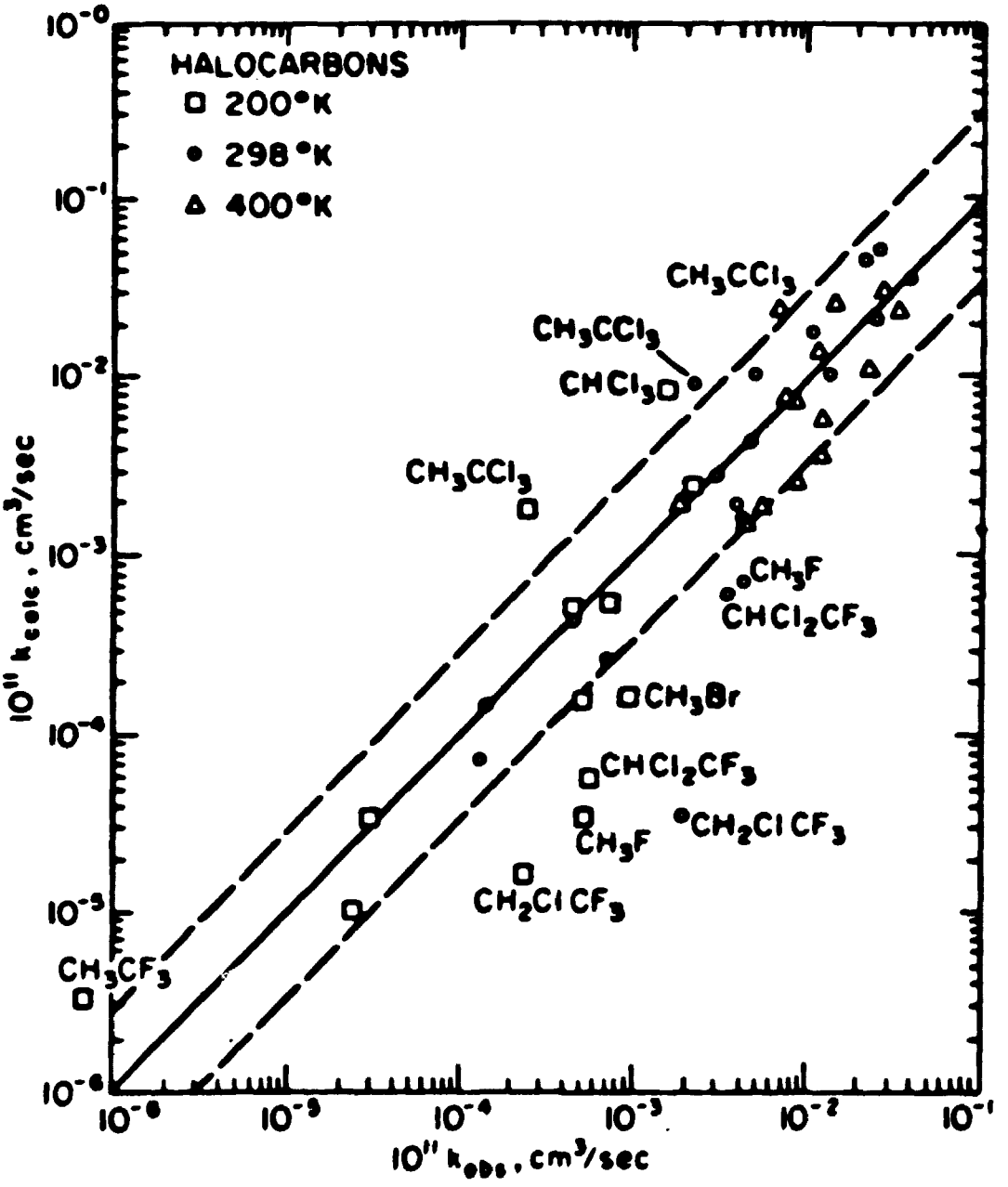

Figure 5.22. Comparison of observed and predicted rate constants for the reaction between OH and haloalkanes. Solid line - a perfect fit; dashed lines - factors of ±3 deviation from perfection. (Heicklen, 1981).

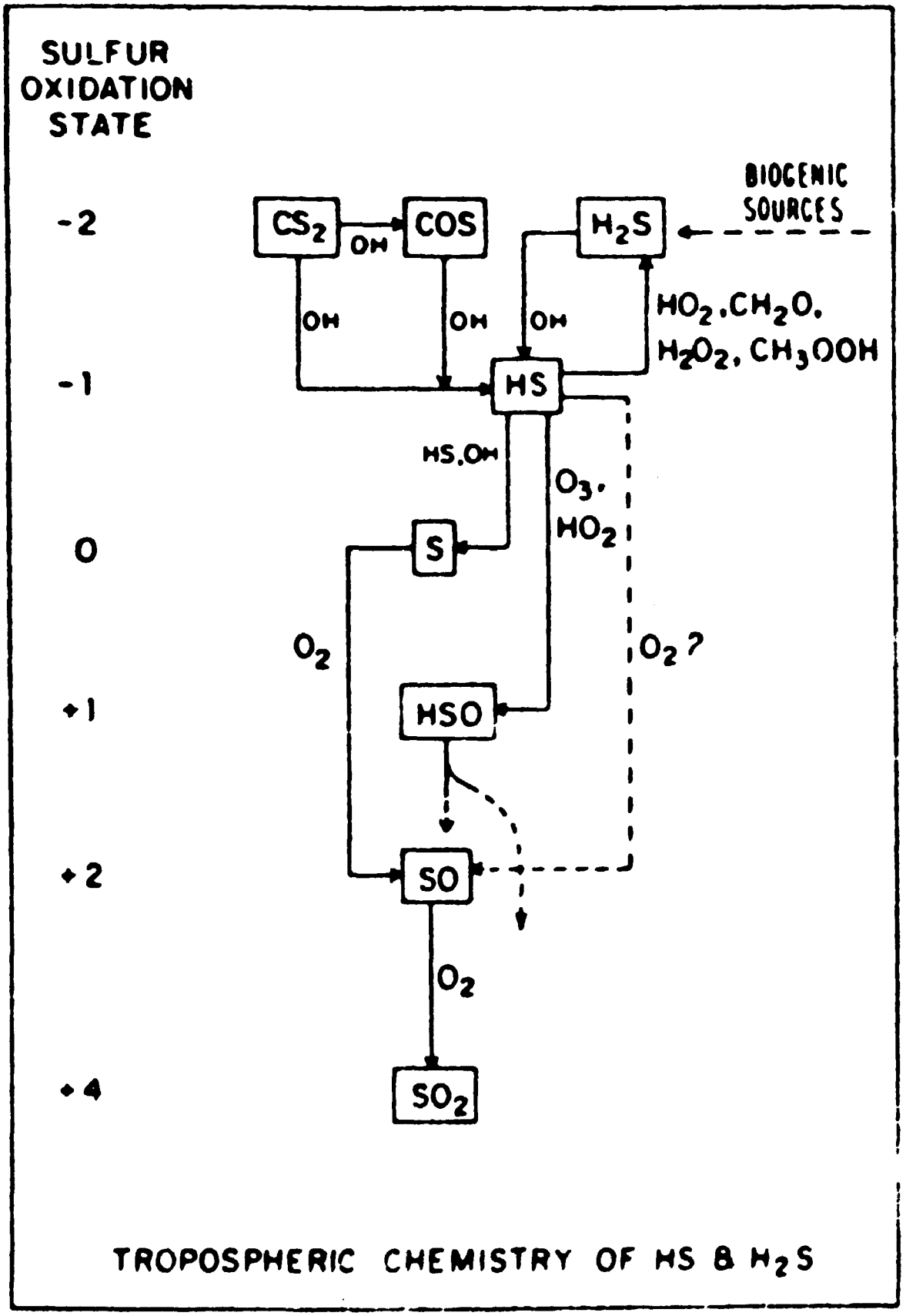

Figure 6.1. Schematic diagram for the chemical transformations of HS in the troposphere. (McElroy et al., 1980).

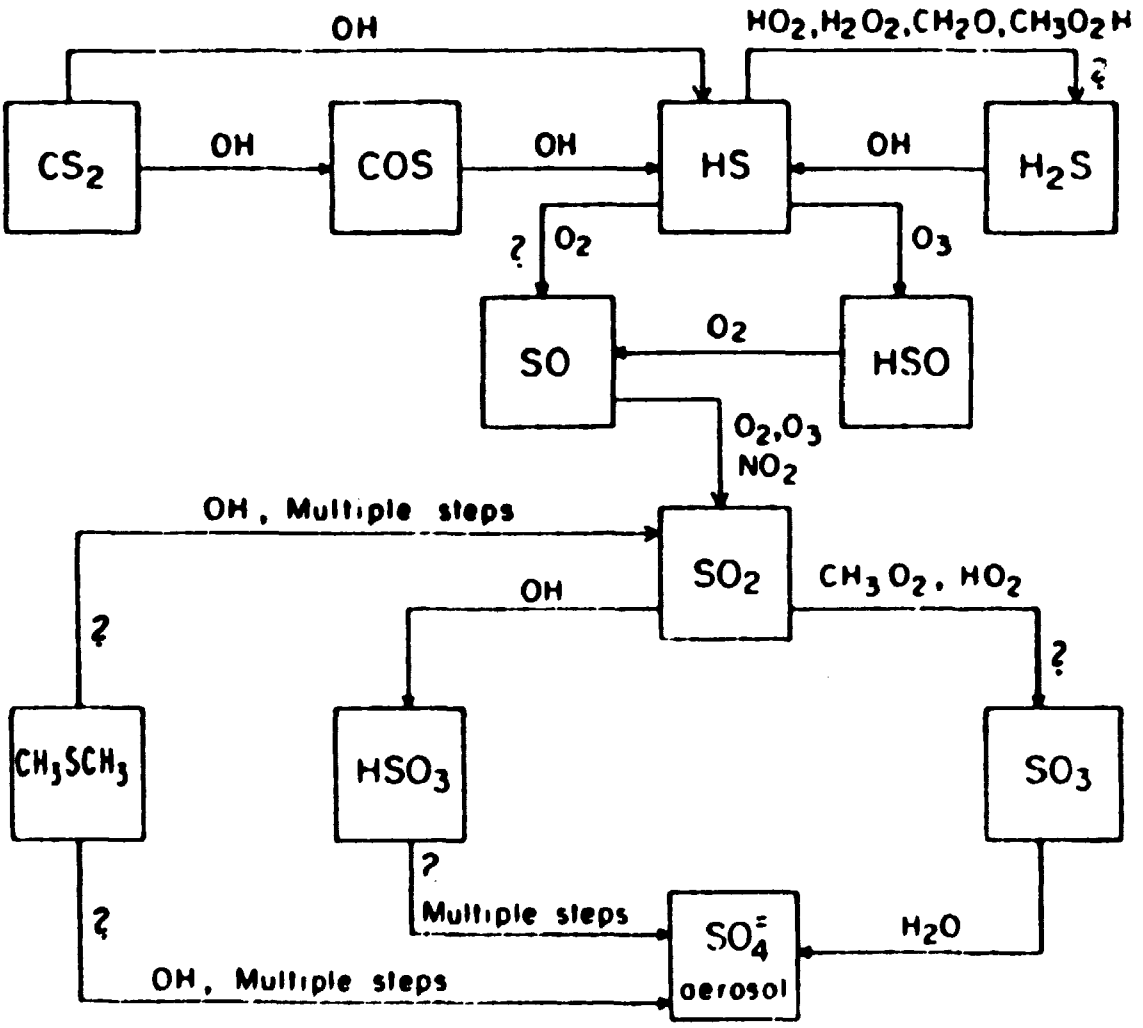

Figure 6.2. Schematic diagram for the major chemical transformations of sulfur compounds. Pathway for which detailed mechanisms have yet to be identified are labelled by question marks. (Sze and Ko, 1980).

	H	H_2S	HS	H_2S_2	S	S_2	HS_2	H_2
H	11	12	13	14	15	16	17	-
H_2S		-	23	-	25	-	-	-
HS			33	34	35	36	37	38
H_2S_2				-	45	-	-	-
S					55	56	57	58
S_2						66	67	-
HS_2							77	78
H_2								-

Figure 6.3. Quadratic array showing the reactions considered in the pulse radiolysis of H_2S and their numbering used in chapter 6.

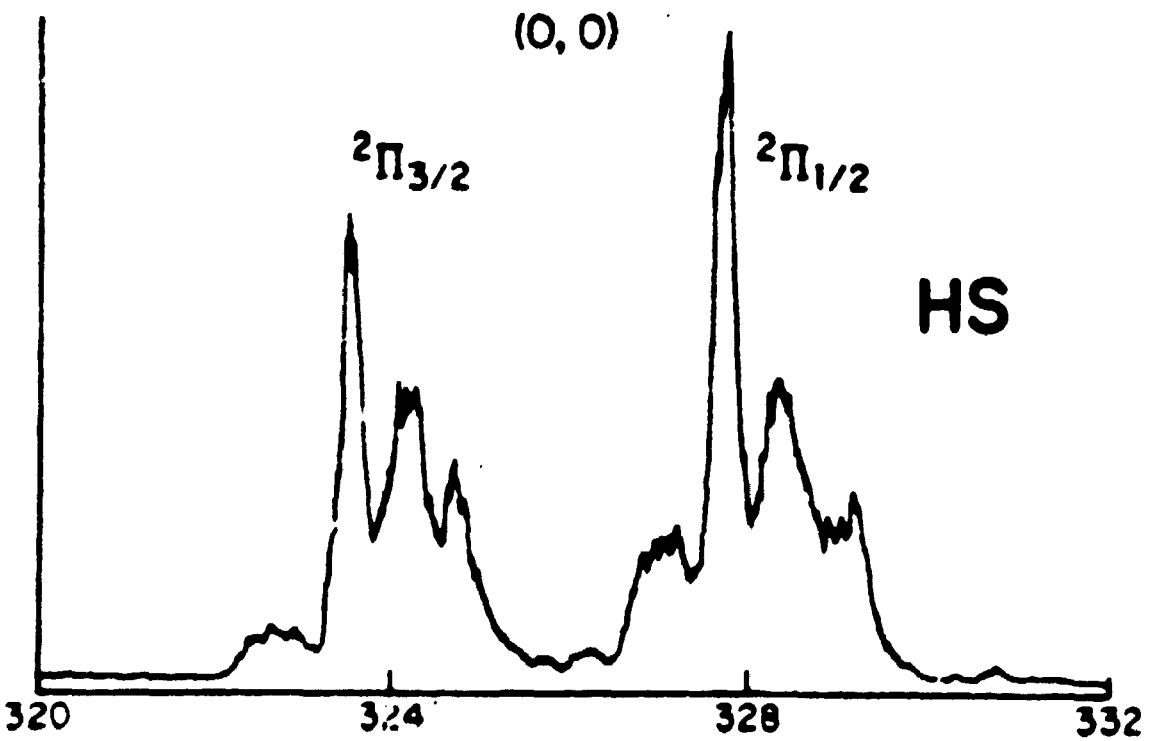

Figure 6.4. Emission spectrum of the HS-transitions used for monitoring the HS-radical. (Tiee, 1981).

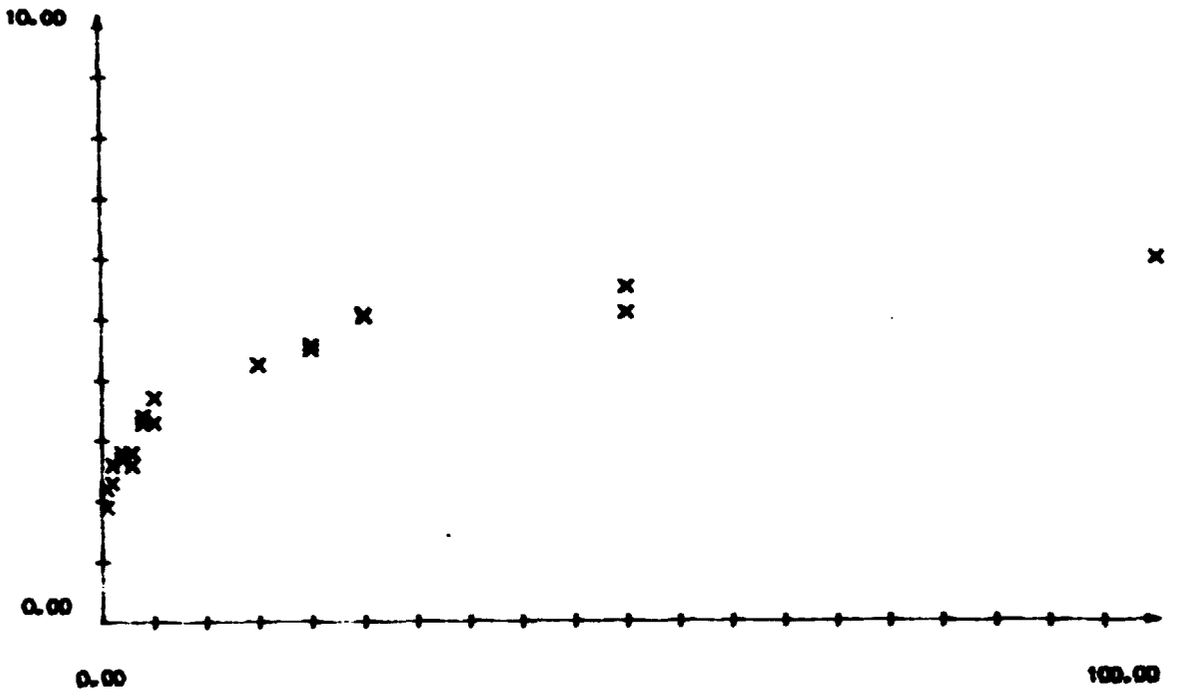

Figure 6.5. Yield of HS in H_2S-Ar mixtures measured by the maximum HS-absorbance at 3241 Å. Abscissa is H_2S partial pressures in mbar and ordinate is 100 × A_{max}.

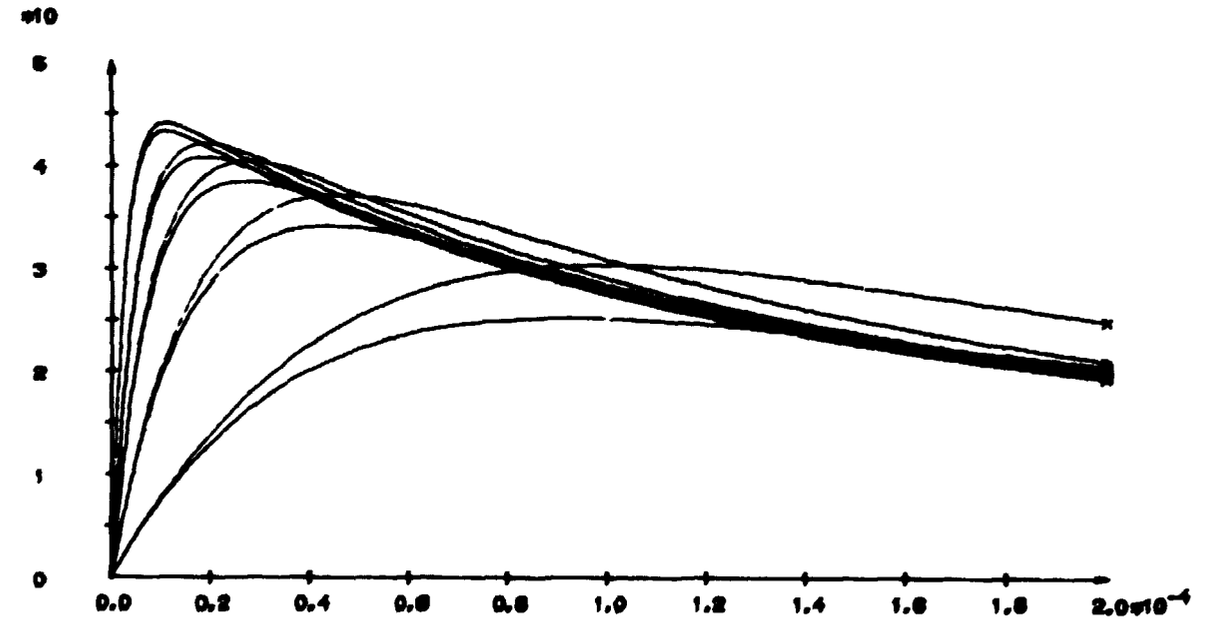

Figure 6.6. Computer simulations of HS-formation and decay for 5 different H_2S-concentrations, with 2 different models for each H_2S-concentration. Units: HS-concentration in M vs. time in s.

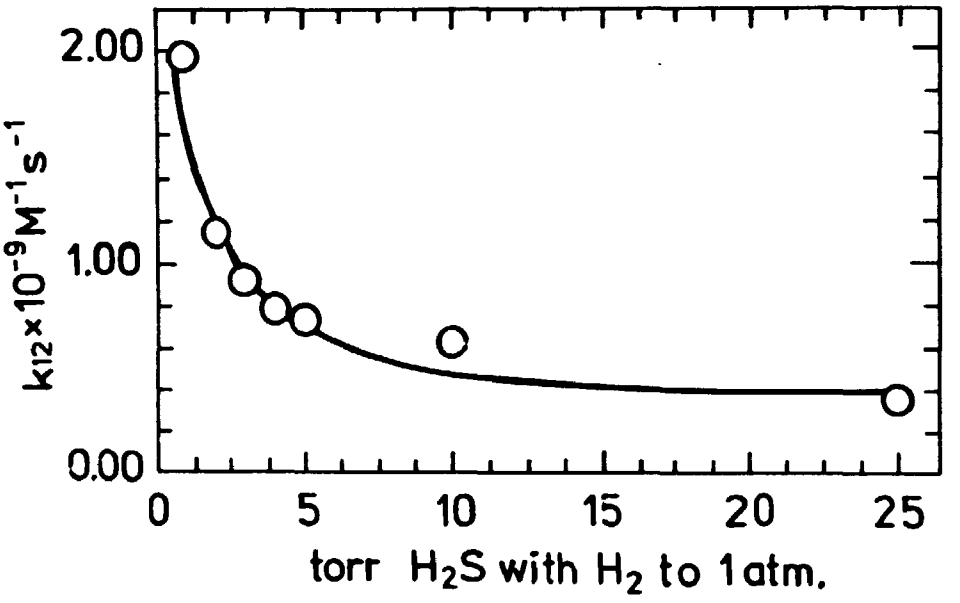

Figure 6.7. Derived values of k(H + H_2S → H_2 + HS) vs. H_2S partial pressure in torr.

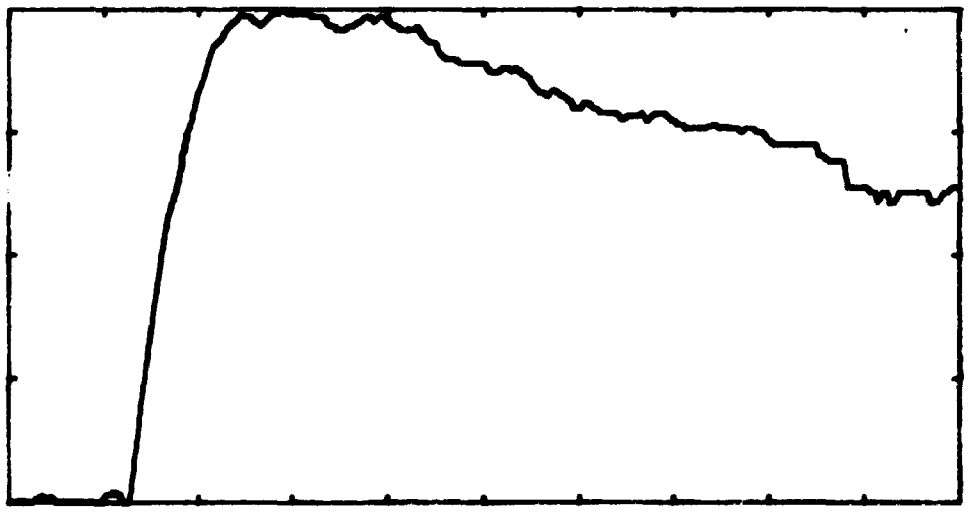

Figure 6.8. HS-formation and decay in 1 atm H_2S monitored at 3241 Å, T = 298±1 K and full timescale = 20 μsec.

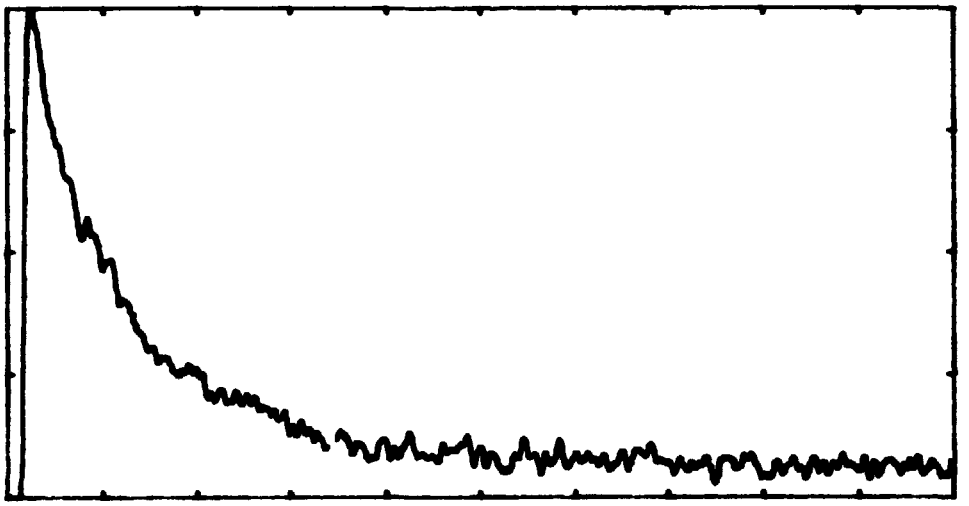

Figure 6.9. HS-formation and decay in 1 atm H_2S monitored at 3241 Å, T = 298±1 K and full timescale = 400 μsec.

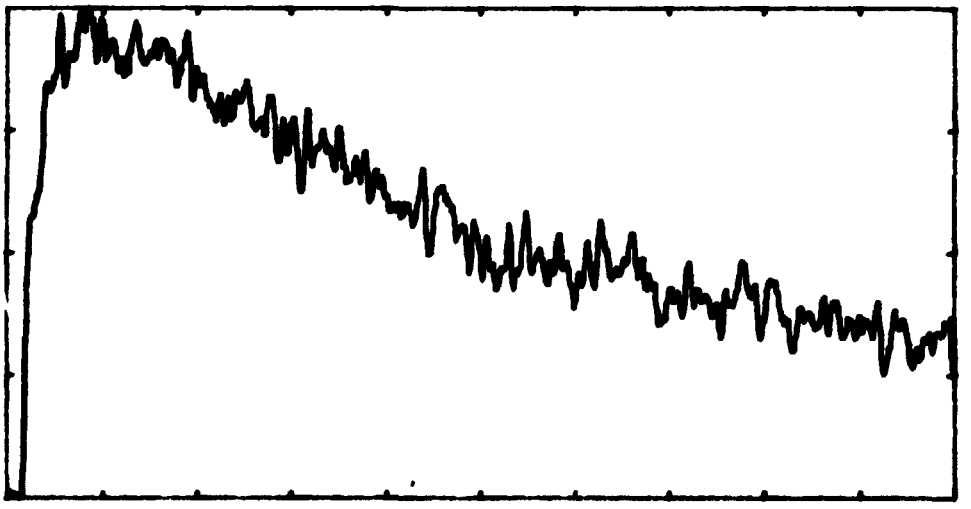

Figure 6.10. HS_2-formation and decay in 1 atm H_2S monitored at 3448 Å, T = 298±1 K and full timescale = 400 μsec.

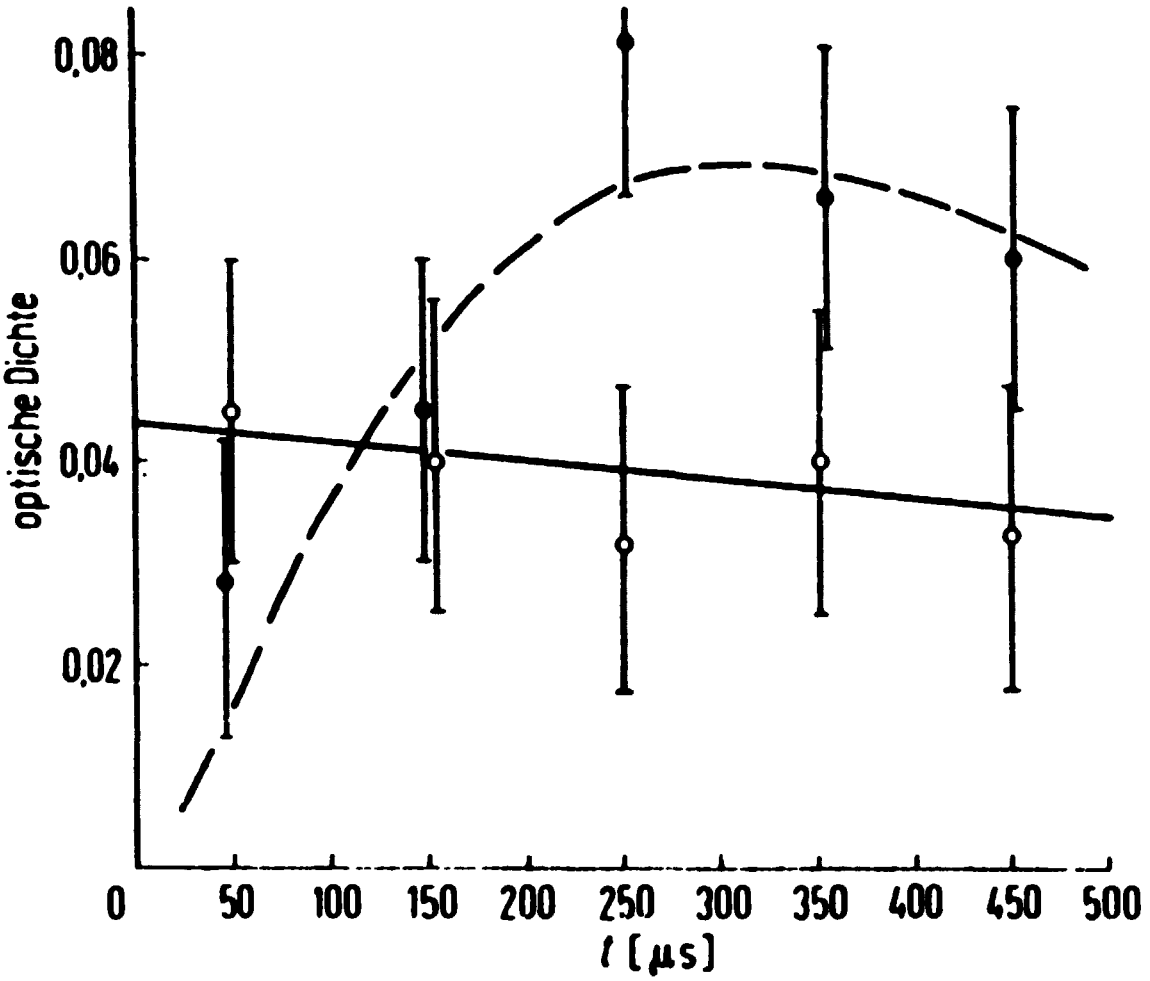

Figure 6.11. Dashed curve is the HS_2-formation in the experiment of Perner and Franken (1969).

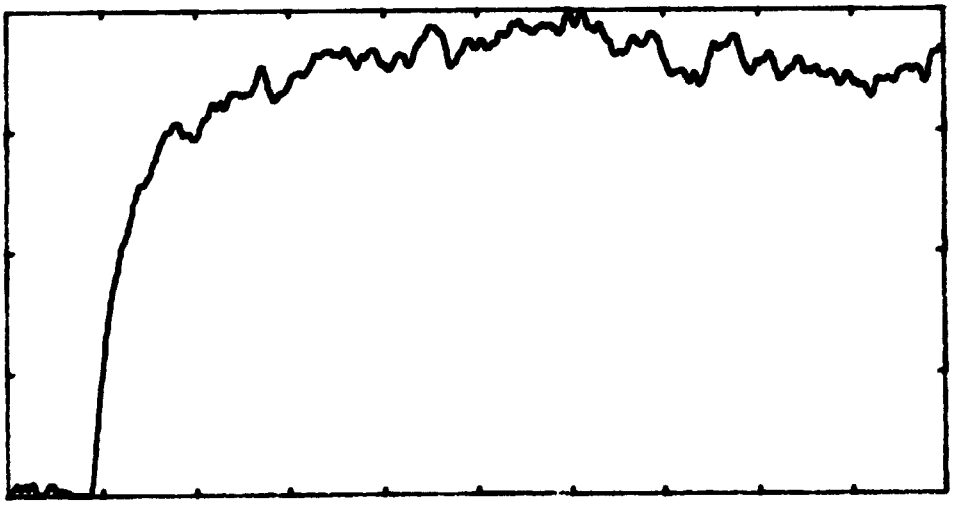

Figure 6.12. HS-formation in 2 mbar H_2S + Ar to 1 atm, monitored at 3241 Å, T = 298±1 K and full timescale = 40 µsec.

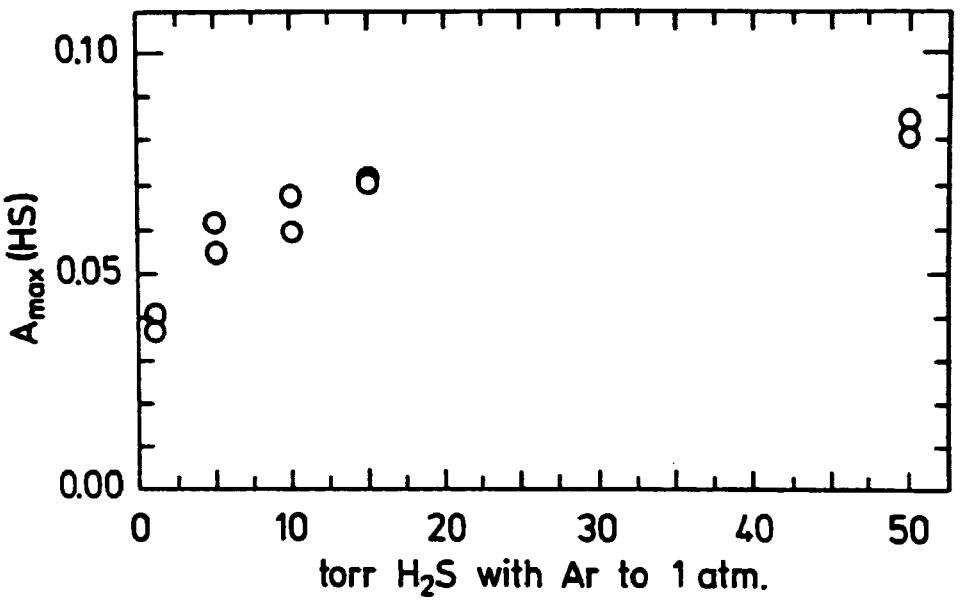

Figur 6.13. Maximum HS-absorbance vs. H_2S partial pressure.

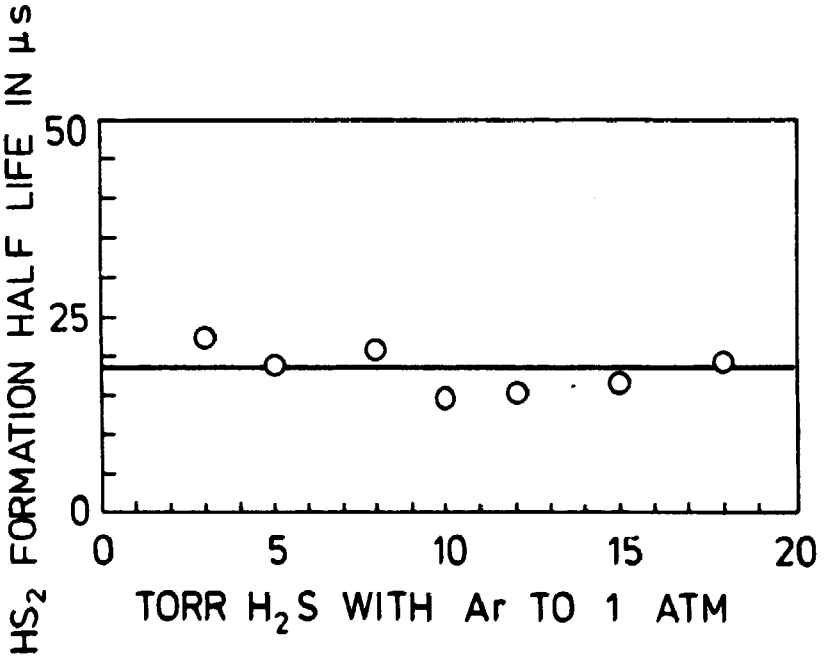

Figure 6.14. HS_2-formation halflife vs. H_2S partial pressure.

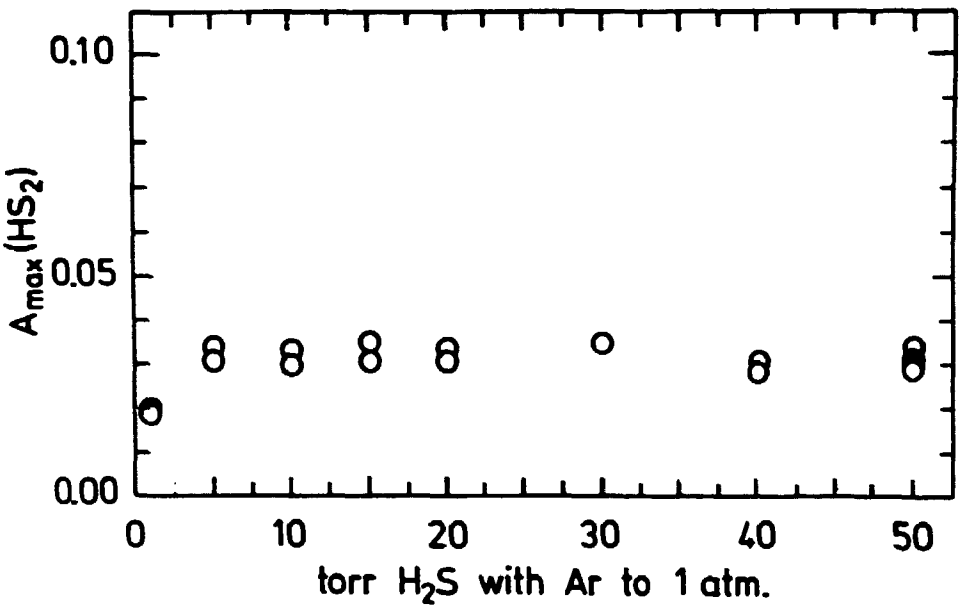

Figure 6.15. Maximum HS_2-absorbance vs. H_2S partial pressure.

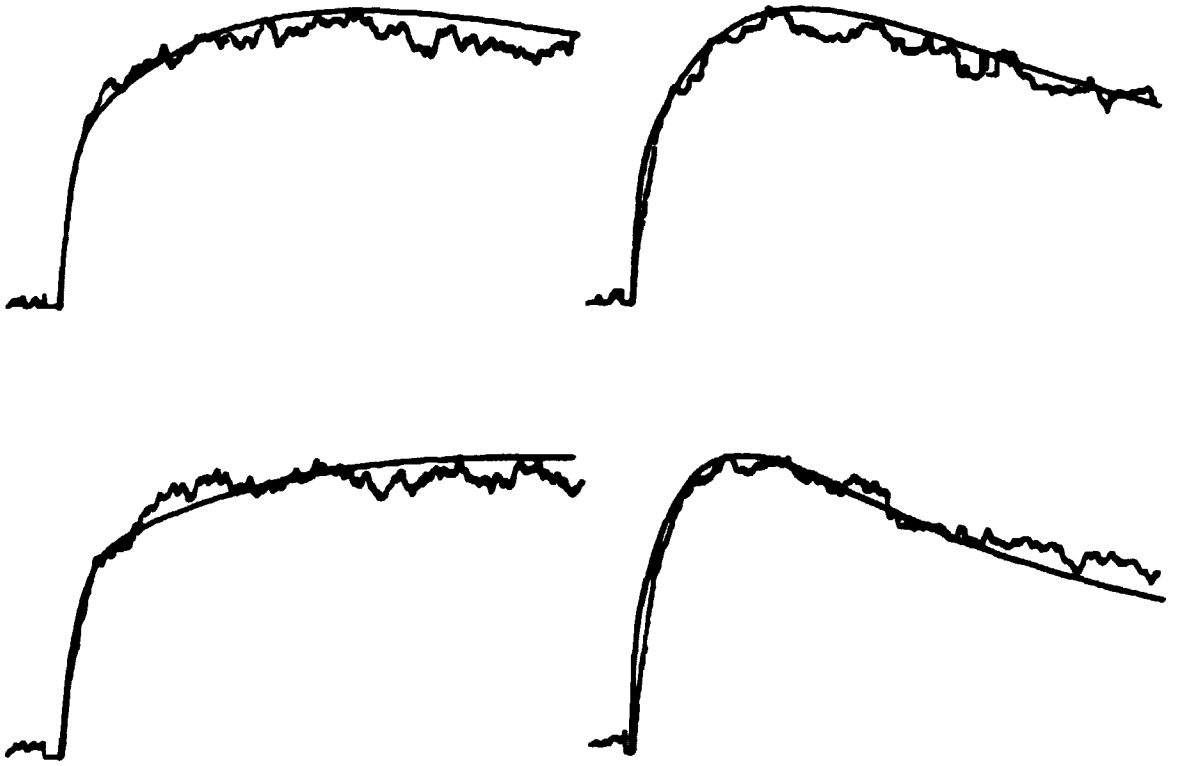

Figure 6.16. Comparison between experimental and computer simulated HS-kinetics in H_2S/Ar-mixtures. Normalized absorbance vs. time. Lower left: 1 mbar H_2S, upper left: 2 mbar H_2S, upper right: 5 mbar H_2S, lower right: 10 mbar H_2S. Total pressure = 1 atm.

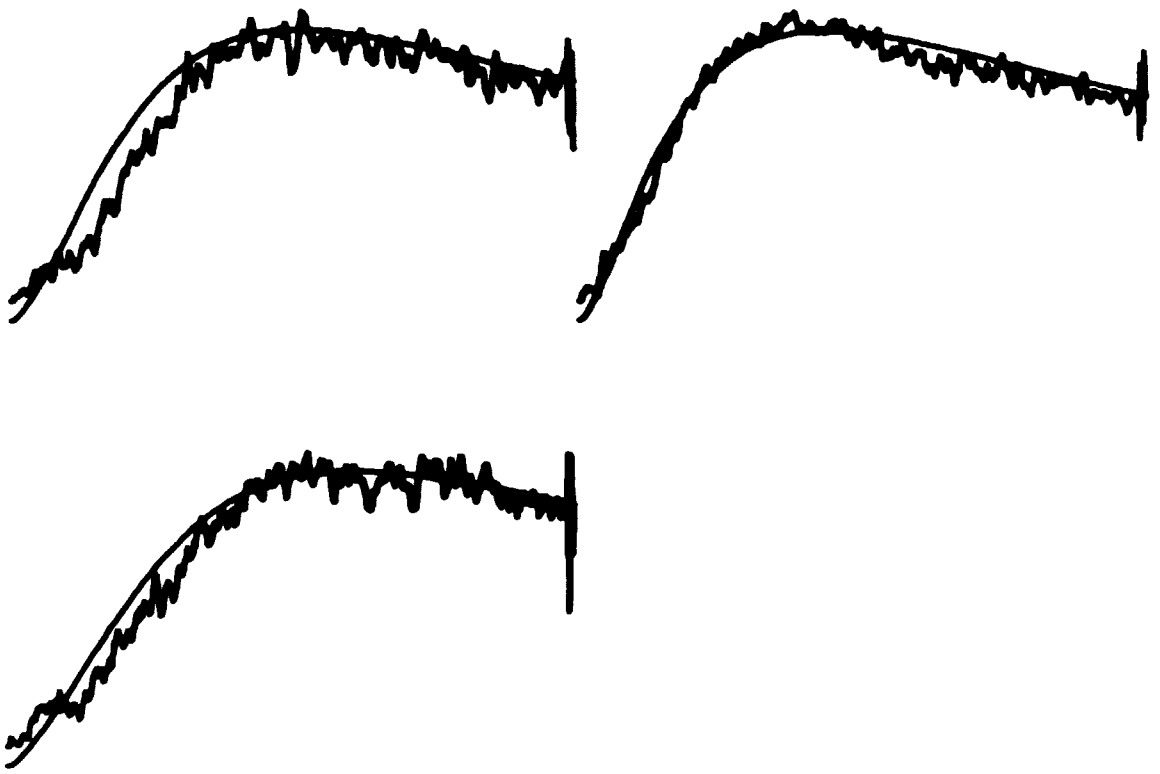

Figure 6.17. Comparison between experimental and computer simulated HS_2-kinetics in H_2S/Ar-mixtures. Normalized absorbance vs. time. Lower left: 1 mbar H_2S, upper left: 2 mbar H_2S, upper right: 5 mbar H_2S. Total pressure = 1 atm.

Sales distributors:
G.E.C. Gad Strøget
Vimmelskaftet 32
DK-1161 Copenhagen K, Denmark

Available on exchange from:
Risø Library, Risø National Laboratory,
P.O.Box 49, DK-4000 Roskilde, Denmark

ISBN 87-550-1002-4
ISSN 0106-2840